

A first order hyperbolic framework for large strain computational solid dynamics. Part III: Thermo-elasticity

Javier Bonet ^{a,1}, Chun Hean Lee ^{b,2}, Antonio J. Gil ^{c,3}, Ataollah Ghavamian ^{c,4}

(a) *University of Greenwich, London, SE10 9LS, United Kingdom*

(b) *Glasgow Computational Engineering Centre, James Watt School of Engineering
University of Glasgow, Glasgow, G12 8QQ, United Kingdom*

(c) *Zienkiewicz Centre for Computational Engineering, College of Engineering
Swansea University, Bay Campus, SA1 8EN, United Kingdom*

Abstract

In Parts I [1] and II [2] of this series, a novel computational framework was presented for the numerical analysis of large strain fast solid dynamics in compressible and nearly/truly incompressible isothermal hyperelasticity. The methodology exploited the use of a system of first order Total Lagrangian conservation laws formulated in terms of the linear momentum and a triplet of deformation measures comprised of the deformation gradient tensor, its co-factor and its Jacobian. Moreover, the consideration of polyconvex constitutive laws was exploited in order to guarantee the hyperbolicity of the system and show the existence of a convex entropy function (sum of kinetic and strain energy per unit undeformed volume) necessary for symmetrisation. In this new paper, the framework is extended to the more general case of thermo-elasticity by incorporating the first law of thermodynamics as an additional conservation law, written in terms of either the entropy (suitable for smooth solutions) or the total energy density (suitable for discontinuous solutions) of the system. The paper is further enhanced with the following key novelties. First, sufficient conditions are put forward in terms of the internal energy density and the entropy measured at reference temperature in order to ensure *ab-initio* the polyconvexity of the internal energy density in terms of the extended set comprised of the triplet of deformation measures and the entropy. Second, the study of the eigenvalue structure of the system is performed as proof of hyperbolicity and with the purpose of obtaining correct time step bounds for explicit time integrators. Application to two well-established thermo-elastic models is presented: Mie-Grüneisen and modified entropic elasticity. Third, the use of polyconvex internal energy constitutive laws enables the definition of a generalised convex entropy function, namely the *ballistic* energy, and associated entropy fluxes, allowing the symmetrisation of the system of conservation laws in terms of entropy-conjugate fields. Fourth, and in line with the previous papers of the series, an explicit stabilised Petrov-Galerkin framework is presented for the numerical solution of the thermo-elastic system of conservation laws when considering the entropy as an unknown of the system. Finally, a series of numerical examples is presented in order to assess the applicability and robustness of the proposed formulation.

Keywords: Large strain thermo-elasticity, Petrov-Galerkin, Explicit dynamics,

¹Corresponding author: j.bonet@greenwich.ac.uk

²Corresponding author: chunhean.lee@glasgow.ac.uk

³Corresponding author: a.j.gil@swansea.ac.uk

⁴Present address: École des Mines de Saint-Étienne, Saint-Étienne, France

1. Introduction

In Parts I [1] and II [2] of this series, a novel computational framework was presented for the numerical analysis of large strain fast solid dynamics in isothermal hyperelasticity. Whilst the aim of Part I was on compressible hyperelasticity, the focus of Part II moved towards nearly and truly incompressible hyperelasticity. The fundamental motivating factor for such work has been the development of a methodology capable of addressing the shortcomings of traditional displacement based formulations, such as: reduced order of convergence for strains and stresses [3], poor performance in bending dominated scenarios [4–7], numerical instabilities of the type of shear/volumetric locking [8, 9] and spurious pressure fluctuations [10–12] and high frequency oscillations in the vicinity of sharp spatial gradients when using Newmark-type time integrators [13, 14].

Apart from the possible use of high order schemes [15], extensive literature on low order schemes (typically preferred by the software industry), is available on a variety of techniques capable of addressing some (if not all) of the above shortcomings. In the case of linear tetrahedral elements, the earliest attempt at employing a system of conservation laws in solid dynamics originates from the work of [16, 17], where the conservation variables of the mixed based approach were the linear momentum \mathbf{p} and the deformation gradient tensor \mathbf{F} . Specifically, an upwind Godunov-type cell centred Finite Volume Method was presented for small strain linear elasticity. With a similar philosophy, an alternative version of cell centred FVM [18], approximated using node based numerical fluxes, was introduced in isothermal hyperelasticity [19, 20]. Recently, Scovazzi and co-authors [21–25] explored a mixed based (velocity-pressure) approach for the applications of transient solid dynamics by utilising a Variational Multi-Scale method. Codina, Cervera and collaborators [26–30] also explored a similar idea of incorporating stabilised nodal stresses with the use of orthogonal subgrid scale method.

In recent years, some of the authors of this manuscript have pursued the same $\{\mathbf{p}, \mathbf{F}\}$ system whilst exploiting well-established fluid inspired spatial discretisation techniques [3, 31–34]. In subsequent papers, the $\{\mathbf{p}, \mathbf{F}\}$ system was then augmented by incorporating a new conservation law for the Jacobian of the deformation J [35] to effectively solve nearly/truly incompressible deformations. Further enhancement of this framework has been reported by the authors [1, 2], when considering isothermal materials governed by a polyconvex constitutive law where the co-factor \mathbf{H} of the deformation plays a dominant role. The full set of unknowns $\{\mathbf{p}, \mathbf{F}, \mathbf{H}, J\}$ yields an elegant system of conservation laws, where the existence of a generalised convex entropy function enables the derivation of a symmetric system of hyperbolic equations, dual of that expressed in terms of entropy conjugates of the conservation variables [2].

Consideration of thermal effects, especially in the context of large strain fast transient dynamics, is fundamental in order to obtain a realistic representation of stresses when a solid undergoes a complex and rapidly evolving deformation pattern. With focus on thermo-elasticity and thermo-inelasticity, numerous authors have worked over the years putting forward a variety of computational schemes where both displacements and thermal variables are solved either monolithically or in staggered fashion [33, 36–40]. Traditionally, authors prefer the use of the temperature θ as the *thermal* unknown to be solved, although alternative schemes in terms of the entropy η are also possible [36, 41].

The aim of this Part III paper is to further extend the work thus far presented in this series to account for strongly thermally-coupled scenarios, through the consideration of non-

reversible thermo-elastic constitutive models⁵. With this in mind, a generalised system of first order conservation laws is presented in terms of the set $\{\mathbf{p}, \mathbf{F}, \mathbf{H}, J, \eta\}$, where the first law of thermodynamics is incorporated as an extra conservation law in addition to the linear momentum and geometric conservation already covered in Parts I and II.

A crucial aspect that requires special attention (especially in the case of coupled problems) is that of the stability of the formulation, from both the continuum and numerical standpoints. With respect to the former, this paper seeks the use of *ab initio* stable polyconvex constitutive internal energy functionals in the most generic thermal case, that is, not only restricted to isothermal or isentropic scenarios [42–46]. Thus, and following the definition of polyconvexity with respect to the extended set of arguments $\{\mathbf{F}, \mathbf{H}, J, \eta\}$, as proposed in [47], a set of sufficient conditions will be put forward for the (i) internal energy density and (ii) the entropy measured at reference temperature, in order to ensure *ab initio* the polyconvexity of the general internal energy density function. As it is well known, polyconvexity is a sufficient guarantor of ellipticity or rank-one convexity (in the quasi-static case) and hyperbolicity⁶ (in the dynamic case). In this paper, the latter condition is demonstrated and, moreover, the study of the eigenvalue structure of the system is carried out with the purpose of obtaining correct time step bounds for explicit time integrators. Application to two well-established thermo-elastic models is presented: Mie-Grüneisen and modified entropic elasticity. The complexity of the algebra is tremendously facilitated by means of the use of a tensor cross product operation which can be originally found in [49, 50] and exploited for the first time in the context of solid mechanics in [51, 52].

The use of polyconvex internal energy density functionals facilitates the transformation of the system of conservation laws into a symmetric set via the introduction of a suitable convex entropy function⁷. In the context of thermo-elasticity, this convex entropy function will be identified with the well-known ballistic energy [53] (also known as Lyapunov function [54, 55]) of the system. Moreover, and although the main focus of the paper is on the use of the entropy as the *thermal* unknown (suitable for the case of smooth fields), it is also shown how the use of the ballistic energy as convex entropy function permits the use of the total energy density as an alternative *thermal* unknown (in the case of discontinuous fields). From the numerical point of view, and in consistency with previous work in this series, an explicit stabilised Petrov-Galerkin framework is employed for the numerical solution of the thermo-elastic system of conservation laws when considering the entropy as an unknown of the system.

The outline of the paper is as follows. Section 2 briefly recaps and summarises the system of Total Lagrangian conservation laws for the case of non-thermal hyperelasticity. Section 3 starts by introducing some fundamental concepts of thermo-elasticity and calorimetry, necessary for the remainder of the paper. The Section then presents alternative representations of the internal energy density before introducing some sufficient conditions that, if ensured, guarantee *ab-initio* the polyconvexity of the internal energy density functional. Section 3 concludes by presenting examples of universally convex functions for the case of volumetric-deviatoric Mie-Grüneisen constitutive models. In Section 4, a proof of hyperbolicity is presented along with accurate time bounds for the volumetric and shear wave speeds. Section 5 demonstrates the existence of a convex entropy function, the so-called ballistic energy, which permits the symmetrisation of the system of conservation laws. Section 6 discusses the time and spatial discretisation and presents

⁵Further inelastic contributions (i.e. plasticity, viscoplasticity, viscoelasticity, thermo-viscoplasticity) are not within the scope of this paper.

⁶Also known as the Legendre-Hadamard condition [48].

⁷Not to be confused with the entropy density field.

the stabilised Petrov-Galerkin Finite Element scheme pursued in this paper, implemented in the form of a Variational MultiScale approach. Section 7 summarises for completeness the solution procedure. In Section 8, an extensive set of numerical examples with emphasis on smooth problems is presented to assess the performance of the proposed method and draw some comparisons against an alternative vertex centred Finite Volume method recently developed by the authors. Section 9 summarises some concluding remarks and current directions of research. In addition, Appendix A computes the volumetric and wave speeds for the modified entropic elasticity case. Appendix B briefly summarises the key ingredients of the formulation whereby the total energy density is preferred, instead of the entropy, as *thermal* unknown. Finally, Appendix C presents the linearisation of the set of conservation laws which is used to derive a closed form solution used to verify the numerical spatial convergence of the formulation.

2. First order conservation laws for non-thermal elasticity

Consider the motion of a non-thermal⁸ elastic body that is described by a time-dependent mapping field $\phi(\mathbf{X}, t)$ which links a material particle from an initial reference configuration $\mathbf{X} \in V_R$ of boundary ∂V_R (with outward unit normal \mathbf{N}) to the time-dependent spatial configuration $\mathbf{x} \in V_R(t)$ of boundary $\partial V_R(t)$ (with outward unit normal \mathbf{n}) according to $\mathbf{x} = \phi(\mathbf{X}, t)$. As presented in Part I [1] and Part II [2] of this series, the motion can be described by a system of first order Total Lagrangian conservation laws as follows:

$$\frac{\partial \mathbf{p}}{\partial t} - \text{DIV} \mathbf{P} = \mathbf{f}_R; \quad (1a)$$

$$\frac{\partial \mathbf{F}}{\partial t} - \text{DIV} \left(\frac{1}{\rho_R} \mathbf{p} \otimes \mathbf{I} \right) = \mathbf{0}; \quad (1b)$$

$$\frac{\partial \mathbf{H}}{\partial t} - \text{CURL} \left(\frac{1}{\rho_R} \mathbf{p} \times \mathbf{F} \right) = \mathbf{0}; \quad (1c)$$

$$\frac{\partial J}{\partial t} - \text{DIV} \left(\frac{1}{\rho_R} \mathbf{H}^T \mathbf{p} \right) = 0. \quad (1d)$$

Here, $\mathbf{p} = \rho_R \mathbf{v}$ is the linear momentum per unit of undeformed volume, ρ_R is the density of the undeformed configuration, \mathbf{v} represents the velocity field, \mathbf{f}_R is the body force per unit of reference volume, \mathbf{F} is the deformation gradient tensor (or fibre map), \mathbf{H} is the co-factor of the deformation gradient tensor (area map), J is the Jacobian of the deformation gradient tensor (volume map), \mathbf{P} represents the first Piola-Kirchhoff stress tensor, \mathbf{I} is the identity tensor, DIV and CURL represent the material divergence and curl operators, respectively. The symbol \otimes is the standard dyadic outer product, whilst \times represents the tensor cross product between vectors and/or second order tensors as that presented in [51, 52]. Finally, for post-processing purposes, the deformed geometry \mathbf{x} can be recovered through time integration of the velocity field denoted as

$$\frac{d\mathbf{x}}{dt} = \frac{\mathbf{p}}{\rho_R}. \quad (2)$$

⁸When using the term non-thermal, two possible scenarios can be considered, namely that of isothermal (constant temperature) or isentropic (constant entropy).

As the system of conservation laws presented above has more equations than needed, suitable compatibility relationships, also known as involutions [56], are necessary, namely⁹,

$$\text{CURL}\mathbf{F} = \mathbf{0}; \quad \text{DIV}\mathbf{H} = \mathbf{0}. \quad (3)$$

In the presence of non-smooth solutions (outside the scope of this paper), above balance equations (1) are accompanied by appropriate Rankine Hugoniot jump conditions. For an in-depth derivation and use of these conditions, the reader is referred to Part I in the series and to further contributions by the authors, typically in the context of non-Finite Element based spatial discretisations [3, 32, 34, 57–61].

For closure of system (1), and to guarantee the existence of real wave speeds in the material (hyperbolicity) for the entire range of possible deformations, suitable constitutive laws compliant with the principle of objectivity (frame invariance) and the second law of Thermodynamics (Coleman-Noll procedure) must be established [62]. In Parts I and II, and for reversible elastodynamics, objective constitutive laws were defined via polyconvex elastic strain energy density functionals [42, 43, 63–67]¹⁰, that is, the strain energy density is written as a convex combination of the triplet of deformation measures $\mathcal{X} = \{\mathbf{F}, \mathbf{H}, J\}$.

3. Thermo-elasticity

3.1. First law of thermodynamics in terms of the total energy

The above system (1) can be extended to more general constitutive models that take into account thermal effects, such as thermo-elasticity. The resulting processes are generally irreversible and require an additional conservation law and variable describing the total balance of energy in the system. This is known as the first law of thermodynamics and is expressed as [68]:

$$\frac{d}{dt} \int_{V_R} E dV_R = \int_{\partial V_R} \mathbf{t} \cdot \mathbf{v} dA - \int_{\partial V_R} Q_B dA + \int_{V_R} \mathbf{f}_R \cdot \mathbf{v} dV_R + \int_{V_R} r_R dV_R, \quad (4)$$

where $E(\mathbf{X}, t)$ is the total energy density (per unit undeformed volume), $\mathbf{t} = \mathbf{P}\mathbf{N}$ the boundary traction vector, $Q_B = \mathbf{Q} \cdot \mathbf{N}$ is the heat flow normal to the boundary ∂V_R , r_R the thermal heat source per unit reference volume. The equivalent pointwise conservation law is given by

$$\frac{\partial E}{\partial t} + \text{DIV}(\mathbf{Q} - \mathbf{P}^T \mathbf{v}) = \mathbf{f}_R \cdot \mathbf{v} + r_R, \quad (5)$$

with jump conditions being defined as [3]

$$U[[E]] = [[\mathbf{Q}]] \cdot \mathbf{N} - [[\mathbf{P}^T \mathbf{v}]] \cdot \mathbf{N}, \quad (6)$$

where $[[\bullet]] := [\bullet]^+ - [\bullet]^-$ denotes the jump operator across a discontinuous surface defined by a unit normal \mathbf{N} (pointing from $[\bullet]^-$ towards $[\bullet]^+$) propagating within the material with normal speed U .

⁹Conservation equations for the cofactor and Jacobian of the deformation are not strictly necessary from a continuum standpoint as these two kinematic fields are strongly related (via compatibility equations or involutions) with the deformation gradient. However, from a semi-discrete viewpoint, this strong compatibility weakens and can be “exploited” in order to add flexibility to a low order numerical scheme circumventing locking related problems.

¹⁰The strain energy density is measured either at a reference temperature (i.e. isothermal hyperelasticity) or at a reference entropy (i.e. isentropic hyperelasticity), depending on the simulation to be carried out.

3.2. First law of thermodynamics in terms of the internal energy and the entropy

The total energy E density in the above first law of thermodynamics includes kinetic and internal energy contributions. Multiplying the linear momentum balance principle (1a) by \mathbf{v} and subtracting it from the above equation (5), after some algebra, gives

$$\frac{\partial \mathcal{E}}{\partial t} + \text{DIV} \mathbf{Q} = \mathbf{P} : \nabla_0 \mathbf{v} + r_R, \quad (7)$$

where $\mathcal{E}(\mathbf{X}, t) = E - \frac{1}{2\rho_R} (\mathbf{p} \cdot \mathbf{p})$ represents the internal energy per unit undeformed volume. Note, however, that the above transformation is only possible in the case of smooth fields. For the Petrov-Galerkin type of finite element solutions envisaged here this will be the case. In strict thermo-elasticity, the internal energy density $\mathcal{E}(\mathbf{X}, t)$ is postulated to depend on the triplet of deformation variables $\boldsymbol{\chi} = \{\mathbf{F}, \mathbf{H}, J\}$ and the so-called entropy density (per unit of undeformed volume) η , that is

$$\mathcal{E}(\mathbf{X}, t) = \mathcal{E}(\boldsymbol{\chi}_\eta); \quad \boldsymbol{\chi}_\eta = \{\boldsymbol{\chi}, \eta\} = \{\mathbf{F}, \mathbf{H}, J, \eta\}, \quad (8)$$

where \mathcal{E} denotes the same internal energy per unit undeformed volume as \mathcal{E} but with a different functional dependency. Here, the entropy density field $\eta(\mathbf{X}, t)$ is defined as the energy dual conjugate variable to the temperature $\theta(\mathbf{X}, t)$, that is

$$\theta(\mathbf{X}, t) = \frac{\partial \mathcal{E}(\boldsymbol{\chi}_\eta)}{\partial \eta} = \Theta(\boldsymbol{\chi}_\eta). \quad (9)$$

Again, the notation θ and Θ is used to denote the same temperature with different functional dependency. Similarly, energy conjugate fields can be defined to the three deformation measures of the triplet $\boldsymbol{\chi}$ as

$$\boldsymbol{\Sigma}_F = \frac{\partial \mathcal{E}(\boldsymbol{\chi}_\eta)}{\partial \mathbf{F}}; \quad \boldsymbol{\Sigma}_H = \frac{\partial \mathcal{E}(\boldsymbol{\chi}_\eta)}{\partial \mathbf{H}}; \quad \Sigma_J = \frac{\partial \mathcal{E}(\boldsymbol{\chi}_\eta)}{\partial J}. \quad (10)$$

By comparing the time rate of the internal strain energy $\mathcal{E}(\mathbf{X}, t)$ to that of its equivalent re-expression $\mathcal{E}(\boldsymbol{\chi}_\eta)$ and, using the properties of the tensor cross product as shown in [1], it is possible to relate the conjugate stresses defined in (10) to the standard first Piola–Kirchhoff stress tensor as

$$\begin{aligned} \frac{\partial \mathcal{E}(\mathbf{X}, t)}{\partial t} &= \frac{\partial \mathcal{E}(\boldsymbol{\chi}_\eta)}{\partial \mathbf{F}} : \frac{\partial \mathbf{F}}{\partial t} + \frac{\partial \mathcal{E}(\boldsymbol{\chi}_\eta)}{\partial \mathbf{H}} : \frac{\partial \mathbf{H}}{\partial t} + \frac{\partial \mathcal{E}(\boldsymbol{\chi}_\eta)}{\partial J} \frac{\partial J}{\partial t} + \frac{\partial \mathcal{E}(\boldsymbol{\chi}_\eta)}{\partial \eta} \frac{\partial \eta}{\partial t} \\ &= \boldsymbol{\Sigma}_F : \nabla_0 \mathbf{v} + \boldsymbol{\Sigma}_H : (\mathbf{F} \times \nabla_0 \mathbf{v}) + \Sigma_J (\mathbf{H} : \nabla_0 \mathbf{v}) + \theta \frac{\partial \eta}{\partial t} \\ &= [\boldsymbol{\Sigma}_F + \boldsymbol{\Sigma}_H \times \mathbf{F} + \Sigma_J \mathbf{H}] : \nabla_0 \mathbf{v} + \theta \frac{\partial \eta}{\partial t}, \end{aligned} \quad (11)$$

which leads to the following relationship

$$\mathbf{P}(\boldsymbol{\chi}_\eta) = \boldsymbol{\Sigma}_F + \boldsymbol{\Sigma}_H \times \mathbf{F} + \Sigma_J \mathbf{H}. \quad (12)$$

It is now possible to re-write the first law of thermodynamics in terms of the entropy η by combining equations (7) and (11) to give a thermal expression in which mechanical terms have been conveniently eliminated to yield [48]

$$\theta \frac{\partial \eta}{\partial t} + \text{DIV} \mathbf{Q} = r_R. \quad (13)$$

Alternatively, noting that $\frac{1}{\theta}\text{DIV}\mathbf{Q} = \text{DIV}\left(\frac{\mathbf{Q}}{\theta}\right) + \frac{1}{\theta^2}\mathbf{Q}\cdot\nabla_0\theta$, a conservation type of law for the entropy emerges as

$$\frac{\partial\eta}{\partial t} + \text{DIV}\left(\frac{\mathbf{Q}}{\theta}\right) = \frac{r_R}{\theta} - \frac{1}{\theta^2}\mathbf{Q}\cdot\nabla_0\theta, \quad (14)$$

where \mathbf{Q}/θ represents the flux of entropy and the right hand side term is the entropy source per unit undeformed volume. Note that this expression (14) for the entropy assumes smooth solutions and it is still an expression of the first law. Integration over an arbitrary volume V_R together with use of the divergence theorem gives

$$\frac{d}{dt}\int_{V_R}\eta dV_R + \int_{\partial V_R}\left(\frac{Q_B}{\theta}\right) dA = \int_{V_R}\left(\frac{r_R}{\theta}\right) dV_R - \int_{V_R}\frac{1}{\theta^2}\mathbf{Q}\cdot\nabla_0\theta dV_R. \quad (15)$$

In relation to the heat flux vector \mathbf{Q} , we consider the typical Fourier law to hold and which can be defined in a Total Lagrangian fashion

$$\mathbf{Q} = -\mathbf{K}\nabla_0\theta; \quad \mathbf{K} = J^{-1}\mathbf{H}^T\mathbf{k}\mathbf{H}. \quad (16)$$

where \mathbf{k} represents the positive semi-definite second order thermal conductivity tensor in the deformed configuration.

3.3. Second law of thermodynamics

Given the fact that heat must flow from hotter to colder regions of the solid and, consequently, the direction of \mathbf{Q} must oppose the direction of the thermal gradient $\nabla_0\theta$ as

$$-\frac{1}{\theta^2}\mathbf{Q}\cdot\nabla_0\theta \geq 0. \quad (17)$$

This implies that equation (15) can be written in the form of an inequality as

$$\frac{d}{dt}\int_{V_R}\eta dV_R + \int_{\partial V_R}\left(\frac{Q_B}{\theta}\right) dA \geq \int_{V_R}\left(\frac{r_R}{\theta}\right) dV_R. \quad (18)$$

This inequality is known as the second law of thermodynamics. Note that in classical rational mechanics [48] equation (18) is accepted a priori as a fundamental principle from which the flow direction equation (17) is then obtained as a consequence. The physical implication of this equation is that the total entropy of an isolated system (i.e. with null second and third terms of above inequality (18)) can only grow. The equivalent differential form of equation (18) is

$$\frac{\partial\eta}{\partial t} + \text{DIV}\left(\frac{\mathbf{Q}}{\theta}\right) \geq \frac{r_R}{\theta}. \quad (19)$$

Note that the physical consequence of this inequality implies that thermo-elastic processes in general cannot be reversed. Typically, a process can only be reversed if the inequality becomes an equality when \mathbf{Q} vanishes. Such processes are known as adiabatic. In addition, if there are no heat sources the entropy value will be preserved in which case the process is known as isentropic.

3.4. General thermal relationships and stability requirements

In general, the Calorimetry relationships between internal energy \mathcal{E} , temperature θ and entropy η can be derived from the definition of the specific heat at constant volume c_v [68, 69]. This requires the re-definition of the entropy η and the internal energy density \mathcal{E} in terms of the triplet of deformation measures $\boldsymbol{\mathcal{X}}$ and the temperature θ of the system, namely, $\boldsymbol{\mathcal{X}}_\theta = \{\boldsymbol{\mathcal{X}}, \theta\} = \{\mathbf{F}, \mathbf{H}, J, \theta\}$. Specifically,

$$c_v \stackrel{\text{def}}{=} \left. \frac{d\mathcal{E}}{d\theta} \right|_{\boldsymbol{\mathcal{X}}=\text{const}} = \frac{\partial \tilde{\mathcal{E}}(\boldsymbol{\mathcal{X}}_\theta)}{\partial \theta}; \quad \tilde{\mathcal{E}}(\boldsymbol{\mathcal{X}}_\theta) = \mathcal{E}(\boldsymbol{\mathcal{X}}, \tilde{\eta}(\boldsymbol{\mathcal{X}}_\theta)); \quad \eta = \tilde{\eta}(\boldsymbol{\mathcal{X}}_\theta), \quad (20)$$

with $c_v = \rho_R C_v > 0$, where ρ_R is the density measured at a reference temperature θ_R and C_v the specific heat per unit mass. As the internal energy $\mathcal{E}(\boldsymbol{\mathcal{X}}, t)$ can be expressed as a function of the set of arguments $\boldsymbol{\mathcal{X}}_\eta$ (8), consequently equation (20) can be recast using the chain rule to yield

$$c_v = \frac{\partial \mathcal{E}(\boldsymbol{\mathcal{X}}_\eta)}{\partial \eta} \frac{\partial \tilde{\eta}(\boldsymbol{\mathcal{X}}_\theta)}{\partial \theta}. \quad (21)$$

Given that $\partial \mathcal{E}(\boldsymbol{\mathcal{X}}_\eta)/\partial \eta = \theta$ (9), a constitutive relationship between the temperature θ and the entropy η at constant deformation can be established

$$\frac{\partial \tilde{\eta}(\boldsymbol{\mathcal{X}}_\theta)}{\partial \theta} = \frac{c_v}{\theta}. \quad (22)$$

In general, the specific heat coefficient c_v is a function of temperature θ . However, this coefficient can be assumed constant for most materials for a reasonably large range of temperature variations [68]. Restricting the derivations to this simple constant heat coefficient case, enables expression (22) to be integrated analytically with respect to the entropy or temperature changes as

$$\int_{\tilde{\eta}_R(\boldsymbol{\mathcal{X}})}^{\tilde{\eta}(\boldsymbol{\mathcal{X}}_\theta)} d\eta = \int_{\theta_R}^{\theta} \frac{c_v}{\theta} d\theta, \quad (23)$$

which leads to a simple relationship between entropy and temperature as

$$\tilde{\eta}(\boldsymbol{\mathcal{X}}_\theta) = \tilde{\eta}_R(\boldsymbol{\mathcal{X}}) + c_v \ln \frac{\theta}{\theta_R}; \quad \tilde{\eta}_R(\boldsymbol{\mathcal{X}}) = \tilde{\eta}(\boldsymbol{\mathcal{X}}, \theta = \theta_R). \quad (24)$$

In this expression, $\tilde{\eta}_R(\boldsymbol{\mathcal{X}})$ denotes the entropy measured at a constant temperature θ_R and expressed as a function of the deformation $\boldsymbol{\mathcal{X}}$ (after the deformation, the temperature is allowed to return to the reference value θ_R). Using equation (24), the reverse relationship yielding the temperature as a function of the entropy and deformation is given by

$$\begin{aligned} \Theta(\boldsymbol{\mathcal{X}}_\eta) &= \theta_R e^{(\eta - \tilde{\eta}_R(\boldsymbol{\mathcal{X}}))/c_v} \\ &= \theta_R e^{-\tilde{\eta}_R(\boldsymbol{\mathcal{X}})/c_v} e^{\eta/c_v} \\ &= \Theta_0(\boldsymbol{\mathcal{X}}) e^{\eta/c_v}; \quad \Theta_0(\boldsymbol{\mathcal{X}}) = \theta_R e^{-\tilde{\eta}_R(\boldsymbol{\mathcal{X}})/c_v} = \Theta(\boldsymbol{\mathcal{X}}, \eta = 0), \end{aligned} \quad (25)$$

where $\Theta_0(\boldsymbol{\mathcal{X}})$ denotes the temperature reached after a state of deformation $\boldsymbol{\mathcal{X}}$ is arrived under isentropic conditions, that is, keeping the entropy constant at its reference value zero. Finally, it is also possible to write an explicit relationship for the internal energy $\mathcal{E}(\boldsymbol{\mathcal{X}}, t)$ in terms of

the set $\boldsymbol{\mathcal{X}}_\eta$, that is, $\mathcal{E}(\boldsymbol{\mathcal{X}}_\eta)$. This is achieved by integrating equation (9) with respect to the entropy field between the limits 0 and a given value η as

$$\int_{\mathcal{E}_0(\boldsymbol{\mathcal{X}})}^{\mathcal{E}(\boldsymbol{\mathcal{X}}_\eta)} d\mathcal{E} = \Theta_0(\boldsymbol{\mathcal{X}}) \int_0^\eta e^{\eta/c_v} d\eta, \quad (26)$$

which then yields

$$\mathcal{E}(\boldsymbol{\mathcal{X}}_\eta) = \mathcal{E}_0(\boldsymbol{\mathcal{X}}) + c_v \Theta_0(\boldsymbol{\mathcal{X}}) \left[e^{\frac{\eta}{c_v}} - 1 \right]; \quad \mathcal{E}_0(\boldsymbol{\mathcal{X}}) = \mathcal{E}(\boldsymbol{\mathcal{X}}, \eta = 0), \quad (27)$$

where the term $\mathcal{E}_0(\boldsymbol{\mathcal{X}})$ represents the amount of internal energy per unit reference volume accumulated when the body is deformed in an isentropic manner.

In order to ensure the existence of real wave speeds in the material for the entire thermo-elastic deformation process, that is, regardless of the amount of deformation $\boldsymbol{\mathcal{X}}$ and thermal state η (or θ), it is important that the function $\mathcal{E}(\boldsymbol{\mathcal{X}}_\eta)$ (27) is convex in its variables [47]. This is an extension of the usual polyconvexity condition for non-thermal processes where the strain energy density is required to be convex on the triplet of deformation variables $\boldsymbol{\mathcal{X}}$.

Note that since it is perfectly possible to envisage isentropic deformation processes taking place where the second term in (27a) vanishes, it is necessary that the function $\mathcal{E}_0(\boldsymbol{\mathcal{X}})$ should be convex in $\boldsymbol{\mathcal{X}}$, that is $\mathcal{E}_0(\boldsymbol{\mathcal{X}})$ shall be polyconvex. However, it is also easy to see that the convexity of $\mathcal{E}_0(\boldsymbol{\mathcal{X}})$ alone does not ensure the convexity of $\mathcal{E}(\boldsymbol{\mathcal{X}}_\eta)$ as per equation (27) for all values of $\boldsymbol{\mathcal{X}}$ and η . Furthermore, since it is also perfectly physically possible to envisage processes taking place at a given constant temperature, for instance θ_R , the energy potential defining the material behaviour at this temperature, namely the Helmholtz free energy function $\psi_R(\boldsymbol{\mathcal{X}})$ must also be polyconvex¹¹. The isothermal Helmholtz free energy potential is related to the internal energy density as

$$\psi_R(\boldsymbol{\mathcal{X}}) = \tilde{\mathcal{E}}_R(\boldsymbol{\mathcal{X}}) - \theta_R \tilde{\eta}_R(\boldsymbol{\mathcal{X}}); \quad \tilde{\mathcal{E}}_R(\boldsymbol{\mathcal{X}}) = \tilde{\mathcal{E}}(\boldsymbol{\mathcal{X}}, \theta = \theta_R) = \mathcal{E}(\boldsymbol{\mathcal{X}}, \tilde{\eta}_R(\boldsymbol{\mathcal{X}})). \quad (28)$$

The internal energy term $\tilde{\mathcal{E}}_R(\boldsymbol{\mathcal{X}})$ represents the energy per unit undeformed volume caused by the deformation after the temperature has been allowed to return back to the reference value θ_R . This is in contrast to $\mathcal{E}_0(\boldsymbol{\mathcal{X}})$, which measures the energy per unit undeformed volume caused by deformation but before any heat flow has been allowed to take place so that the entropy, rather than the temperature, remains at its reference zero value. In summary, for a well defined constitutive model, the following three conditions must be satisfied, namely

- (i) $\mathcal{E}(\boldsymbol{\mathcal{X}}_\eta)$ is convex in $\{\boldsymbol{\mathcal{X}}_\eta\} = \{\boldsymbol{\mathcal{X}}, \eta\} = \{\boldsymbol{F}, \boldsymbol{H}, J, \eta\}$,
- (ii) $\mathcal{E}_0(\boldsymbol{\mathcal{X}})$ is convex in $\boldsymbol{\mathcal{X}} = \{\boldsymbol{F}, \boldsymbol{H}, J\}$, and
- (iii) $\psi_R(\boldsymbol{\mathcal{X}})$ is convex in $\boldsymbol{\mathcal{X}} = \{\boldsymbol{F}, \boldsymbol{H}, J\}$.

When defining the internal energy density, it is very tempting to do so in terms of simple polyconvex functions for $\mathcal{E}_0(\boldsymbol{\mathcal{X}})$ or $\psi_R(\boldsymbol{\mathcal{X}})$ as shown in Parts I or II [1, 2], for instance,

$$\mathcal{E}_0(\boldsymbol{\mathcal{X}}) = \varsigma_0 (J^{-2/3} II_{\boldsymbol{F}} - 3) + \xi_0 \left(J^{-2} II_{\boldsymbol{H}}^{3/2} - 3\sqrt{3} \right) + \frac{\kappa_0}{2} (J - 1)^2; \quad \{\varsigma_0, \xi_0, \kappa_0\} \geq 0 \quad (29)$$

¹¹ $\mathcal{E}_0(\boldsymbol{\mathcal{X}})$ and $\psi_R(\boldsymbol{\mathcal{X}})$ correspond correspond to the classical strain energy potentials used in non-thermal isentropic and isothermal simulations, respectively.

or

$$\psi_R(\boldsymbol{\mathcal{X}}) = \varsigma_R (J^{-2/3} II_{\mathbf{F}} - 3) + \xi_R \left(J^{-2} II_{\mathbf{H}}^{3/2} - 3\sqrt{3} \right) + \frac{\kappa_R}{2} (J - 1)^2; \quad \{\varsigma_R, \xi_R, \kappa_R\} \geq 0, \quad (30)$$

where $II_{\mathbf{F}} = \mathbf{F} : \mathbf{F}$ and $II_{\mathbf{H}} = \mathbf{H} : \mathbf{H}$. Appropriate values for the material parameters $\varsigma_{0,R}$ and $\xi_{0,R}$ can be defined in terms of the shear modulus μ , that is, $2\varsigma_{0,R} + 3\sqrt{3}\xi_{0,R} = \mu_{0,R}$ [2].

Unfortunately, neither the use of (29) nor (30) alone is sufficient to ensure that condition (i) is satisfied for general thermo-elastic materials where the thermo-mechanical coupling is determined by, for instance, a Mie-Grüneisen model. The next section describes sufficient conditions for (i), (ii) and (iii) to be satisfied.

3.5. Polyconvex thermo-mechanical internal energy functionals

This section presents conditions that are sufficient for $\mathcal{E}(\boldsymbol{\mathcal{X}}_\eta)$ to be universally polyconvex and presents some simple examples of such energy functions. Several examples of universally polyconvex strain energy models are proposed for materials governed by a general Mie-Grüneisen coupling model. The relationship between the resulting polyconvex models' coefficients and the standard coefficients $\{\varsigma_0, \xi_0, \kappa_0\}$ and $\{\varsigma_R, \xi_R, \kappa_R\}$ given in (29) and (30) can then be derived. Additionally, alternative polyconvex strain energy models for modified entropic elasticity [70] are also presented in Appendix A for completeness.

3.5.1. Sufficient conditions for a polyconvex energy function

In order to derive sufficient conditions to satisfy (i), (ii) and (iii), note first that expression (27) can be re-written as

$$\begin{aligned} \mathcal{E}(\boldsymbol{\mathcal{X}}_\eta) &= \mathcal{E}_0(\boldsymbol{\mathcal{X}}) + c_v \Theta_0(\boldsymbol{\mathcal{X}}) \left[e^{\frac{\eta}{c_v}} - 1 \right] \\ &= \mathcal{E}_0(\boldsymbol{\mathcal{X}}) + c_v (\theta_R - \Theta_0(\boldsymbol{\mathcal{X}})) + c_v (\Theta_0(\boldsymbol{\mathcal{X}}) e^{\eta/c_v} - \theta_R) \\ &= \tilde{\mathcal{E}}_R(\boldsymbol{\mathcal{X}}) + c_v (\Theta_0(\boldsymbol{\mathcal{X}}) e^{\eta/c_v} - \theta_R) \\ &= \tilde{\mathcal{E}}_R(\boldsymbol{\mathcal{X}}) + c_v \theta_R \left(e^{\frac{\eta - \tilde{\eta}_R(\boldsymbol{\mathcal{X}})}{c_v}} - 1 \right), \end{aligned} \quad (31)$$

where the following relationship (obtained from directly integrating (20) with respect to the temperature field between θ_R and $\Theta_0(\boldsymbol{\mathcal{X}})$) has been used

$$\tilde{\mathcal{E}}_R(\boldsymbol{\mathcal{X}}) = \mathcal{E}_0(\boldsymbol{\mathcal{X}}) + c_v (\theta_R - \Theta_0(\boldsymbol{\mathcal{X}})). \quad (32)$$

Proposition 1. *Convexity conditions (i), (ii) and (iii) are satisfied for any value of $\boldsymbol{\mathcal{X}}_\eta$ if both $\tilde{\mathcal{E}}_R(\boldsymbol{\mathcal{X}})$ and $-\tilde{\eta}_R(\boldsymbol{\mathcal{X}})$ are convex in $\boldsymbol{\mathcal{X}}$, that is, they are both polyconvex functionals.*

Proof. Condition (iii) is an obvious consequence of equation (28). In order to prove that conditions (i) and (ii) are also satisfied, it is first necessary to show that the exponential of a polyconvex function is also a polyconvex function, that is, if $\phi(\boldsymbol{\alpha})$ is a polyconvex function in $\boldsymbol{\alpha}$, then $\varphi(\boldsymbol{\alpha}) = e^{\phi(\boldsymbol{\alpha})}$ is also polyconvex in $\boldsymbol{\alpha}$. This is achieved by noting that the Hessian of φ ($[\mathbb{H}]_\varphi = \frac{\partial^2 \varphi}{\partial \boldsymbol{\alpha} \partial \boldsymbol{\alpha}}$) and the Hessian of ϕ ($[\mathbb{H}]_\phi = \frac{\partial^2 \phi}{\partial \boldsymbol{\alpha} \partial \boldsymbol{\alpha}}$) are related via the chain rule, to give

$$[\mathbb{H}]_\varphi = \left[[\mathbb{H}]_\phi + \frac{\partial \phi}{\partial \boldsymbol{\alpha}} \otimes \frac{\partial \phi}{\partial \boldsymbol{\alpha}} \right] e^{\phi(\boldsymbol{\alpha})}. \quad (33)$$

Hence,

$$\delta\boldsymbol{\alpha} \cdot [\mathbb{H}_\phi] \delta\boldsymbol{\alpha} = \left[\delta\boldsymbol{\alpha} \cdot [\mathbb{H}_\phi] \delta\boldsymbol{\alpha} + \left(\delta\boldsymbol{\alpha} \cdot \frac{\partial\phi}{\partial\boldsymbol{\alpha}} \right)^2 \right] e^{\phi(\boldsymbol{\alpha})} \geq 0; \quad \forall \delta\boldsymbol{\alpha}, \quad (34)$$

provided $[\mathbb{H}_\phi]$ is positive semi-definite.

This implies that if $-\tilde{\eta}_R(\boldsymbol{\mathcal{X}})$ is convex in $\boldsymbol{\mathcal{X}}$, then $\Theta_0(\boldsymbol{\mathcal{X}}) = \theta_R e^{-\frac{\tilde{\eta}_R(\boldsymbol{\mathcal{X}})}{c_v}}$ is also convex in $\boldsymbol{\mathcal{X}}$. Consequently, if both $\tilde{\mathcal{E}}_R(\boldsymbol{\mathcal{X}})$ and $-\tilde{\eta}_R(\boldsymbol{\mathcal{X}})$ are polyconvex, then equation (32) implies that condition (ii) is also satisfied. Finally, if $-\tilde{\eta}_R(\boldsymbol{\mathcal{X}})$ is polyconvex, then $(\eta - \tilde{\eta}_R(\boldsymbol{\mathcal{X}}))/c_v$ is convex in $\boldsymbol{\mathcal{X}}_\eta$ and therefore equation (31) implies that condition (i) is also satisfied, which concludes the proof of the above proposition. \square

3.5.2. Distortional-volumetric energy decomposition

A more general formulation valid for a wide range of materials, including most metals, relies on the assumption that the shear or distortional behaviour of the material can be split from the volumetric response [71] and, more crucially, that the thermo-mechanical coupling is only associated with the volumetric component of the deformation, that is $\tilde{\eta}_R(\boldsymbol{\mathcal{X}}) \approx \tilde{\eta}_R(J)$. This assumption closely matches the intuitive expectation that changes of temperature only lead to changes in volume and not the shape distortion of the material. Mathematically, these assumptions are expressed by means of an additive decomposition of the internal energy $\mathcal{E}(\boldsymbol{\mathcal{X}}_\eta)$ into thermally coupled volumetric $U(J, \eta)$ and non-thermally coupled distortional $\mathcal{E}'(\boldsymbol{\mathcal{X}})$ components. Comparing this with expression (31), and considering a similar deviatoric-volumetric energy split for $\tilde{\mathcal{E}}_R(\boldsymbol{\mathcal{X}}) = \tilde{\mathcal{E}}'_R(\boldsymbol{\mathcal{X}}) + \tilde{U}_R(J)$ in (31), gives

$$\mathcal{E}(\boldsymbol{\mathcal{X}}_\eta) = \tilde{\mathcal{E}}'_R(\boldsymbol{\mathcal{X}}) + U(J, \eta); \quad U(J, \eta) = \tilde{U}_R(J) + c_v \theta_R \left(e^{\frac{\eta - \tilde{\eta}_R(J)}{c_v}} - 1 \right); \quad \tilde{U}_R(J) = U(J, \tilde{\eta}_R(J)). \quad (35)$$

The evaluation of the first Piola-Kirchhoff stress now emerges as a deviatoric-pressure decomposition given by

$$\mathbf{P}(\boldsymbol{\mathcal{X}}_\eta) = \mathbf{P}'(\boldsymbol{\mathcal{X}}) + p(J, \eta) \mathbf{H}; \quad p = \frac{\partial U(J, \eta)}{\partial J}, \quad (36)$$

with the deviatoric first Piola-Kirchhoff stress $\mathbf{P}'(\boldsymbol{\mathcal{X}})$ being defined as

$$\mathbf{P}'(\boldsymbol{\mathcal{X}}) = \boldsymbol{\Sigma}_F + \boldsymbol{\Sigma}_H \times \mathbf{F} + \boldsymbol{\Sigma}'_J \mathbf{H}; \quad \boldsymbol{\Sigma}_F = \frac{\partial \tilde{\mathcal{E}}'_R(\boldsymbol{\mathcal{X}})}{\partial \mathbf{F}}; \quad \boldsymbol{\Sigma}_H = \frac{\partial \tilde{\mathcal{E}}'_R(\boldsymbol{\mathcal{X}})}{\partial \mathbf{H}}; \quad \boldsymbol{\Sigma}'_J = \frac{\partial \tilde{\mathcal{E}}'_R(\boldsymbol{\mathcal{X}})}{\partial J}. \quad (37)$$

Using the volumetric energy representation in (35), the pressure $p(J, \eta)$ can be written as

$$\begin{aligned} p(J, \eta) &= \frac{d\tilde{U}_R(J)}{dJ} + \theta_R \left(e^{\frac{\eta - \tilde{\eta}_R(J)}{c_v}} \right) \left(-\frac{d\tilde{\eta}_R(J)}{dJ} \right) \\ &= \tilde{p}_R(J) - \theta_R \frac{d\tilde{\eta}_R(J)}{dJ} e^{\frac{\eta - \tilde{\eta}_R(J)}{c_v}}; \quad \tilde{p}_R(J) = \frac{d\tilde{U}_R(J)}{dJ}. \end{aligned} \quad (38)$$

In the above expression, $\tilde{p}_R(J) = p(J, \tilde{\eta}_R(J))$ describes the way in which the pressure in the solid changes as a consequence of changes in volume at constant temperature.

Furthermore, the symmetric positive semi-definite Hessian operator $[\mathbb{H}_\mathcal{E}]$ of the strain energy functional \mathcal{E} is introduced by computing the second derivative of \mathcal{E} (35) with respect to the set

\mathcal{X}_η , to give

$$[\mathbb{H}_\mathcal{E}] = \begin{bmatrix} \mathcal{E}_{\mathbf{F}\mathbf{F}} & \mathcal{E}_{\mathbf{F}\mathbf{H}} & \mathcal{E}_{\mathbf{F}J} & \mathcal{E}_{\mathbf{F}\eta} \\ \mathcal{E}_{\mathbf{H}\mathbf{F}} & \mathcal{E}_{\mathbf{H}\mathbf{H}} & \mathcal{E}_{\mathbf{H}J} & \mathcal{E}_{\mathbf{H}\eta} \\ \mathcal{E}_{J\mathbf{F}} & \mathcal{E}_{J\mathbf{H}} & \mathcal{E}_{JJ} & \mathcal{E}_{J\eta} \\ \mathcal{E}_{\eta\mathbf{F}} & \mathcal{E}_{\eta\mathbf{H}} & \mathcal{E}_{\eta J} & \mathcal{E}_{\eta\eta} \end{bmatrix} = \begin{bmatrix} \frac{\partial^2 \mathcal{E}}{\partial \mathbf{F} \partial \mathbf{F}} & \frac{\partial^2 \mathcal{E}}{\partial \mathbf{F} \partial \mathbf{H}} & \frac{\partial^2 \mathcal{E}}{\partial \mathbf{F} \partial J} & \frac{\partial^2 \mathcal{E}}{\partial \mathbf{F} \partial \eta} \\ \frac{\partial^2 \mathcal{E}}{\partial \mathbf{H} \partial \mathbf{F}} & \frac{\partial^2 \mathcal{E}}{\partial \mathbf{H} \partial \mathbf{H}} & \frac{\partial^2 \mathcal{E}}{\partial \mathbf{H} \partial J} & \frac{\partial^2 \mathcal{E}}{\partial \mathbf{H} \partial \eta} \\ \frac{\partial^2 \mathcal{E}}{\partial J \partial \mathbf{F}} & \frac{\partial^2 \mathcal{E}}{\partial J \partial \mathbf{H}} & \frac{\partial^2 \mathcal{E}}{\partial J \partial J} & \frac{\partial^2 \mathcal{E}}{\partial J \partial \eta} \\ \frac{\partial^2 \mathcal{E}}{\partial \eta \partial \mathbf{F}} & \frac{\partial^2 \mathcal{E}}{\partial \eta \partial \mathbf{H}} & \frac{\partial^2 \mathcal{E}}{\partial \eta \partial J} & \frac{\partial^2 \mathcal{E}}{\partial \eta \partial \eta} \end{bmatrix}. \quad (39)$$

3.5.3. Universally polyconvex energy functions

One of the most commonly used constitutive models describing the volumetric thermal coupling in solids is given by the Mie-Grüneisen equation of state. In this model, the nonlinear relationship [68, 69] between the pressure and thermal energy is¹²

$$J \frac{dp}{d\mathcal{E}} \Big|_{J=\text{constant}} = -\Gamma_0 J^q, \quad (40)$$

where Γ_0 is a positive material constant and q a coefficient that varies from zero (for a perfect gas) to one (for solid materials). Above expression simply means the way pressure p changes with thermal energy at confined volumes ($J = \text{constant}$) is only a function of J and not the temperature θ (nor η).

Using the above Mie-Grüneisen relation (40), it is now possible to obtain an explicit expression for $\tilde{\eta}_R(J)$. This is achieved by combing equations (9), (27) and (38) to give

$$\frac{dp}{d\mathcal{E}} \Big|_{J=\text{constant}} = \frac{1}{\frac{\partial \mathcal{E}(\mathcal{X}_\eta)}{\partial \eta}} \frac{\partial p(J, \eta)}{\partial \eta} = \frac{1}{\theta} \frac{\partial p(J, \eta)}{\partial \eta} = -\frac{1}{c_v} \frac{d\tilde{\eta}_R(J)}{dJ} = -\Gamma_0 J^{q-1}, \quad (41)$$

from which $\tilde{\eta}_R(J)$ can be integrated to give¹³

$$-\tilde{\eta}_R(J) = c_v \Gamma_0 \frac{1 - J^q}{q}. \quad (42)$$

Crucially, differentiating equation (42) twice with respect to J implies the convexity of $-\tilde{\eta}_R(J)$, that is

$$-\frac{d^2 \tilde{\eta}_R(J)}{dJ^2} = (1 - q)c_v \Gamma_0 J^{q-2} \geq 0 \quad \forall 0 \leq q \leq 1 \quad \text{and} \quad \{c_v, \Gamma_0\} > 0. \quad (43)$$

In order to complete the constitutive model, as given in (35), it is necessary to ensure that $\tilde{\mathcal{E}}_R(\mathcal{X})$ is also polyconvex. In fact, it would be tempting to choose a function $\tilde{\mathcal{E}}_R(\mathcal{X})$ as those in (29) or (30). This, however, would lead to a non-vanishing state of stress at the reference

¹²In linear elasticity, an isotropic material with a linear thermal expansion coefficient $\alpha_{\Delta t}$ (measured per Kelvin), as observed experimentally, will experience a volumetric expansion equal to $3\alpha_{\Delta t}$ per unit of increased temperature. If the volume remains constant, the relation between the pressure variation and the thermal change is given as $\frac{dp}{d\mathcal{E}} \Big|_{J=1} = -\frac{3\alpha_{\Delta t}\kappa}{c_v}$. Comparing this with equation (40) at $J = 1$, the parameter Γ_0 can then be related to the linear thermal expansion as $\Gamma_0 = 3\alpha_{\Delta t}\kappa/c_v$.

¹³For the limiting case of $q = 0$, the thermo-mechanical coupling term (42) becomes

$$-\tilde{\eta}_R(J) = -c_v \Gamma_0 \ln J,$$

which indeed is the expression used for perfect gases [33].

configuration ($\boldsymbol{\mathcal{X}}_I = \{\mathbf{F} = \mathbf{I}, \mathbf{H} = \mathbf{I}, J = 1\}$ and $\eta = 0$), which is contrary to the definition of a stress-free reference configuration. In order to resolve this problem, it is important that $\tilde{\mathcal{E}}_R(\boldsymbol{\mathcal{X}})$ satisfies appropriate initial conditions at $\boldsymbol{\mathcal{X}}_I = \{\mathbf{I}, \mathbf{I}, 1\}$. In particular, the first Piola-Kirchhoff stresses at the reference configuration $\{\boldsymbol{\mathcal{X}}_I, \eta = 0\}$ should vanish and, therefore, differentiating equation (32) gives

$$\mathbf{0} = \left[\frac{\partial \mathcal{E}_0}{\partial \mathbf{F}} + \frac{\partial \mathcal{E}_0}{\partial \mathbf{H}} \boldsymbol{\times} \mathbf{F} + \frac{\partial \mathcal{E}_0}{\partial J} \mathbf{H} \right]_{\boldsymbol{\mathcal{X}}_I} = \left[\frac{\partial \tilde{\mathcal{E}}_R}{\partial \mathbf{F}} + \frac{\partial \tilde{\mathcal{E}}_R}{\partial \mathbf{H}} \boldsymbol{\times} \mathbf{I} + \frac{\partial \tilde{\mathcal{E}}_R}{\partial J} \mathbf{I} \right]_{\boldsymbol{\mathcal{X}}_I} + \theta_R \left(-\frac{d\tilde{\eta}_R(J)}{dJ} \right) \Big|_{J=1} \mathbf{I}, \quad (44)$$

where equation (25) and the fact that $\tilde{\eta}_R(J = 1) = 0$ have been used. By doing this, equation (44) gives an initial condition for $\tilde{\mathcal{E}}_R(\boldsymbol{\mathcal{X}})$ in terms of $\tilde{\eta}_R(J)$ as

$$\left[\frac{\partial \tilde{\mathcal{E}}_R}{\partial \mathbf{F}} + \frac{\partial \tilde{\mathcal{E}}_R}{\partial \mathbf{H}} \boldsymbol{\times} \mathbf{I} + \frac{\partial \tilde{\mathcal{E}}_R}{\partial J} \mathbf{I} \right]_{\boldsymbol{\mathcal{X}}_I} = \theta_R \frac{d\tilde{\eta}_R}{dJ} \Big|_{J=1} \mathbf{I}. \quad (45)$$

It is worth noticing that the same expression (45) could have been derived from the isothermal potential $\psi_R(\boldsymbol{\mathcal{X}})$ by using equation (28) together with the isothermal stress free condition. Using the deviatoric-volumetric energy decomposition for a Mie-Grüneisen model, that is $\tilde{\mathcal{E}}_R(\boldsymbol{\mathcal{X}}) = \tilde{\mathcal{E}}'_R(\boldsymbol{\mathcal{X}}) + \tilde{U}_R(J)$, expression (45) implies

$$\mathbf{0} = \left[\frac{\partial \tilde{\mathcal{E}}'_R}{\partial \mathbf{F}} + \frac{\partial \tilde{\mathcal{E}}'_R}{\partial \mathbf{H}} \boldsymbol{\times} \mathbf{I} + \frac{\partial \tilde{\mathcal{E}}'_R}{\partial J} \mathbf{I} \right]_{\boldsymbol{\mathcal{X}}_I}; \quad \frac{d\tilde{U}_R}{dJ} \Big|_{J=1} = \theta_R \frac{d\tilde{\eta}_R}{dJ} \Big|_{J=1} = c_v \Gamma_0 \theta_R. \quad (46)$$

Inspired by expression (29) or (30), one simple polyconvex energy function that satisfies the above conditions (46) is

$$\tilde{\mathcal{E}}'_R(\boldsymbol{\mathcal{X}}) = \varsigma (J^{-2/3} II_{\mathbf{F}} - 3) + \xi (J^{-2} II_{\mathbf{H}}^{3/2} - 3\sqrt{3}); \quad \tilde{U}_R(J) = \frac{\kappa}{2} (J-1)^2 + c_v \Gamma_0 \theta_R (J-1), \quad (47)$$

which gives a universally polyconvex strain energy function for Mie-Grüneisen model as

$$\mathcal{E}(\boldsymbol{\mathcal{X}}_\eta) = \tilde{\mathcal{E}}'_R(\boldsymbol{\mathcal{X}}) + \tilde{U}_R(J) + c_v \theta_R (e^{(\eta - \tilde{\eta}_R(J))/c_v} - 1) \quad (48)$$

where $2\varsigma + 3\sqrt{3}\xi = \mu$. The above function is convex for any value of $\boldsymbol{\mathcal{X}}_\eta$ provided that $\{\mu, \kappa, \Gamma_0, c_v\} \geq 0$ and $0 \leq q \leq 1$. Given the fact that only volumetric thermal coupling is considered in this model, the shear modulus μ used in the deviatoric component $\tilde{\mathcal{E}}'_R(\boldsymbol{\mathcal{X}})$ of (47) is related with μ_0 and μ_R , given in expressions (29) and (30) respectively, as $\mu = \mu_0 = \mu_R$.

Remark 1: The equivalent Helmholtz free energy potential of (48) can also be derived. The relationship between the internal energy and the Helmholtz free energy function described as $\psi(\boldsymbol{\mathcal{X}}_\theta) = \tilde{\mathcal{E}}(\boldsymbol{\mathcal{X}}_\theta) - \theta \tilde{\eta}(\boldsymbol{\mathcal{X}}_\theta)$, combined with the respective volumetric-distortional decomposition of ψ and \mathcal{E} , implies that

$$\psi'_R(\boldsymbol{\mathcal{X}}) = \tilde{\mathcal{E}}'_R(\boldsymbol{\mathcal{X}}); \quad \psi_{\text{vol}}(J, \theta) = U(J, \tilde{\eta}(J, \theta)) - \theta \tilde{\eta}(J, \theta). \quad (49)$$

Notice that there is no difference between the distortional internal energy or distortional Helmholtz free energy since the thermal effects are confined to the volumetric components. By defining the volumetric component of Helmholtz free energy at reference temperature

$$\psi_{R,\text{vol}}(J) = U(J, \tilde{\eta}_R(J)) - \theta_R \tilde{\eta}_R(J) = \tilde{U}_R(J) - \theta_R \tilde{\eta}_R(J), \quad (50)$$

and combining the relationship between entropy and temperature (25) gives

$$\psi(\boldsymbol{\mathcal{X}}_\theta) = \psi_R(\boldsymbol{\mathcal{X}}) - \vartheta \tilde{\eta}_R(J) + T(\theta); \quad T(\theta) = c_v \left(\vartheta - \theta \ln \frac{\theta}{\theta_R} \right), \quad (51)$$

where $\vartheta = \theta - \theta_R$ is the temperature increment. In (51), the first term, that is $\psi_R(\boldsymbol{\mathcal{X}}) = \psi'_R(\boldsymbol{\mathcal{X}}) + \psi_{R,\text{vol}}(J)$, represents the material behaviour at the reference temperature, the second term accounts for the thermo-mechanical coupling and the third term $T(\theta)$ is purely thermal and embodies the temperature-entropy relationships described in the previous section.

Finally, it is interesting to find the relationship between κ as in equation (47) and the traditional κ_0 and κ_R as

$$\kappa_0 = \left. \frac{d^2 U_0(J)}{dJ^2} \right|_{J=1}; \quad \kappa_R = \left. \frac{d^2 \psi_{R,\text{vol}}(J)}{dJ^2} \right|_{J=1}, \quad (52)$$

that is the initial bulk modulus at constant entropy and constant temperature, respectively. Noting that the volumetric components of equations (32) and (28) implies that

$$U_0(J) = \tilde{U}_R(J) + c_v \theta_R \left(e^{\frac{\Gamma_0(1-J^q)}{q}} - 1 \right); \quad (53a)$$

$$\psi_{R,\text{vol}}(J) = \tilde{U}_R(J) - \theta_R c_v \Gamma_0 \frac{J^q - 1}{q}, \quad (53b)$$

where \tilde{U}_R is already defined in (47). Simple double differentiation of the above expressions gives at $J = 1$ the following bulk moduli relationships

$$\kappa_R = \kappa + c_v \theta_R \Gamma_0 (1 - q); \quad \kappa_0 = \kappa + c_v \theta_R \Gamma_0^2. \quad (54)$$

Notice that for the particular case of $q = 1$, then $\kappa = \kappa_R$.

3.5.4. Stress evaluation and Hessian operator

Recalling equation (36), the first Piola-Kirchhoff stress tensor is evaluated by differentiating the internal energy expression given by equation (48) with respect to the extended set of deformation variables $\boldsymbol{\mathcal{X}}$. After some algebraic manipulation, the conjugate stresses become

$$\boldsymbol{\Sigma}_F = 2\zeta J^{-2/3} \mathbf{F}; \quad \boldsymbol{\Sigma}_H = 3\xi J^{-2} II_H^{1/2} \mathbf{H}; \quad \Sigma_J = \Sigma'_J + p \quad (55)$$

with

$$\Sigma'_J = -\frac{2\zeta}{3} J^{-5/3} III_F - 2\xi J^{-3} III_H^{3/2}; \quad p = \kappa(J - 1) + c_v \Gamma_0 \theta_R \left(1 - J^{q-1} e^{\frac{\zeta}{c_v}} e^{\Gamma_0 \frac{1-J^q}{q}} \right). \quad (56)$$

Moreover, the Hessian operator $[\mathbb{H}_\mathcal{E}]$ of the universally polyconvex strain energy function given in expression (48) adopts the following expression

$$[\mathbb{H}_\mathcal{E}] = \begin{bmatrix} \mathcal{E}_{FF} & \mathbf{0} & \mathcal{E}_{FJ} & \mathbf{0} \\ \mathbf{0} & \mathcal{E}_{HH} & \mathcal{E}_{HJ} & \mathbf{0} \\ \mathcal{E}_{JF} & \mathcal{E}_{JH} & \mathcal{E}_{JJ} & \mathcal{E}_{J\eta} \\ \mathbf{0} & \mathbf{0} & \mathcal{E}_{\eta J} & \mathcal{E}_{\eta\eta} \end{bmatrix}, \quad (57)$$

with components

$$\begin{aligned}
\mathcal{E}_{\mathbf{F}\mathbf{F}} &= \frac{\partial^2 \tilde{\mathcal{E}}'_R}{\partial \mathbf{F} \partial \mathbf{F}} = 2\varsigma J^{-2/3} \mathcal{I}; & \mathcal{E}_{\mathbf{H}\mathbf{H}} &= \frac{\partial^2 \tilde{\mathcal{E}}'_R}{\partial \mathbf{H} \partial \mathbf{H}} = 3\xi J^{-2} I I_{\mathbf{H}}^{1/2} [I I_{\mathbf{H}}^{-1} \mathbf{H} \otimes \mathbf{H} + \mathcal{I}], \\
\mathcal{E}_{\mathbf{F}J} &= \mathcal{E}_{J\mathbf{F}} = \frac{\partial^2 \tilde{\mathcal{E}}'_R}{\partial \mathbf{F} \partial J} = -\frac{4\varsigma}{3} J^{-5/3} \mathbf{F}; & \mathcal{E}_{\mathbf{H}J} &= \mathcal{E}_{J\mathbf{H}} = \frac{\partial^2 \tilde{\mathcal{E}}'_R}{\partial \mathbf{H} \partial J} = -6\xi J^{-3} I I_{\mathbf{H}}^{1/2} \mathbf{H}, \\
\mathcal{E}_{\eta\eta} &= \frac{\partial^2 U}{\partial \eta \partial \eta} = \frac{\theta}{c_v}; & \mathcal{E}_{J\eta} &= \mathcal{E}_{\eta J} = \frac{\partial^2 U}{\partial J \partial \eta} = -\Gamma_0 J^{q-1} \theta, \\
\mathcal{E}_{JJ} &= \frac{\partial^2 \mathcal{E}}{\partial J \partial J} = \gamma + \kappa + \kappa_\eta,
\end{aligned} \tag{58}$$

where $\gamma = \frac{10\varsigma}{9} J^{-8/3} I I_{\mathbf{F}} + 6\xi J^{-4} I I_{\mathbf{H}}^{3/2}$ and $\kappa_\eta = \theta c_v \Gamma_0 J^{q-2} [\Gamma_0 J^q + (1-q)]$. Here, \mathcal{I} represents the fourth order identity tensor defined in indicial notation as $[\mathcal{I}]_{iIjJ} = \delta_{ij} \delta_{IJ}$. It is easy to prove that the above Hessian matrix (57) is positive definite for parameters $\{\mu, \kappa, c_v, \Gamma_0\} > 0$ and $0 \leq q \leq 1$ (refer to Part II [2] of this series where the non-thermal component of this Hessian matrix is studied).

3.6. Combined equations

At this juncture, it is important to emphasise that the (conductive) nature of the heat flux vector \mathbf{Q} (16) is very different to the (convective) nature of the fluxes featuring in the linear momentum balance equation (1a) and the geometric conservation laws for $\{\mathbf{F}, \mathbf{H}, J\}$ described in (1b)-(1d). Convective fluxes $\mathcal{F}_I^c(\mathbf{u})$ are functions of the conservation variables, whereas conductive fluxes $\mathcal{F}_I^v(\mathbf{u}, \nabla_0 \mathbf{u})$ depend also on the gradients of these variables. Combining all the balance laws described in expressions (1a)-(1d) and (14), a full set of first order conservation laws can be established for thermo-elasticity as

$$\frac{\partial \mathbf{u}}{\partial t} + \sum_{I=1}^3 \frac{\partial \mathcal{F}_I^c(\mathbf{u})}{\partial X_I} + \sum_{I=1}^3 \frac{\partial \mathcal{F}_I^v(\mathbf{u}, \nabla_0 \mathbf{u})}{\partial X_I} = \mathcal{S}, \tag{59}$$

with vector of variables \mathbf{u} , convective flux vector $\mathcal{F}_I^c(\mathbf{u})$, conductive flux vector $\mathcal{F}_I^v(\mathbf{u}, \nabla_0 \mathbf{u})$ are

$$\mathbf{u} = \begin{bmatrix} p \\ \mathbf{F} \\ \mathbf{H} \\ J \\ \eta \end{bmatrix}; \quad \mathcal{F}_I^c = - \begin{bmatrix} P \mathbf{E}_I \\ \frac{1}{\rho_R} \mathbf{p} \otimes \mathbf{E}_I \\ \mathbf{F} \times \left(\frac{1}{\rho_R} \mathbf{p} \otimes \mathbf{E}_I \right) \\ \mathbf{H} : \left(\frac{1}{\rho_R} \mathbf{p} \otimes \mathbf{E}_I \right) \\ 0 \end{bmatrix}; \quad \mathcal{F}_I^v = \begin{bmatrix} \mathbf{0} \\ \mathbf{0} \\ \mathbf{0} \\ 0 \\ \frac{1}{\Theta} \mathbf{Q} \cdot \mathbf{E}_I \end{bmatrix}, \tag{60}$$

and source terms \mathcal{S} given by

$$\mathcal{S} = \begin{bmatrix} \mathbf{f}_R \\ \mathbf{0} \\ \mathbf{0} \\ 0 \\ \frac{r_R}{\Theta} - \frac{1}{\Theta^2} \mathbf{Q} \cdot (\nabla_0 \Theta) \end{bmatrix}, \tag{61}$$

where the Cartesian coordinate basis are

$$\mathbf{E}_1 = \begin{bmatrix} 1 \\ 0 \\ 0 \end{bmatrix}; \quad \mathbf{E}_2 = \begin{bmatrix} 0 \\ 1 \\ 0 \end{bmatrix}; \quad \mathbf{E}_3 = \begin{bmatrix} 0 \\ 0 \\ 1 \end{bmatrix}. \tag{62}$$

Since the number of unknowns is greater than the number of equations, appropriate constitutive equations are required to close the above system (59). For instance, in the case of Mie-Grüneisen thermo-elastic model, the first Piola–Kirchhoff stress \mathbf{P} and the relationship between the entropy and temperature are

$$\mathbf{P}(\boldsymbol{\chi}_\eta) = \mathbf{P}'(\boldsymbol{\chi}) + p(J, \eta)\mathbf{H}; \quad \Theta(J, \eta) = \theta_R e^{\eta/c_v} e^{\Gamma_0(1-J^q)/q}, \quad (63)$$

respectively, where the deviatoric stress \mathbf{P}' and pressure p are defined in equations (55) and (56). In addition, the material heat flux vector \mathbf{Q} (16) is related to the deformation and thermal gradient $\nabla_0\Theta$ and is repeated here for convenience

$$\mathbf{Q} = -\mathbf{K}\nabla_0\Theta; \quad \mathbf{K} = J^{-1}\mathbf{H}^T \mathbf{k}\mathbf{H}. \quad (64)$$

Finally, for the complete definition of the initial boundary value problem, initial and boundary (essential and natural) conditions must be suitably specified.

Remark 2: It is also interesting to view the resulting convective flux \mathcal{F}_I^c , as given in (60), to be additively decomposed into a convective flux $\mathcal{F}_I^{c,\mathbf{F}}$ associated with \mathbf{F} , a convective flux $\mathcal{F}_I^{c,\mathbf{H}}$ associated with \mathbf{H} and a convective flux $\mathcal{F}_I^{c,J}$ of J , as

$$\mathcal{F}_I^c = \mathcal{F}_I^{c,\mathbf{F}} + \mathcal{F}_I^{c,\mathbf{H}} + \mathcal{F}_I^{c,J}, \quad (65)$$

with their components

$$\mathcal{F}_I^{c,\mathbf{F}} = - \begin{bmatrix} \Sigma_{\mathbf{F}} \mathbf{E}_I \\ \frac{1}{\rho_R} \mathbf{p} \otimes \mathbf{E}_I \\ \mathbf{0} \\ 0 \\ 0 \end{bmatrix}; \quad \mathcal{F}_I^{c,\mathbf{H}} = - \begin{bmatrix} (\Sigma_{\mathbf{H}} \times \mathbf{F}) \mathbf{E}_I \\ \mathbf{0} \\ \mathbf{F} \times \left(\frac{1}{\rho_R} \mathbf{p} \otimes \mathbf{E}_I \right) \\ 0 \\ 0 \end{bmatrix}; \quad \mathcal{F}_I^{c,J} = - \begin{bmatrix} (\Sigma_J \mathbf{H}) \mathbf{E}_I \\ \mathbf{0} \\ \mathbf{0} \\ \mathbf{H} : \left(\frac{1}{\rho_R} \mathbf{p} \otimes \mathbf{E}_I \right) \\ 0 \end{bmatrix}. \quad (66)$$

For the Petrov-Galerkin type of discretisation envisaged in this paper, and taking advantage of the above flux vector splitting type of approach, we can then introduce suitable Petrov-Galerkin weights specifically designed for the hyperbolic system (59) under consideration.

4. Hyperbolicity

As shown in this series [1, 2], the study of the eigenvalue structure of the system (59) is crucial in order to guarantee its hyperbolicity. In Reference [33], the authors verified the hyperbolic nature of the problem for a (non-polyconvex) Mie-Grüneisen thermo-elastic model, hence not universally guaranteeing the existence of real wave speeds at any state of thermo-elastic deformation $\boldsymbol{\chi}_\eta$. In addition, the procedure presented therein required the formation of the flux Jacobian matrix (namely, the derivative of the fluxes $\mathcal{F}(\mathbf{U})$ with respect to conservation variables \mathbf{U}), which sometimes can be quite cumbersome.

With the use of the polyconvex Mie-Grüneisen model (48), and taking advantage of the tensor cross product operation [49, 50] recently re-introduced in [1, 2] in computational solid mechanics, we examine the hyperbolicity of the system (59) in a convection dominated scenario, that is, neglecting the contribution of the conductive heat flux \mathbf{Q} . For completeness, the same

procedure is also applied to the case of a modified entropic elasticity model, which is included in Appendix A.

The eigenvalues (or wave speeds) of the system (59) can be determined by identifying possible plane wave solutions (in the absence of source terms) of the type [1]

$$\mathbf{u} = \phi(\mathbf{X} \cdot \mathbf{N} - c_\alpha t) \mathbf{u}_\alpha = \phi(\mathbf{X} \cdot \mathbf{N} - c_\alpha t) \begin{bmatrix} \mathbf{p}_\alpha \\ \mathbf{F}_\alpha \\ \mathbf{H}_\alpha \\ J_\alpha \\ \eta_\alpha \end{bmatrix}, \quad (67)$$

where ϕ denotes a scalar real valued function, c_α is the wave speed corresponding to the eigenmode \mathbf{u}_α and \mathbf{N} is the direction of propagation. Substitution of the above equation into expression (59) leads to a characteristic equation of the system given by

$$\mathcal{A}_N \mathbf{u}_\alpha = c_\alpha \mathbf{u}_\alpha; \quad \mathcal{A}_N = \frac{\partial \mathcal{F}_N}{\partial \mathbf{u}}; \quad \mathcal{F}_N = \sum_{I=1}^3 \mathcal{F}_I N_I. \quad (68)$$

However, above eigenvalue problem (68) unfortunately requires the explicit expression for the (convective) flux Jacobian matrix \mathcal{A}_N . To avoid this, it is important to note that above equation can be re-written by utilising the concept of directional derivative [71] to give

$$D\mathcal{F}_N[\mathbf{u}_\alpha] = c_\alpha \mathbf{u}_\alpha. \quad (69)$$

Considering each individual component of this system (60)

$$- \begin{bmatrix} D(\mathbf{PN})[\mathbf{F}_\alpha, \mathbf{H}_\alpha, J_\alpha, \eta_\alpha] \\ D(\mathbf{v} \otimes \mathbf{N})[\mathbf{v}_\alpha] \\ D(\mathbf{F} \times (\mathbf{v} \otimes \mathbf{N}))[\mathbf{v}_\alpha, \mathbf{F}_\alpha] \\ D(\mathbf{H} : (\mathbf{v} \otimes \mathbf{N}))[\mathbf{v}_\alpha, \mathbf{H}_\alpha] \\ 0 \end{bmatrix} = c_\alpha \begin{bmatrix} \rho_R \mathbf{v}_\alpha \\ \mathbf{F}_\alpha \\ \mathbf{H}_\alpha \\ J_\alpha \\ \eta_\alpha \end{bmatrix}. \quad (70)$$

For the case where $c_\alpha \neq 0$, the geometric equations $\{\mathbf{F}_\alpha, \mathbf{H}_\alpha, J_\alpha\}$, as well as the entropy equation η_α , of the system, result in

$$\mathbf{F}_\alpha = -\frac{1}{c_\alpha} \mathbf{v}_\alpha \otimes \mathbf{N}; \quad (71a)$$

$$\mathbf{H}_\alpha = -\frac{1}{c_\alpha} [\mathbf{F}_\alpha \times (\mathbf{v} \otimes \mathbf{N}) + \mathbf{F} \times (\mathbf{v}_\alpha \otimes \mathbf{N})]; \quad (71b)$$

$$J_\alpha = -\frac{1}{c_\alpha} [\mathbf{H}_\alpha : (\mathbf{v} \otimes \mathbf{N}) + \mathbf{H} : (\mathbf{v}_\alpha \otimes \mathbf{N})]; \quad (71c)$$

$$\eta_\alpha = 0. \quad (71d)$$

Substitution of (71a) into (71b) yields

$$\mathbf{H}_\alpha = -\frac{1}{c_\alpha} \left[\underbrace{(\mathbf{v}_\alpha \otimes \mathbf{N}) \times (\mathbf{v} \otimes \mathbf{N})}_0 + \mathbf{F} \times (\mathbf{v}_\alpha \otimes \mathbf{N}) \right] = -\frac{1}{c_\alpha} \mathbf{F} \times (\mathbf{v}_\alpha \otimes \mathbf{N}). \quad (72)$$

It is possible to demonstrate after some algebra that the first term on the right hand side of (71c) is zero, yielding the reduced equation

$$J_\alpha = -\frac{1}{c_\alpha} \mathbf{H} : (\mathbf{v}_\alpha \otimes \mathbf{N}). \quad (73)$$

Substitution of (71a), (72) and (73) into (70a) results in

$$\rho_R c_\alpha^2 \mathbf{v}_\alpha = D(\mathbf{P}\mathbf{N})[\mathbf{v}_\alpha \otimes \mathbf{N}, \mathbf{F} \times (\mathbf{v}_\alpha \otimes \mathbf{N}), \mathbf{H} : (\mathbf{v}_\alpha \otimes \mathbf{N}), 0] \quad (74)$$

For convenience, above expression can also be pre-multiplied by a generic virtual velocity field $\delta \mathbf{v}$ to give¹⁴

$$\begin{aligned} \rho_R c_\alpha^2 \delta \mathbf{v} \cdot \mathbf{v}_\alpha &= (\delta \mathbf{v} \otimes \mathbf{N}) : D\mathbf{P}[\mathbf{v}_\alpha \otimes \mathbf{N}, \mathbf{F} \times (\mathbf{v}_\alpha \otimes \mathbf{N}), \mathbf{H} : (\mathbf{v}_\alpha \otimes \mathbf{N}), 0] \\ &= (\delta \mathbf{v} \otimes \mathbf{N}) : D(\Sigma_{\mathbf{F}} + \Sigma_{\mathbf{H}} \times \mathbf{F} + \Sigma_J \mathbf{H})[\mathbf{v}_\alpha \otimes \mathbf{N}, \mathbf{F} \times (\mathbf{v}_\alpha \otimes \mathbf{N}), \mathbf{H} : (\mathbf{v}_\alpha \otimes \mathbf{N}), 0] \\ &= \underbrace{\begin{bmatrix} (\delta \mathbf{v} \otimes \mathbf{N}) : \\ \mathbf{F} \times (\delta \mathbf{v} \otimes \mathbf{N}) : \\ \mathbf{H} : (\delta \mathbf{v} \otimes \mathbf{N}) \\ 0 \end{bmatrix}^T}_{\text{Constitutive term}} [\mathbb{H}_{\mathcal{E}}] \underbrace{\begin{bmatrix} : (\mathbf{v}_\alpha \otimes \mathbf{N}) \\ : \mathbf{F} \times (\mathbf{v}_\alpha \otimes \mathbf{N}) \\ \mathbf{H} : (\mathbf{v}_\alpha \otimes \mathbf{N}) \\ 0 \end{bmatrix}}_{\text{Geometric term}} \\ &+ \underbrace{(\Sigma_{\mathbf{H}} + \Sigma_J \mathbf{F}) : [(\delta \mathbf{v} \otimes \mathbf{N}) \times (\mathbf{v}_\alpha \otimes \mathbf{N})]}_{\text{Geometric term}}. \end{aligned} \quad (75)$$

Taking $\delta \mathbf{v} = \mathbf{v}_\alpha$, the geometric term in above equation (75) goes to zero and this leads to the satisfaction of well known Legendre-Hadamard condition, namely

$$\rho_R c_\alpha^2 = \begin{bmatrix} (\mathbf{v}_\alpha \otimes \mathbf{N}) : \\ \mathbf{F} \times (\mathbf{v}_\alpha \otimes \mathbf{N}) : \\ \mathbf{H} : (\mathbf{v}_\alpha \otimes \mathbf{N}) \\ 0 \end{bmatrix}^T [\mathbb{H}_{\mathcal{E}}] \begin{bmatrix} : (\mathbf{v}_\alpha \otimes \mathbf{N}) \\ : \mathbf{F} \times (\mathbf{v}_\alpha \otimes \mathbf{N}) \\ \mathbf{H} : (\mathbf{v}_\alpha \otimes \mathbf{N}) \\ 0 \end{bmatrix} \geq 0, \quad (76)$$

if and only if $[\mathbb{H}_{\mathcal{E}}]$ is a positive semi-definite matrix. This is indeed the case in this paper since the Hessian operator (57) is evaluated based on a polyconvex internal energy function.

Remark 3: In general, it is also possible [72, 73] to re-write equation (75c) in an alternative manner by relating the Hessian components with a fourth order elasticity tensor \mathbf{C} , described as follows

$$\rho_R c_\alpha^2 \delta \mathbf{v} \cdot \mathbf{v}_\alpha = (\delta \mathbf{v} \otimes \mathbf{N}) : \mathbf{C} : (\mathbf{v}_\alpha \otimes \mathbf{N}) = \delta \mathbf{v} \cdot (\mathbf{C}_{\mathbf{N}\mathbf{N}} \mathbf{v}_\alpha), \quad (77)$$

with the acoustic tensor $\mathbf{C}_{\mathbf{N}\mathbf{N}}$ being defined as

$$[\mathbf{C}_{\mathbf{N}\mathbf{N}}]_{ij} = [\mathbf{C}]_{iIjJ} N_I N_J. \quad (78)$$

Comparison of (75) and (77) enables the fourth order elasticity tensor \mathbf{C} to be obtained as a summation of a material contribution \mathbf{C}_m (depending upon second derivatives of \mathcal{E}) and a

¹⁴It is interesting to see how the use of the tensor cross product allows for simple expressions of the resulting tangent operator which neatly separates material from geometrical dependencies.

geometrical contribution \mathbf{C}_g , namely $\mathbf{C} = \mathbf{C}_m + \mathbf{C}_g$, with components

$$\begin{aligned} \mathbf{C}_m = & \mathcal{E}_{\mathbf{F}\mathbf{F}} + \mathbf{F} \times \mathcal{E}_{\mathbf{H}\mathbf{H}} \times \mathbf{F} + \mathcal{E}_{\mathbf{J}\mathbf{J}} \mathbf{H} \otimes \mathbf{H} + \mathcal{E}_{\mathbf{F}\mathbf{H}} \times \mathbf{F} + \mathbf{F} \times \mathcal{E}_{\mathbf{H}\mathbf{F}} + \mathcal{E}_{\mathbf{F}\mathbf{J}} \otimes \mathbf{H} \\ & + \mathbf{H} \otimes \mathcal{E}_{\mathbf{J}\mathbf{F}} + \mathbf{F} \times \mathcal{E}_{\mathbf{H}\mathbf{J}} \otimes \mathbf{H} + \mathbf{H} \otimes \mathcal{E}_{\mathbf{J}\mathbf{H}} \times \mathbf{F}, \end{aligned} \quad (79a)$$

$$\mathbf{C}_g = \mathcal{I} \times (\Sigma_{\mathbf{H}} + \Sigma_{\mathbf{J}} \mathbf{F}). \quad (79b)$$

Here, $[\mathcal{I}]_{ijj} = \delta_{ij} \delta_{IJ}$ and notice also that the contribution of the geometrical component \mathbf{C}_g in (77) vanishes when $\delta \mathbf{v} = \mathbf{v}_\alpha$, that is $(\mathbf{v}_\alpha \otimes \mathbf{N}) : \mathbf{C}_g : (\mathbf{v}_\alpha \otimes \mathbf{N}) = 0$.

Utilising the Hessian operator described in (57), the thermo-mechanical acoustic tensor for Mie-Grüneisen model \mathbf{C}_{NN} (78) becomes

$$\mathbf{C}_{NN} = \mathbf{C}_{NN}^{\mathcal{X}} + \kappa_\eta \Lambda_H^2 \mathbf{n} \otimes \mathbf{n}. \quad (80)$$

In this equation, the first term $\mathbf{C}_{NN}^{\mathcal{X}}$, already presented in Part II [2], refers to a non-thermal acoustic tensor and the second term represents an additional contribution characterised by thermal effects. For convenience, the non-thermal acoustic tensor is repeated here (refer to equation (40) in [2]) as

$$\mathbf{C}_{NN}^{\mathcal{X}} = \alpha \mathbf{I} + \beta \Lambda_T^2 \mathbf{I} - \beta \Lambda_T + [\zeta \Lambda_F \Lambda_H + \beta \Lambda_M (\Lambda_M I I_{\mathbf{H}}^{-1} - 4J^{-1} \Lambda_H) + (\gamma + \kappa) \Lambda_H^2] \mathbf{n} \otimes \mathbf{n}, \quad (81)$$

and the following notations are used

$$\begin{aligned} \Lambda_H \mathbf{n} &= \mathbf{H} \mathbf{N}; \\ \Lambda_F \mathbf{n} &= \mathbf{F} \mathbf{N}; \\ \Lambda_M \mathbf{n} &= (\mathbf{F} \mathbf{T}_1) \times (\mathbf{H} \mathbf{T}_2) + (\mathbf{H} \mathbf{T}_1) \times (\mathbf{F} \mathbf{T}_2); \\ \Lambda_T &= (\mathbf{F} \mathbf{T}_1) \otimes (\mathbf{F} \mathbf{T}_1) + (\mathbf{F} \mathbf{T}_2) \otimes (\mathbf{F} \mathbf{T}_2); \\ \Lambda_T^2 &= (\mathbf{F} \mathbf{T}_1) \cdot (\mathbf{F} \mathbf{T}_1) + (\mathbf{F} \mathbf{T}_2) \cdot (\mathbf{F} \mathbf{T}_2); \\ \alpha &= 2\zeta_R J^{-2/3}; \\ \beta &= 3\xi_R J^{-2} I I_{\mathbf{H}}^{1/2}; \\ \gamma &= \frac{10}{9} \zeta_R J^{-8/3} I I_{\mathbf{F}} + 6\xi_R J^{-4} I I_{\mathbf{H}}^{3/2}; \\ \zeta &= -\frac{8}{3} \zeta_R J^{-5/3}. \end{aligned} \quad (82)$$

Instead of deriving a close form solution for the wave speed for any possible orientation \mathbf{N} , it is sufficient to obtain bounds of the wave speeds by assuming \mathbf{N} is a principal direction. In this particular case, the first two eigenvalues correspond to pressure waves are obtained by taking $\mathbf{v}_\alpha = \mathbf{n}$, where \mathbf{n} is a unit vector orthogonal to the vectors $\mathbf{F} \mathbf{T}_{1,2} = \mathbf{t}_{1,2}$ which lie on the propagation surface. This is achieved by substituting equation (80) into (77) and taking $\delta \mathbf{v} = \mathbf{v}_\alpha = \mathbf{n}$ to give,

$$\rho_R c_p^2 = \alpha + \beta \Lambda_T^2 + \zeta \Lambda_H \Lambda_F + \beta \Lambda_M [\Lambda_M I I_{\mathbf{H}}^{-1} - 4J^{-1} \Lambda_H] + (\gamma + \kappa + \kappa_\eta) \Lambda_H^2. \quad (83)$$

As a result, the first set of eigenvalues corresponding to pressure wave c_p is

$$c_{1,2} = \pm c_p, \quad (84)$$

where

$$c_p = \sqrt{\frac{\alpha + \beta\Lambda_T^2 + \zeta\Lambda_H\Lambda_F + \beta\Lambda_M [\Lambda_M II_{\mathbf{H}}^{-1} - 4J^{-1}\Lambda_H] + (\gamma + \kappa)\Lambda_H^2}{\rho_R} + \frac{\kappa_\eta\Lambda_H^2}{\rho_R}}. \quad (85)$$

Here, $\kappa_\eta = \theta_{c_v}\Gamma_0 J^{q-2} [\Gamma_0 J^q + (1-q)] > 0$ provided that $\{\theta, c_v, \Gamma_0\} > 0$ and $0 \leq q \leq 1$. Similarly, by taking $\delta\mathbf{v} = \mathbf{v}_\alpha = \mathbf{t}_{1,2}$, the remaining four eigenvalues corresponding to shear wave speeds

$$c_{3,4} = \pm c_{s1}; \quad c_{5,6} = \pm c_{s2}; \quad c_{s1} = \sqrt{\frac{\alpha + \beta(\Lambda_T^2 - \lambda_1^2)}{\rho_R}}; \quad c_{s2} = \sqrt{\frac{\alpha + \beta(\Lambda_T^2 - \lambda_2^2)}{\rho_R}}, \quad (86)$$

where $\lambda_{1,2}^2$ are the eigenvalues of Λ_T . In this model, due to coupling of thermal and mechanical effects only in the volumetric contribution, it is worth emphasising that only pressure waves (85) take into account the combined effect of mechanical deformation and temperature. On the contrary, the shear waves described in (86) however remain unaltered with respect to temperature.

5. Entropy based balance laws for thermo-elasticity

Using the entropy as thermal variable allows the so-called ballistic free energy function B [53] to be chosen as a generalised convex entropy function S [1] of the hyperbolic set of equations (59) defined by

$$S(\mathbf{p}, \mathcal{X}_\eta) = B(\mathbf{p}, \mathcal{X}_\eta) = \underbrace{\frac{1}{2\rho_R}\mathbf{p} \cdot \mathbf{p}}_{\text{Kinetic energy}} + \underbrace{\mathcal{E}(\mathcal{X}_\eta)}_{\text{Internal energy}} \underbrace{-\theta_R\eta}_{\text{Thermal conduction}} = \mathbb{E}(\mathbf{p}, \mathcal{X}_\eta) - \theta_R\eta, \quad (87)$$

where the total energy \mathbb{E} is the summation of kinetic and internal energies such that $\mathbb{E}(\mathbf{p}, \mathcal{X}_\eta) = \frac{1}{2\rho_R}\mathbf{p} \cdot \mathbf{p} + \mathcal{E}(\mathcal{X}_\eta)$. Above generalised convex entropy function S clearly represents the total energy \mathbb{E} and thermal energy contributions per unit of undeformed volume. A conjugate set of entropy variables \mathbf{v} is obtained through the derivatives of S (87) as

$$\mathbf{v} = \frac{\partial S}{\partial \mathcal{U}} = \begin{bmatrix} \frac{\partial S}{\partial \mathbf{p}} \\ \frac{\partial S}{\partial \mathbf{F}} \\ \frac{\partial S}{\partial \mathbf{H}} \\ \frac{\partial S}{\partial J} \\ \frac{\partial S}{\partial \eta} \end{bmatrix} = \begin{bmatrix} \mathbf{v} \\ \Sigma_{\mathbf{F}} \\ \Sigma_{\mathbf{H}} \\ \Sigma_J \\ \vartheta \end{bmatrix}. \quad (88)$$

The Hessian operator $[\mathbb{H}_S]$ associated with the convex entropy function S can now follow by taking derivatives of the conjugate variables described above

$$[\mathbb{H}_S] = \frac{\partial \mathbf{v}}{\partial \mathcal{U}} = \frac{\partial S}{\partial \mathcal{U} \partial \mathcal{U}} = \left[\begin{array}{c|c} \frac{1}{\rho_R} \mathbf{I} & \mathbf{0} \\ \hline \mathbf{0} & [\mathbb{H}_\mathcal{E}] \end{array} \right], \quad (89)$$

where \mathbf{I} symbolises the second order identity tensor and $[\mathbb{H}_\mathcal{E}]$ represents the Hessian operator of the energy function $\mathcal{E}(\mathcal{X}_\eta)$ (39).

Remark 4: It is possible to provide interesting relationships between ballistic free energy B and total energy \mathbb{E} in non-thermal scenarios. For the isentropic case (where $\eta = 0$), it is easy to show that the ballistic free energy B in (87) is simply the total energy per unit of undeformed volume described as

$$B_0(\mathbf{p}, \boldsymbol{\chi}) = \frac{1}{2\rho_R} \mathbf{p} \cdot \mathbf{p} + \mathcal{E}_0(\boldsymbol{\chi}) = \mathbb{E}_0(\mathbf{p}, \boldsymbol{\chi}); \quad B_0 = B(\mathbf{p}, \boldsymbol{\chi}, \eta = 0); \quad \mathbb{E}_0 = \mathbb{E}(\mathbf{p}, \boldsymbol{\chi}, \eta = 0). \quad (90)$$

Notice that B_0 and \mathbb{E}_0 represent the ballistic energy and total energy at isentropic conditions, respectively. On the other hand, in the case of isothermal process (for instance, $\theta = \theta_R$), we demonstrate that the ballistic free energy \tilde{B}_R is the total energy per unit undeformed volume minus the entropy energy component due to changes in deformation, which is equivalent to the kinetic energy plus the Helmholtz's free energy at the reference temperature. This is achieved by first re-expressing $B(\mathbf{p}, \boldsymbol{\chi}_\eta) = \tilde{B}(\mathbf{p}, \boldsymbol{\chi}_\theta)$ and $\mathcal{E}(\boldsymbol{\chi}_\eta) = \tilde{\mathcal{E}}(\boldsymbol{\chi}_\theta)$, combined with the transformation $\psi_R(\boldsymbol{\chi}) = \tilde{\mathcal{E}}_R(\boldsymbol{\chi}) - \theta_R \tilde{\eta}_R(\boldsymbol{\chi})$, to yield

$$\tilde{B}_R(\mathbf{p}, \boldsymbol{\chi}) = \frac{1}{2\rho_R} \mathbf{p} \cdot \mathbf{p} + \tilde{\mathcal{E}}_R(\boldsymbol{\chi}) - \theta_R \tilde{\eta}_R(\boldsymbol{\chi}) = \tilde{\mathbb{E}}_R(\mathbf{p}, \boldsymbol{\chi}) - \theta_R \tilde{\eta}_R(\boldsymbol{\chi}) = \frac{1}{2\rho_R} \mathbf{p} \cdot \mathbf{p} + \psi_R(\boldsymbol{\chi}). \quad (91)$$

Here, $\tilde{\mathbb{E}}_R = \frac{1}{2\rho_R} \mathbf{p} \cdot \mathbf{p} + \tilde{\mathcal{E}}_R(\boldsymbol{\chi}) = \tilde{\mathbb{E}}(\mathbf{p}, \boldsymbol{\chi}, \theta = \theta_R)$ represents the total energy accumulated at reference temperature θ_R .

Remark 5: As shown in [74], another option to address irreversible thermal effects is the introduction of a variable describing the total balance energy E of the system as given in (5). In this case, an alternative set of conservation variables is thus considered, namely $\hat{\mathbf{U}} = [\mathbf{p}, \mathbf{F}, \mathbf{H}, J, E]^T$ [74]. This approach is necessary in the case of non-smooth solutions, which will not be the focus of this publication. For completeness, a suitable generalised convex entropy function and its conjugate entropy variables are derived and summarised in Appendix B.

Pre-multiplication of system (59) with the Hessian $[\mathbb{H}_S]$ leads to the symmetric form of the conservation laws as [74–76]

$$[\mathbb{H}_S]^{-1} \frac{\partial}{\partial t} \begin{bmatrix} \mathbf{v} \\ \Sigma_{\mathbf{F}} \\ \Sigma_{\mathbf{H}} \\ \Sigma_J \\ \vartheta \end{bmatrix} - \begin{bmatrix} \text{DIV} \Sigma_{\mathbf{F}} + \text{CURL} \Sigma_{\mathbf{H}} \times \mathbf{F} + \mathbf{H} (\nabla_0 \Sigma_J) \\ \nabla_0 \mathbf{v} \\ \mathbf{F} \times \nabla_0 \mathbf{v} \\ \mathbf{H} : \nabla_0 \mathbf{v} \\ 0 \end{bmatrix} = \begin{bmatrix} 0 \\ 0 \\ 0 \\ 0 \\ \text{DIV} \left(\frac{1}{\theta} \mathbf{K} \nabla_0 \theta \right) \end{bmatrix} + \begin{bmatrix} \mathbf{f}_R \\ 0 \\ 0 \\ 0 \\ \frac{r_R}{\theta} + \frac{1}{\theta^2} (\mathbf{K} \nabla_0 \theta) \cdot \nabla_0 \theta \end{bmatrix}. \quad (92)$$

Here, $[\mathbf{A} \times \mathbf{B}]_i = \mathcal{E}_{ijk} A_{jL} B_{kL}$ for any second order tensors \mathbf{A} and \mathbf{B} . The above set of symmetric equations for the entropy conjugate variables can also be written in the transformed form

as [2]

$$\frac{\partial \mathbf{v}}{\partial t} - \frac{1}{\rho_R} (\text{DIV} \Sigma_{\mathbf{F}} + \text{CURL} \Sigma_{\mathbf{H}} \times \mathbf{F} + \mathbf{H} \nabla_0 \Sigma_J) = \frac{1}{\rho_R} \mathbf{f}_R; \quad (93a)$$

$$\frac{\partial \Sigma_{\mathbf{F}}}{\partial t} - (\mathcal{E}_{\mathbf{F}\mathbf{F}} + \mathcal{E}_{\mathbf{F}J} \otimes \mathbf{H}) : \nabla_0 \mathbf{v} = \mathbf{0}; \quad (93b)$$

$$\frac{\partial \Sigma_{\mathbf{H}}}{\partial t} - (\mathcal{E}_{\mathbf{H}\mathbf{H}} \times \mathbf{F} + \mathcal{E}_{\mathbf{H}J} \otimes \mathbf{H}) : \nabla_0 \mathbf{v} = \mathbf{0}; \quad (93c)$$

$$\frac{\partial \Sigma_J}{\partial t} - (\mathcal{E}_{J\mathbf{F}} + \mathcal{E}_{J\mathbf{H}} \times \mathbf{F} + \mathcal{E}_{JJ} \mathbf{H}) : \nabla_0 \mathbf{v} = 0; \quad (93d)$$

$$\frac{\partial \vartheta}{\partial t} - \mathcal{E}_{\eta J} \mathbf{H} : \nabla_0 \mathbf{v} = \frac{1}{c_v} (r_R + \text{DIV}(\mathbf{K} \nabla_0 \theta)), \quad (93e)$$

with Hessian components defined in (58).

6. Stabilised variational formulation

In line with previous work in this series [1, 2], a stabilised variational statement for the set of conservation laws (59) is introduced by means of a Petrov-Galerkin approach [76–82] whereby the conjugate weight functions $\delta \mathbf{V}$ are suitably augmented via a (convective) flux splitting type of approach (65) as

$$\delta \mathbf{V}^{st} = \delta \mathbf{V} + \left(\frac{\partial \mathcal{F}_I^c}{\partial \mathbf{U}} \tilde{\boldsymbol{\tau}} \right)^T \frac{\partial \delta \mathbf{V}}{\partial X_I} = \delta \mathbf{V} + \left(\frac{\partial \mathcal{F}_I^{c,\mathbf{F}}}{\partial \mathbf{U}} \tilde{\boldsymbol{\tau}}_{\mathbf{F}} + \frac{\partial \mathcal{F}_I^{c,\mathbf{H}}}{\partial \mathbf{U}} \tilde{\boldsymbol{\tau}}_{\mathbf{H}} + \frac{\partial \mathcal{F}_I^{c,J}}{\partial \mathbf{U}} \tilde{\boldsymbol{\tau}}_J \right)^T \frac{\partial \delta \mathbf{V}}{\partial X_I}. \quad (94)$$

Here, $\{\tilde{\boldsymbol{\tau}}_{\mathbf{F}}, \tilde{\boldsymbol{\tau}}_{\mathbf{H}}, \tilde{\boldsymbol{\tau}}_J\}$ denote matrices of stabilisation parameters tailor-made for the hyperbolic system given in (59) as

$$\tilde{\boldsymbol{\tau}}_{\mathbf{F}} = \begin{bmatrix} \mathbf{0} & \mathbf{0} & \mathbf{0} & \mathbf{0} & \mathbf{0} \\ \mathbf{0} & \tau_{\mathbf{F}} \mathbf{I} & \mathbf{0} & \mathbf{0} & \mathbf{0} \\ \mathbf{0} & \mathbf{0} & \mathbf{0} & \mathbf{0} & \mathbf{0} \\ \mathbf{0} & \mathbf{0} & \mathbf{0} & \mathbf{0} & \mathbf{0} \\ \mathbf{0} & \mathbf{0} & \mathbf{0} & \mathbf{0} & \mathbf{0} \end{bmatrix}; \quad \tilde{\boldsymbol{\tau}}_{\mathbf{H}} = \begin{bmatrix} \mathbf{0} & \mathbf{0} & \mathbf{0} & \mathbf{0} & \mathbf{0} \\ \mathbf{0} & \mathbf{0} & \mathbf{0} & \mathbf{0} & \mathbf{0} \\ \mathbf{0} & \mathbf{0} & \tau_{\mathbf{H}} \mathbf{I} & \mathbf{0} & \mathbf{0} \\ \mathbf{0} & \mathbf{0} & \mathbf{0} & \mathbf{0} & \mathbf{0} \\ \mathbf{0} & \mathbf{0} & \mathbf{0} & \mathbf{0} & \mathbf{0} \end{bmatrix}; \quad \tilde{\boldsymbol{\tau}}_J = \begin{bmatrix} \tau_p \mathbf{I} & \mathbf{0} & \mathbf{0} & \mathbf{0} & \mathbf{0} \\ \mathbf{0} & \mathbf{0} & \mathbf{0} & \mathbf{0} & \mathbf{0} \\ \mathbf{0} & \mathbf{0} & \mathbf{0} & \mathbf{0} & \mathbf{0} \\ \mathbf{0} & \mathbf{0} & \mathbf{0} & \tau_J & \mathbf{0} \\ \mathbf{0} & \mathbf{0} & \mathbf{0} & \mathbf{0} & \tau_\eta \end{bmatrix}. \quad (95)$$

With these at hand, the individual components of (94) can be obtained as

$$\delta \mathbf{v}^{st} = \delta \mathbf{v} - \frac{\tau_p}{\rho_R} (\mathbf{H} \nabla_0 \delta \Sigma_J); \quad (96a)$$

$$\delta \Sigma_{\mathbf{F}}^{st} = \delta \Sigma_{\mathbf{F}} - \tau_{\mathbf{F}} \mathcal{E}_{\mathbf{F}\mathbf{F}} : \nabla_0 \delta \mathbf{v}; \quad (96b)$$

$$\delta \Sigma_{\mathbf{H}}^{st} = \delta \Sigma_{\mathbf{H}} - \tau_{\mathbf{H}} \mathcal{E}_{\mathbf{H}\mathbf{H}} : (\mathbf{F} \times \nabla_0 \delta \mathbf{v}); \quad (96c)$$

$$\delta \Sigma_J^{st} = \delta \Sigma_J - \tau_J \mathcal{E}_{JJ} \mathbf{H} : \nabla_0 \delta \mathbf{v}; \quad (96d)$$

$$\delta \vartheta^{st} = \delta \vartheta - \tau_\eta \mathcal{E}_{\eta J} \mathbf{H} : \nabla_0 \delta \mathbf{v}. \quad (96e)$$

Notice that the units of the above five τ -parameters (i.e. τ_p , $\tau_{\mathbf{F}}$, $\tau_{\mathbf{H}}$, τ_J and τ_η) are those of time and are chosen as a fraction of the time step for explicit integration schemes [83]. The

residuals \mathcal{R} of the conservation laws are defined by

$$\mathcal{R} = \begin{bmatrix} \mathcal{R}_p \\ \mathcal{R}_F \\ \mathcal{R}_H \\ \mathcal{R}_J \\ \mathcal{R}_\eta \end{bmatrix} = \begin{bmatrix} \text{DIV}P + \dot{f}_R - \dot{p} \\ \nabla_0 \mathbf{v} - \dot{\mathbf{F}} \\ \mathbf{F} \times \nabla_0 \mathbf{v} - \dot{\mathbf{H}} \\ \mathbf{H} : \nabla_0 \mathbf{v} - \dot{J} \\ r_R - \text{DIV}Q - \theta \dot{\eta} \end{bmatrix}, \quad (97)$$

where the dot over a variable is used to denote differentiation in time. It is now possible to derive a (stabilised) weak statement by multiplying appropriate conjugate virtual fields $\delta \mathbf{V}^{st}$ with the corresponding residuals \mathcal{R} , and integrating over the initial reference volume V_R , to give

$$0 = \int_{V_R} (\delta \mathbf{v}^{st} \cdot \mathcal{R}_p + \delta \Sigma_F^{st} : \mathcal{R}_F + \delta \Sigma_H^{st} : \mathcal{R}_H + \delta \Sigma_J^{st} \mathcal{R}_J + \delta \vartheta^{st} \mathcal{R}_\eta) dV_R. \quad (98)$$

By re-grouping expression (98) according to each virtual conjugate variable, it is possible to first extract the terms containing the virtual velocity field $\delta \mathbf{v}$ as

$$0 = \int_{V_R} \delta \mathbf{v} \cdot \mathcal{R}_p dV_R - \int_{V_R} [\tau_F \mathcal{E}_{FF} : \mathcal{R}_F + \tau_H \mathcal{E}_{HH} : \mathcal{R}_H + \tau_J \mathcal{E}_{JJ} \mathcal{R}_J \mathbf{H} + \tau_\eta \mathcal{E}_{\eta J} \mathcal{R}_\eta \mathbf{H}] : \nabla_0 \delta \mathbf{v} dV_R. \quad (99)$$

Integrating by parts the first term on the right hand side of (99), and expanding the resulting equation yields

$$\int_{V_R} \delta \mathbf{v} \cdot \frac{\partial \mathbf{p}}{\partial t} dV_R = \int_{V_R} \delta \mathbf{v} \cdot \mathbf{f}_R dV_R + \int_{\partial V_R} \delta \mathbf{v} \cdot \mathbf{t}_B dA - \int_{V_R} \mathbf{P}^{st} : \nabla_0 \delta \mathbf{v} dV_R, \quad (100)$$

where the stabilised first Piola Kirchhoff stress being defined as

$$\mathbf{P}^{st} = \Sigma_F^{st} + \Sigma_H^{st} \times \mathbf{F} + \Sigma_J^{st} \mathbf{H} \quad (101)$$

with the corresponding stabilised conjugate stresses as

$$\Sigma_F^{st} = \Sigma_F + \tau_F \mathcal{E}_{FF} : \mathcal{R}_F; \quad \Sigma_H^{st} = \Sigma_H + \tau_H \mathcal{E}_{HH} : \mathcal{R}_H; \quad \Sigma_J^{st} = \Sigma_J + \tau_J \mathcal{E}_{JJ} \mathcal{R}_J + \tau_\eta \mathcal{E}_{J\eta} \mathcal{R}_\eta. \quad (102)$$

Following a Variational Multi-Scale (VMS) stabilisation procedure [2, 21–24], these stresses (102) can be alternatively approximated in terms of stabilised strains as

$$\Sigma_F^{st} \approx \Sigma_F(\mathbf{F}^{st}, \mathbf{H}, J, \eta); \quad \Sigma_H^{st} \approx \Sigma_H(\mathbf{F}, \mathbf{H}^{st}, J, \eta); \quad \Sigma_J^{st} \approx \Sigma_J(\mathbf{F}, \mathbf{H}, J^{st}, \eta^{st}), \quad (103)$$

where

$$\mathbf{F}^{st} = \mathbf{F} + \tau_F \mathcal{R}_F; \quad \mathbf{H}^{st} = \mathbf{H} + \tau_H \mathcal{R}_H; \quad J^{st} = J + \tau_J \mathcal{R}_J; \quad \eta^{st} = \eta + \tau_\eta \mathcal{R}_\eta. \quad (104)$$

In the above expression (104), the residual terms $\{\mathcal{R}_F, \mathcal{R}_H, \mathcal{R}_J\}$ represent the difference between the time rate of the corresponding strain variable and its evaluation in terms of the material gradient of the velocities. To reduce the implicitness of the formulation, a simple procedure is used whereby time integrated geometric terms $\{\mathcal{R}_F^x, \mathcal{R}_H^x, \mathcal{R}_J^x\}$ are incorporated in (104a,b,c) to give [31, 84]

$$\mathbf{F}^{st} = \mathbf{F} + \tau_F \mathcal{R}_F + \zeta_F \mathcal{R}_F^x; \quad \mathcal{R}_F^x = \mathbf{F}_x - \mathbf{F}; \quad (105a)$$

$$\mathbf{H}^{st} = \mathbf{H} + \tau_H \mathcal{R}_H + \zeta_H \mathcal{R}_H^x; \quad \mathcal{R}_H^x = \frac{1}{2} (\mathbf{F}_x \times \mathbf{F}_x) - \mathbf{H}; \quad (105b)$$

$$J^{st} = J + \tau_J \mathcal{R}_J + \zeta_J \mathcal{R}_J^x; \quad \mathcal{R}_J^x = \det \mathbf{F}_x - J, \quad (105c)$$

where $\mathbf{F}_x = \nabla_0 \phi(\mathbf{X}, t)$ and $\zeta_{\mathbf{F}}, \zeta_{\mathbf{H}}, \zeta_J$ are dimensionless stabilisation parameters usually in the range of $[0, 0.5]$ [1, 2, 31, 35, 84].

It is important to notice that both approaches (e.g. Petrov-Galerkin (102) and VMS (103) [81, 85, 86]) are not strictly identical, except for the linear constitutive law [1]. From the implementation point of view, the VMS approach (102) is slightly more advantageous as it avoids the need to explicitly compute the Hessian components for the computation of the stabilisation terms.

With focus on linear tetrahedral finite elements, we can introduce the linear shape functions N_a (where $a = 1 \dots N$, N being the total number of nodes in the underlying mesh) for the interpolation of the momentum and virtual velocity fields, to give a set of equations for the rate of change of momentum at each node a given as

$$\sum_{b=1}^N M_{ab} \dot{\mathbf{p}}_b = \int_{V_R} N_a \mathbf{f}_R dV_R + \int_{\partial V_R} N_a \mathbf{t}_B dA - \int_{V_R} \mathbf{P}^{st} \nabla_0 N_a dV_R, \quad (106)$$

where the consistent mass-like contribution¹⁵ $M_{ab} = \int_{V_R} N_a N_b dV_R$. Similarly, the enhanced conjugate stress measures (96) can be introduced into the weighted residual equation (98) to give a set of strain update equations as

$$\sum_{b=1}^N M_{ab} \dot{\mathbf{F}}_b = \int_{V_R} N_a \nabla_0 \left(\frac{1}{\rho_R} \mathbf{p} \right) dV_R; \quad (107a)$$

$$\sum_{b=1}^N M_{ab} \dot{\mathbf{H}}_b = \int_{V_R} N_a \mathbf{F} \times \nabla_0 \left(\frac{1}{\rho_R} \mathbf{p} \right) dV_R; \quad (107b)$$

$$\sum_{b=1}^N M_{ab} \dot{J}_b = \int_{V_R} N_a \mathbf{H} : \nabla_0 \left(\frac{1}{\rho_R} \mathbf{p} \right) dV_R - \int_{V_R} \frac{\tau_{\mathbf{p}}}{\rho_R} (\mathbf{H}^T \mathcal{R}_{\mathbf{p}}) \cdot \nabla_0 N_a dV_R. \quad (107c)$$

Finally, the entropy update equation can now follow

$$\sum_{b=1}^N M_{ab} \dot{\eta}_b = \int_{V_R} \left(\frac{\mathbf{Q}}{\theta} \right) \cdot \nabla_0 N_a dV_R + \int_{V_R} N_a \frac{r_R}{\theta} dV_R - \int_{V_R} \frac{1}{\theta^2} (\nabla_0 \theta \cdot \mathbf{Q}) N_a dV_R - \int_{\partial V_R} N_a \left(\frac{Q_B}{\theta} \right) dA. \quad (108)$$

The main advantage of integrating by parts as shown above is to enable the imposition of the boundary conditions via boundary fluxes. This is indeed useful for the momentum equation (106) and the entropy equation (108) as both expressions introduce naturally the boundary tractions \mathbf{t}_B and the boundary heat flux Q_B , but less important in the case of geometric conservation laws. Hence, as shown in (107a)-(107c), the strain update equations for $\{\mathbf{F}, \mathbf{H}, J\}$ are obtained without utilising integration by parts.

Moreover, by setting $\tau_J = \tau_\eta = 0$, and by assigning $\tau_{\mathbf{H}} = \tau_{\mathbf{F}}$ and $\zeta_{\mathbf{H}} = \zeta_J = \zeta_{\mathbf{F}}$, expressions (106), (107a), (107b), (107c) and (108) are fully decoupled and can be solved in a sequential manner, without resorting to a more computationally expensive iterative algorithm. For instance, equations (107a), (107b) and (108) are first solved to obtain $\{\dot{\mathbf{F}}, \dot{\mathbf{H}}, \dot{\eta}\}$ which can then be substituted into (106) to deduce $\dot{\mathbf{p}}$. Once $\dot{\mathbf{p}}$ is determined, \dot{J} can finally be obtained

¹⁵Notice that M_{ab} is called consistent mass-like component as its units are not of mass but of volume.

Table 1: A summary of the semi-discrete version of Petrov-Galerkin Finite Element Method

Linear momentum equation	$\sum_{b=1}^N M_{ab} \dot{\mathbf{p}}_b = \mathbf{E}_a^p - \mathbf{T}_a^p$ $\mathbf{E}_a^p = \int_{V_R} N_a \mathbf{f}_R dV_R + \int_{\partial V_R} N_a \mathbf{t}_B dA; \quad \mathbf{T}_a^p = \int_{V_R} \mathbf{P}^{st} \nabla_0 N_a dV_R$
Fibre map evolution equation	$\sum_{b=1}^N M_{ab} \dot{\mathbf{F}}_b = \mathbf{T}_a^F$ $\mathbf{T}_a^F = \int_{V_R} N_a \nabla_0 \left(\frac{1}{\rho_R} \mathbf{p} \right) dV_R$
Area map evolution equation	$\sum_{b=1}^N M_{ab} \dot{\mathbf{H}}_b = \mathbf{T}_a^H$ $\mathbf{T}_a^H = \int_{V_R} N_a \mathbf{F} \times \nabla_0 \left(\frac{1}{\rho_R} \mathbf{p} \right) dV_R$
Volume map evolution equation	$\sum_{b=1}^N M_{ab} \dot{J}_b = T_a^J$ $T_a^J = \int_{V_R} N_a \mathbf{H} : \nabla_0 \left(\frac{1}{\rho_R} \mathbf{p} \right) dV_R - \int_{V_R} \frac{\tau_p}{\rho_R} (\mathbf{H}^T \mathcal{R}_p) \cdot \nabla_0 N_a dV_R$
Entropy equation	$\sum_{b=1}^N M_{ab} \dot{\eta}_b = E_a^\eta - T_a^\eta$ $E_a^\eta = \int_{V_R} N_a \frac{r_B}{\theta} dV_R - \int_{\partial V_R} N_a \left(\frac{Q_B}{\theta} \right) dA$ $T_a^\eta = \int_{V_R} \frac{1}{\theta^2} (\nabla_0 \theta \cdot \mathbf{Q}) N_a dV_R - \int_{V_R} \left(\frac{Q}{\theta} \right) \cdot \nabla_0 N_a dV_R$

from (107c). Hence, the semi-discrete version of the five-field $\mathbf{p}\text{-}\mathbf{F}\text{-}\mathbf{H}\text{-}J\text{-}\eta$ conservation formulation (see equations (106)-(108)) for thermo-elasticity is reduced to the consideration of three stabilising parameters, namely $\{\tau_{\mathbf{F}}, \zeta_{\mathbf{F}}, \tau_{\mathbf{p}}\}$.

Finally, above set of stabilised semi-discrete nodal equations along with the geometry \mathbf{x} (2) can then be explicitly integrated from time step t^n to t^{n+1} . In this case, an explicit one-step two-stage Total Variation Diminishing (TVD) Runge–Kutta time integrator [1, 2] is preferred due to its excellent TVD properties. The evaluation of the maximum time increment Δt is intimately related to the minimum size of element h_{\min} , the maximum (pressure) wave speed $c_{p,\max}$ (85) and the Courant–Friedrichs–Lewy number α_{CFL} , described as

$$\Delta t = \alpha_{\text{CFL}} \frac{h_{\min}}{c_{p,\max}}. \quad (109)$$

For the numerical examples presented in this paper, a value of $\alpha_{\text{CFL}} = 0.3$ has been chosen to ensure both the accuracy and stability of the algorithm.

Finally, in order to guarantee the conservation of angular momentum within a system, the scheme is suitably modified via a posteriori global projection procedure already described in [1].

7. Solution procedure

For the purpose of implementation, equations (106), (107a), (107b), (107c) and (108) can be summarised in Table 1. Following the standard element by element assembly [71], these expressions can then be collected into a single system of equations written in vector format as

$$\mathbf{M} \dot{\mathbf{U}}^p = \mathbf{E}^p - \mathbf{T}^p; \quad \mathbf{M} \dot{\mathbf{U}}^F = \mathbf{T}^F; \quad \mathbf{M} \dot{\mathbf{U}}^H = \mathbf{T}^H; \quad \mathbf{M} \dot{\mathbf{U}}^J = \mathbf{T}^J; \quad \mathbf{M} \dot{\mathbf{U}}^\eta = \mathbf{E}^\eta - \mathbf{T}^\eta. \quad (110)$$

Here, \mathbf{M} represents a consistent mass-like matrix, \mathbf{U} is the vector of nodal unknowns

$$\mathbf{M} = \begin{bmatrix} M_{11} \mathbf{I}_{3 \times 3} & M_{12} \mathbf{I}_{3 \times 3} & \dots & M_{1N} \mathbf{I}_{3 \times 3} \\ M_{21} \mathbf{I}_{3 \times 3} & M_{22} \mathbf{I}_{3 \times 3} & \dots & M_{2N} \mathbf{I}_{3 \times 3} \\ \vdots & \vdots & & \vdots \\ M_{N1} \mathbf{I}_{3 \times 3} & M_{N2} \mathbf{I}_{3 \times 3} & \dots & M_{NN} \mathbf{I}_{3 \times 3} \end{bmatrix}; \quad \mathbf{U}^{[\bullet]} = \begin{bmatrix} [\bullet]_1 \\ [\bullet]_2 \\ \vdots \\ [\bullet]_N \end{bmatrix} \quad (111)$$

Algorithm 1: Petrov-Galerkin Finite Element Method for thermo-elasticity

Input : Initial geometry \mathbf{X} ; Material properties; Solution parameters; Initial conditions $\{\mathbf{U}_0^p, \mathbf{U}_0^F, \mathbf{U}_0^H, \mathbf{U}_0^J, \mathbf{U}_0^\eta\}$, Mass matrix
Output: Current value of conservation variables $\{\mathbf{U}_N^p, \mathbf{U}_N^F, \mathbf{U}_N^H, \mathbf{U}_N^J, \mathbf{U}_N^\eta\}$ and current geometry \mathbf{x}_N

```
for iTIME = 1:Number of time steps do
    Compute maximum wave speed;
    Evaluate time increment  $\Delta t$ ;
    for iRK=1:2 do
        Incorporate (Neumann) boundary contributions:  $\mathbf{E}^p$  and  $\mathbf{E}^\eta$ ;
        Compute  $\{\dot{\mathbf{U}}^F, \dot{\mathbf{U}}^H, \dot{\mathbf{U}}^\eta\}$ ;
        Evaluate the equivalent internal force vector  $\mathbf{T}^p$  and  $\dot{\mathbf{U}}^p$ ;
        Activate angular momentum projection algorithm [1];
        Compute  $\dot{\mathbf{U}}^J$ ;
        Update mesh coordinates  $\mathbf{x}$ ;
        Update conservation variables  $\{\mathbf{U}^p, \mathbf{U}^F, \mathbf{U}^H, \mathbf{U}^J, \mathbf{U}^\eta\}$ ;
        Apply strong boundary conditions on  $\mathbf{U}^p$  and  $\mathbf{U}^\eta$ ;
    end
    Update conservation variables  $\{\mathbf{U}^p, \mathbf{U}^F, \mathbf{U}^H, \mathbf{U}^J, \mathbf{U}^\eta\}$ , mesh coordinates  $\mathbf{x}$  and time;
    Apply strong boundary conditions on  $\mathbf{U}^p$  and  $\mathbf{U}^\eta$ ;
    Output results;
end
```

with $\mathbf{I}_{3 \times 3}$ the second order identity tensor. Similarly, $\mathbf{E}^{[\bullet]}$ and $\mathbf{T}^{[\bullet]}$ are the equivalent external and internal vectors defined as

$$\mathbf{E}^{[\bullet]} = \begin{bmatrix} \mathbf{E}_1^{[\bullet]} \\ \mathbf{E}_2^{[\bullet]} \\ \vdots \\ \mathbf{E}_N^{[\bullet]} \end{bmatrix}; \quad \mathbf{T}^{[\bullet]} = \begin{bmatrix} \mathbf{T}_1^{[\bullet]} \\ \mathbf{T}_2^{[\bullet]} \\ \vdots \\ \mathbf{T}_N^{[\bullet]} \end{bmatrix}, \quad (112)$$

respectively. In order to speed up the algorithm, the consistent mass-like matrix contributions are replaced by its lumped counterpart \mathbf{M}^L without affecting the order of convergence [1]. This is defined as

$$\mathbf{M}^L = \begin{bmatrix} M_{11}^L \mathbf{I}_{3 \times 3} & \mathbf{0}_{3 \times 3} & \cdots & \mathbf{0}_{3 \times 3} \\ \mathbf{0}_{3 \times 3} & M_{22}^L \mathbf{I}_{3 \times 3} & \cdots & \mathbf{0}_{3 \times 3} \\ \vdots & \vdots & \ddots & \vdots \\ \mathbf{0}_{3 \times 3} & \mathbf{0}_{3 \times 3} & \cdots & M_{NN}^L \mathbf{I}_{3 \times 3} \end{bmatrix}; \quad M_{aa}^L = \sum_{b=1}^N M_{ab}. \quad (113)$$

For completeness, Algorithm 1 summarises the complete algorithmic description of the Petrov-Galerkin type of Finite Element Method described above, with all necessary numerical ingredients.

8. Numerical examples

In this section, a wide spectrum of three dimensional numerical examples are presented in order to assess the performance, effectiveness and applicability of the Petrov-Galerkin Finite Element Method (PG-FEM) described above. It is crucial to show that the overall PG-FEM linear tetrahedral formulation

- achieves second order convergence not only for velocities and stresses (or strains), but now also include temperature (or entropy),
- circumvents locking difficulties and hour-glassing,
- preserves the total angular momentum over a long term response, and
- guarantees a non-negative rate of production of entropy in an isolated system.

In the following numerical computations, the thermal conductivity tensor is particularised for the case of isotropy, whereby it can be expressed in terms of the scalar conductivity field h , that is $\mathbf{k} = h\mathbf{I}$ (16). The global a posteriori angular momentum projection algorithm as shown in [1] is activated unless otherwise stated.

8.1. Convergence

The main objective of this example is to demonstrate the order of convergence of the proposed framework. A linear thermo-elastic constitutive model [62] is used and its detailed derivation is presented in Appendix C. Following a similar procedure as that described in Part I [1] and Part II [2], the analysis of an *ad-hoc* manufactured solution is now extended to

thermo-elasticity. We consider a cubic shaped domain of unit length¹⁶. The exact fields associated with the mapping description $\phi(\mathbf{X}, t)$ and the temperature profile $\theta(\mathbf{X}, t)$ are specifically chosen as

$$\phi^{\text{exact}}(\mathbf{X}, t) = \mathbf{X} + U_0 \cos(\xi\pi t) \begin{bmatrix} \sin(\frac{\pi X}{2}) \cos(\frac{\pi Y}{2}) \cos(\frac{\pi Z}{2}) \\ \cos(\frac{\pi X}{2}) \sin(\frac{\pi Y}{2}) \cos(\frac{\pi Z}{2}) \\ \cos(\frac{\pi X}{2}) \cos(\frac{\pi Y}{2}) \sin(\frac{\pi Z}{2}) \end{bmatrix} \quad (114)$$

and

$$\theta^{\text{exact}}(\mathbf{X}, t) = \theta_R \left(1 - \frac{3\pi}{2} U_0 \cos(\xi\pi t) \Gamma_0 \left[\cos\left(\frac{\pi X}{2}\right) \cos\left(\frac{\pi Y}{2}\right) \cos\left(\frac{\pi Z}{2}\right) \right] \right). \quad (115)$$

Here, the parameter ξ is defined as

$$\xi = \frac{\sqrt{3}}{2} \sqrt{\left(\frac{2\mu_R + \lambda_R}{\rho_R} \right) + \left(\frac{\theta_R \Gamma_0^2 c_v}{\rho_R} \right)}. \quad (116)$$

For values of U_0 below 0.001 m, the solution can be considered to be linear. Consequently, the exact deformation gradient tensor $\mathbf{F}^{\text{exact}}$ and the exact temperature gradient can now be computed

$$\mathbf{F}^{\text{exact}}(\mathbf{X}, t) = \mathbf{I} + \nabla_0 \phi^{\text{exact}}, \quad \nabla_0 \theta^{\text{exact}}(\mathbf{X}, t) = \frac{3\pi^2 \theta_R \Gamma_0}{4} U_0 \cos(\xi\pi t) \begin{bmatrix} \sin(\frac{\pi X}{2}) \cos(\frac{\pi Y}{2}) \cos(\frac{\pi Z}{2}) \\ \cos(\frac{\pi X}{2}) \sin(\frac{\pi Y}{2}) \cos(\frac{\pi Z}{2}) \\ \cos(\frac{\pi X}{2}) \cos(\frac{\pi Y}{2}) \sin(\frac{\pi Z}{2}) \end{bmatrix}. \quad (117)$$

Here, the material gradient of a mapping is given as

$$\nabla_0 \phi^{\text{exact}} = \alpha \begin{bmatrix} \cos\left(\frac{\pi X}{2}\right) \cos\left(\frac{\pi Y}{2}\right) \cos\left(\frac{\pi Z}{2}\right) & -\sin\left(\frac{\pi X}{2}\right) \sin\left(\frac{\pi Y}{2}\right) \cos\left(\frac{\pi Z}{2}\right) & -\sin\left(\frac{\pi X}{2}\right) \cos\left(\frac{\pi Y}{2}\right) \sin\left(\frac{\pi Z}{2}\right) \\ -\sin\left(\frac{\pi X}{2}\right) \sin\left(\frac{\pi Y}{2}\right) \cos\left(\frac{\pi Z}{2}\right) & \cos\left(\frac{\pi X}{2}\right) \cos\left(\frac{\pi Y}{2}\right) \cos\left(\frac{\pi Z}{2}\right) & -\cos\left(\frac{\pi X}{2}\right) \sin\left(\frac{\pi Y}{2}\right) \sin\left(\frac{\pi Z}{2}\right) \\ -\sin\left(\frac{\pi X}{2}\right) \cos\left(\frac{\pi Y}{2}\right) \sin\left(\frac{\pi Z}{2}\right) & -\cos\left(\frac{\pi X}{2}\right) \sin\left(\frac{\pi Y}{2}\right) \sin\left(\frac{\pi Z}{2}\right) & \cos\left(\frac{\pi X}{2}\right) \cos\left(\frac{\pi Y}{2}\right) \cos\left(\frac{\pi Z}{2}\right) \end{bmatrix} \quad (118)$$

with $\alpha = \frac{U_0 \pi \cos(\xi\pi t)}{2}$. This enables the evaluation of exact fields for both area and volume mappings described as [1]

$$\mathbf{H}^{\text{exact}}(\mathbf{X}, t) = \frac{1}{2} \mathbf{F}^{\text{exact}} \times \mathbf{F}^{\text{exact}}; \quad J^{\text{exact}}(\mathbf{X}, t) = \frac{1}{3} \mathbf{H}^{\text{exact}} : \mathbf{F}^{\text{exact}}. \quad (119)$$

With these at hand, and recalling that both the first Piola (C.12) and the (linearised) relation between entropy and temperature (C.11), we can obtain the exact expressions for the body force \mathbf{f}_R and the entropy source term s_R , as given in (61). Using the chain rule, and after

¹⁶The geometry of this problem can be found in Part I [1] on pg. 716, but with $\{X_1, X_2, X_3\}$ now being replaced by $\{X, Y, Z\}$.

some simple algebra, the body force in this case vanishes and this is demonstrated as below

$$\begin{aligned}
\mathbf{f}_R &= \frac{\partial(\rho_R \mathbf{v})}{\partial t} - \text{DIV} \mathbf{P}^{\text{exact}} \\
&= \frac{\partial}{\partial t} \left(\rho_R \frac{\partial \phi^{\text{exact}}}{\partial t} \right) - \left[\frac{\partial \mathbf{P}^{\text{exact}}}{\partial \mathbf{F}} \bullet \nabla_0 \mathbf{F}^{\text{exact}} + \frac{\partial \mathbf{P}^{\text{exact}}}{\partial \theta} (\nabla_0 \theta^{\text{exact}}) \right] \\
&= \rho_R \frac{\partial^2 \phi^{\text{exact}}}{\partial t^2} - \left[\frac{\partial \mathbf{P}^{\text{exact}}}{\partial \mathbf{F}} \bullet (\nabla_0 (\nabla_0 \phi^{\text{exact}})) + \frac{\partial \mathbf{P}^{\text{exact}}}{\partial \theta} (\nabla_0 \theta^{\text{exact}}) \right] \\
&= \mathbf{0}.
\end{aligned} \tag{120}$$

Here, the symbol \bullet indicates the inner product between a fourth order tensor \mathcal{D} and a third order tensor \mathcal{A} , defined as $[\mathcal{D} \bullet \mathcal{A}]_i = \mathcal{C}_{iIjJ} \mathcal{A}_{jJI}$. Analogously, by making use of (C.11) and a simple isotropic conductivity tensor $\mathbf{K} = h\mathbf{I}$ (where h is a non-negative thermal conductivity), the entropy source term s_R becomes

$$\begin{aligned}
s_R &= \text{DIV} \mathbf{Q}^{\text{exact}} + \theta^{\text{exact}} \frac{\partial \tilde{\eta}(\mathbf{F}, \theta)}{\partial t} \\
&= \text{DIV} (-\mathbf{K} \nabla_0 \theta^{\text{exact}}) + \theta^{\text{exact}} \left(\frac{\partial \tilde{\eta}}{\partial \mathbf{F}} : \frac{\partial \mathbf{F}^{\text{exact}}}{\partial t} + \frac{\partial \tilde{\eta}}{\partial \theta} \frac{\partial \theta^{\text{exact}}}{\partial t} \right) \\
&= -h \text{DIV} (\nabla_0 \theta^{\text{exact}}) + \theta^{\text{exact}} \left(c_v \Gamma_0 \mathbf{I} : \nabla_0 \left(\frac{\partial \phi^{\text{exact}}}{\partial t} \right) + \frac{c_v}{\theta_R} \frac{\partial \theta^{\text{exact}}}{\partial t} \right) \\
&= -h \text{DIV} (\nabla_0 \theta^{\text{exact}}) + \theta^{\text{exact}} \left(c_v \Gamma_0 \nabla_0 \cdot \left(\frac{\partial \phi^{\text{exact}}}{\partial t} \right) + \frac{c_v}{\theta_R} \frac{\partial \theta^{\text{exact}}}{\partial t} \right) \\
&= -\frac{9\pi^3}{8} h \theta_R \Gamma_0 U_0 \cos(\xi \pi t) \left[\cos \left(\frac{\pi X}{2} \right) \cos \left(\frac{\pi Y}{2} \right) \cos \left(\frac{\pi Z}{2} \right) \right].
\end{aligned} \tag{121}$$

Dirichlet boundary conditions compatible with the exact fields $\{\phi^{\text{exact}}, \theta^{\text{exact}}\}$, as described in (114) and (115), are applied on the boundary of the domain. In particular, the cube has symmetric boundary conditions (i.e. restricted to tangential movement) at the faces $X = 0$, $Y = 0$ and $Z = 0$ and skew symmetric boundary conditions (i.e. restricted to normal movement) at the faces $X = 1$, $Y = 1$ and $Z = 1$. Moreover, and according to (115), fixed reference temperature θ_R must be constantly applied at any time at those three boundary faces $X = 1$, $Y = 1$ and $Z = 1$.

The problem is initialised with the mapping field $\phi|_{t=0} = \phi^{\text{exact}}(\mathbf{X}, t = 0)$ (114) and, subsequently, the initial deformation gradient, its co-factor and its Jacobian can be obtained as

$$\mathbf{F}|_{t=0} = \mathbf{F}^{\text{exact}}(\mathbf{X}, t = 0); \quad \mathbf{H}|_{t=0} = \mathbf{H}^{\text{exact}}(\mathbf{X}, t = 0); \quad J|_{t=0} = J^{\text{exact}}(\mathbf{X}, t = 0). \tag{122}$$

An initial distribution of the entropy is given in terms on an initial temperature distribution, by using the following (linearised) relation between the entropy and temperature (refer to (C.11))

$$\eta|_{t=0} = \tilde{\eta} \left(\mathbf{F}|_{t=0}, \theta|_{t=0} \right) = c_v \Gamma_0 \left(\text{tr} \mathbf{F}|_{t=0} - 3 \right) + c_v \left(\frac{\theta|_{t=0}}{\theta_R} - 1 \right); \quad \theta|_{t=0} = \theta^{\text{exact}}(\mathbf{X}, t = 0). \tag{123}$$

A list of parameters used for this simulation is summarised in Table 2. As compared to the closed form solutions described in (114) and (115), Tables 3 and 4 show the L_2 global convergence analysis at time $t = 8 \times 10^{-4}$ s for (1) the components of the velocity \mathbf{v} , (2) the components of the first Piola-Kirchhoff stress tensor \mathbf{P} and (3) the temperature θ . Their corresponding graphical representations are depicted in Figure 1. As expected, the proposed computational framework achieves equal second order convergence for all the variables solved, namely velocity, the stress tensor and the temperature. This equal order convergence for all derived variables is one of the advantages of the proposed framework.

Table 2: Linear thermo-elasticity: problem and material parameters used in the simulation

Problem parameter	U_0	5×10^{-4}	m
Lamé parameters	μ	6.5385	MPa
	λ	9.8077	MPa
Specific heat capacity	C_v	1	$\text{JK}^{-1}\text{kg}^{-1}$
Reference temperature	θ_R	293.15	K
Thermal conductivity	h	10	$\text{WK}^{-1}\text{m}^{-1}$
Material density	ρ_R	1100	kgm^{-3}
Mie-Grüneisen coefficients	q	1	
	Γ_0	8.5889	

Table 3: Linear thermo-elasticity: numerical values for the relative error of $\{v_x, v_y, v_z, \theta\}$ as compared to the exact solution, measured with L_2 norm. Convergence rate calculated using the results of the two finest meshes.

	v_x (m/s)	v_y (m/s)	v_z (m/s)	θ (K)
1/3	6.553×10^{-3}	6.547×10^{-3}	6.489×10^{-3}	1.019×10^{-1}
1/6	1.906×10^{-3}	1.880×10^{-3}	1.875×10^{-3}	2.537×10^{-2}
1/12	4.373×10^{-4}	4.402×10^{-4}	4.768×10^{-4}	6.837×10^{-3}
1/24	1.086×10^{-4}	1.018×10^{-4}	1.231×10^{-4}	1.644×10^{-3}
conv. rate	2.056	2.113	1.954	2.025

Table 4: Linear thermo-elasticity: numerical values for the relative error of $\{P_{xX}, P_{yY}, P_{zZ}\}$ as compared to the exact solution, measured with L_2 norm. Convergence rate calculated using the results of the two finest meshes.

	P_{xX} (Pa)	P_{yY} (Pa)	P_{zZ} (Pa)
1/3	1.538×10^3	1.543×10^3	1.553×10^3
1/6	3.902×10^2	3.91×10^2	3.967×10^2
1/12	1.13×10^2	1.108×10^2	1.109×10^2
1/24	2.776×10^1	2.833×10^1	2.724×10^1
conv. rate	2.025	1.967	2.026

8.2. Conservation

8.2.1. L-shaped block

As previously explored in References [37, 39, 87, 88], the main objective of this classical benchmark problem is to examine the capability of the proposed PG-FEM scheme in preserving

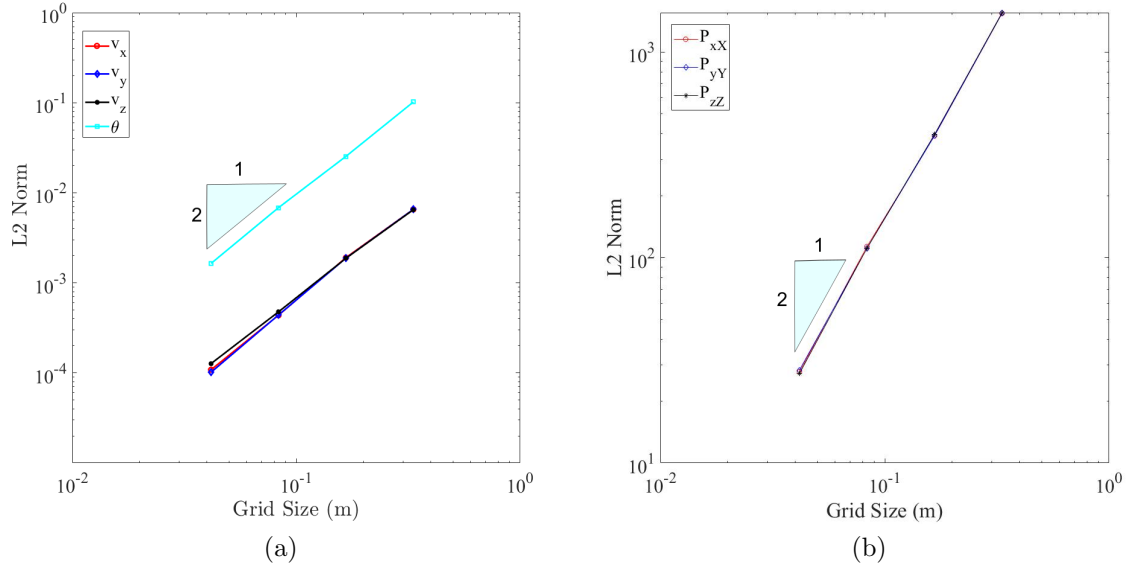


Figure 1: Linear thermo-elasticity: L_2 global convergence analysis at time $t = 8 \times 10^{-4}$ s for (a) the components of velocity and temperature and (b) the components of the first Piola Kirchoff stress tensor. Results obtained using a linear thermo-elastic model as described in equation (C.12). The material properties used are summarised in Table 2.

both the linear and angular momenta of a system. The geometry of the problem is displayed in Figure 2a. The L-shaped structure is subjected to an external torque induced by a pair of time-varying boundary forces $\mathbf{F}_1(t)$ and $\mathbf{F}_2(t)$ acting on two of its boundary faces, described as

$$\mathbf{F}_1(t) = -\mathbf{F}_2(t) = \begin{bmatrix} 150 \\ 300 \\ 450 \end{bmatrix} f(t); \quad f(t) = \begin{cases} t & 0 \leq t < 2.5 \text{ s}, \\ 5 - t & 2.5 \text{ s} \leq t < 5 \text{ s}, \\ 0 & t \geq 5 \text{ s}. \end{cases}$$

Moreover, the initial distribution of the temperature profile on the structure is not entirely homogeneous, that is

$$\theta|_{t=0} = \begin{cases} 300 \text{ K} & Y = 10 \text{ m}, \\ 250 \text{ K} & X = 6 \text{ m}, \\ \theta_R & \text{elsewhere.} \end{cases}$$

In this example, a polyconvex Mie-Grüneisen thermo-elastic model as presented in Section 3.5.3 is considered. The values of all the relevant material and geometrical parameters used can be found in Table 5. For completeness, three different levels of mesh refinement are considered (see Figure 2b-d). For instance, $\{\mathbf{Mesh}\#\mathbf{I}, \mathbf{Mesh}\#\mathbf{II}, \mathbf{Mesh}\#\mathbf{III}\}$ comprise $\{3, 862, 12, 216, 28, 059\}$ linear tetrahedral finite elements, respectively.

First, a mesh refinement study is carried out. This can be seen in the first three columns of Figure 3. It is remarkable that the deformation pattern, together with pressure and temperature profiles, predicted using a small number of elements ($\mathbf{Mesh}\#\mathbf{I}$) agrees extremely well with those results obtained using finer discretisations (i.e. $\mathbf{Mesh}\#\mathbf{II}$ and $\mathbf{Mesh}\#\mathbf{III}$). For benchmarking

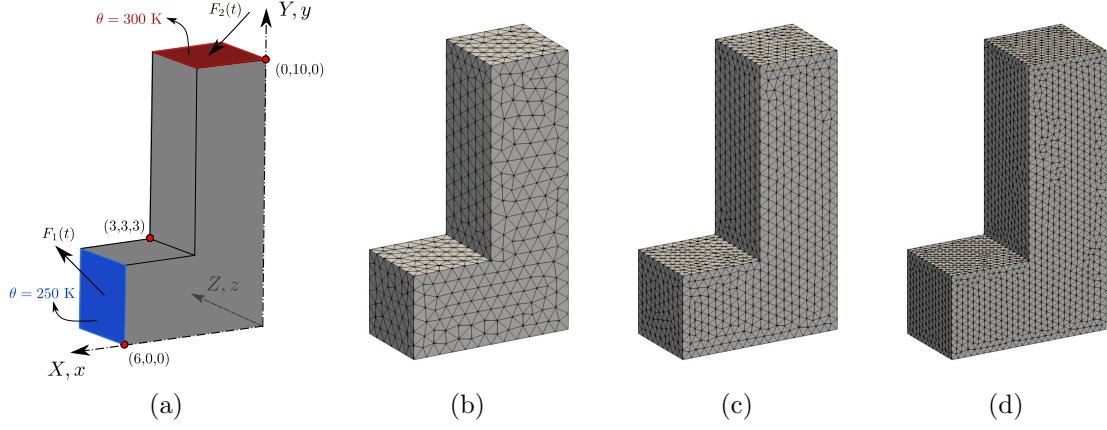


Figure 2: L-shaped block: (a) geometry and its finite element discretisation, namely (b) **Mesh#I** (3,862 linear tetrahedra), (c) **Mesh#II** (12,216 linear tetrahedra) and (d) **Mesh#III** (28,059 linear tetrahedra).

Table 5: L-shaped block: material parameters used in the simulation

Lamé parameters	μ	19.423	kPa
	λ	29.135	kPa
Specific heat capacity	C_v	1	$\text{JK}^{-1}\text{kg}^{-1}$
Reference temperature	θ_R	293.15	K
Thermal conductivity	h	10	$\text{WK}^{-1}\text{m}^{-1}$
Material density	ρ_R	1100	kgm^{-3}
Mie-Grüneisen coefficients	q	1	
	Γ_0	0.0255	

Table 6: Rotating disk: material parameters used in the simulation

Lamé parameters	μ	0.4986	kPa
	λ	10.834	kPa
Specific heat capacity	C_v	10	$\text{JK}^{-1}\text{kg}^{-1}$
Reference temperature	θ_R	308.15	K
Thermal conductivity	h	10	$\text{WK}^{-1}\text{m}^{-1}$
Material density	ρ_R	10	kgm^{-3}
Mie-Grüneisen coefficients	q	1	
	Γ_0	0.0745	

purposes, an alternative in-house Upwind Vertex Centred Finite Volume Method (Upwind-VCFVM) [33] with ultrafine discretisation (i.e. 81,222 number of linear tetrahedral meshes) is also employed and compared. Comparing the results of PG-FEM and Upwind-VCFVM, practically identical results are observed (see Figure 3).

Second, Figures 4a,b demonstrate the ability of the proposed algorithm in preserving both the linear momentum and angular momentum of the system. The total linear momentum, $\mathbf{L}^{\text{total}} = \int_{V_R} \mathbf{p} dV_R$, is very zero at all times as no movement of the centre of mass is appreciated. The total angular momentum, $\mathbf{A}^{\text{total}} = \int_{V_R} \mathbf{x} \times \mathbf{p} dV_R$, is expected to be conserved after the loading phase, that is when time $t > 5$ s. Another interesting variable of interest is the global entropy $\eta^{\text{total}} = \int_{V_R} \eta dV_R$, which increases over time for the entire simulation. This is seen in Figure 4c. In addition, Figure 4d illustrates the time histories of different forms of energy. These include kinetic energy $K^{\text{total}} = \int_{V_R} \frac{1}{2\rho_R} \mathbf{p} \cdot \mathbf{p} dV_R$, internal energy associated with mechanical contribution $\mathcal{E}_{\mathbf{x}}^{\text{total}} = \int_{V_R} \tilde{\mathcal{E}}_R(\mathbf{x}) dV_R$ and internal energy associated with thermal effects $\mathcal{E}_{\eta}^{\text{total}} = \int_{V_R} c_v \theta_R \left(e^{\frac{\eta - \tilde{\eta}_R(\mathbf{x})}{c_v}} - 1 \right) dV_R$. In the absence of boundary heat flux, the external power only arises as a result of external boundary traction, that is $\dot{\psi}_{\text{ext}} = \int_{\partial V_R} \mathbf{t} \cdot \mathbf{v} dA$. With these at hand, the total energy $\mathbb{E}^{\text{total}}$, mathematically defined as $\mathbb{E}^{\text{total}} = K^{\text{total}} + \mathcal{E}_{\mathbf{x}}^{\text{total}} + \mathcal{E}_{\eta}^{\text{total}} - \psi_{\text{ext}}$, can now be computed. This consequently leads to an alternative energy measure known as ballistic energy, that is $S^{\text{total}} = \mathbb{E}^{\text{total}} - \theta_R \eta^{\text{total}}$. Due to the fact that a residual-based upwinding stabilisation term is introduced in our PG-FEM, a slight decrease in the total energy is unavoidable after the loading phase.

Third, and for qualitative comparison purposes, Figure 5a monitors the temperature evolution at three different positions, namely point A at position $[0, 10, 0]^T$, point B at $[6, 0, 0]^T$ and point C at $[3, 3, 3]^T$. Additionally, the time history of the velocity component v_x is also monitored at point A. It is clear that the solution converges with a progressive level of refinement. Finally, a series of deformed states are shown in Figures 6 and 7, where the colour contour plot indicates, respectively, the temperature and pressure representations.

8.2.2. Rotating disk

Similar to the objectives described in the above section, another interesting problem previously explored by other authors [37, 39] is considered. A rotating disk (refer to Figure 8) is first initialised by the following rotational velocity defined as

$$\mathbf{v}|_{t=0} = \boldsymbol{\omega} \times \mathbf{X}, \quad \text{with} \quad \boldsymbol{\omega} = \begin{bmatrix} 1 \\ 1 \\ 1 \end{bmatrix}, \quad (124)$$

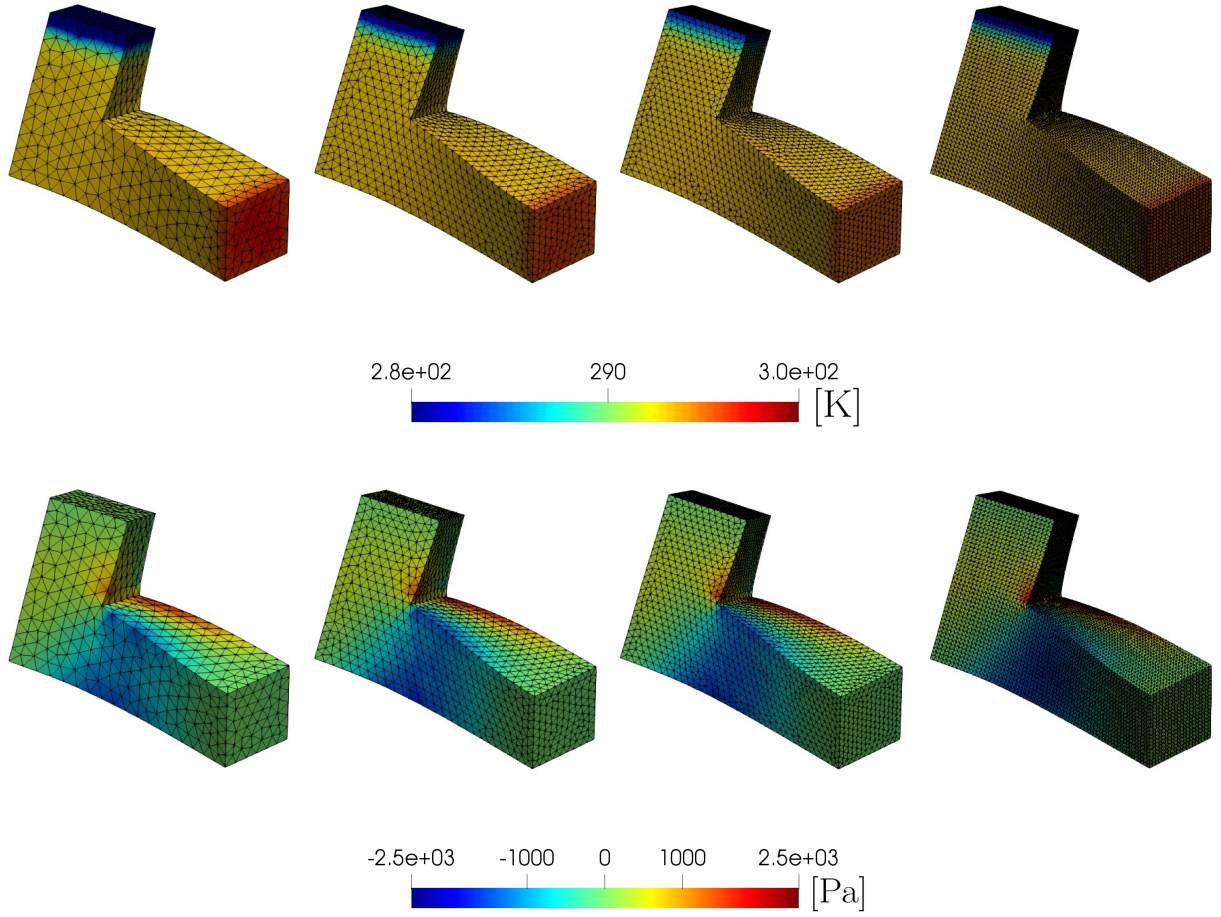


Figure 3: L-shaped block: comparison of deformed shapes at time $t = 11$ s. The first three columns show the mesh refinement of a structure simulated using PG-FEM, whereas the last column shows a deformed structure via Upwind-VCFVM. The first row depicts the temperature contour and the second row illustrates pressure contour. A polyconvex Mie-Grüneisen thermo-elastic constitutive model as described in (48) is used. Their corresponding material parameters are summarised in Table 5.

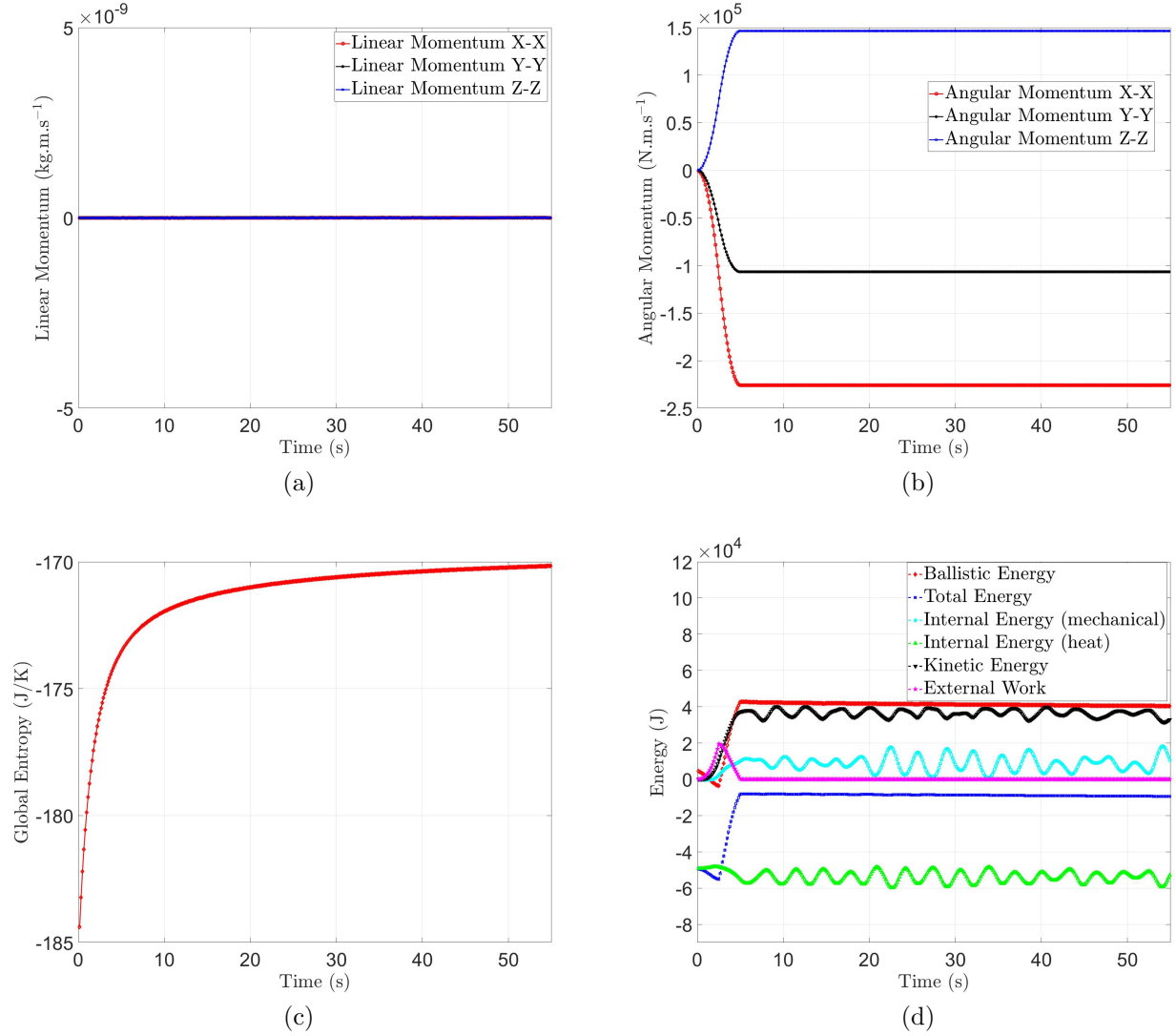


Figure 4: L-shaped block: time evolution of (a) global linear momentum, (b) global angular momentum, (c) global entropy, and (d) different energy measures. A polyconvex Mie-Grüneisen thermo-elastic constitutive model as described in (48) is used. Their corresponding material parameters are summarised in Table 5.

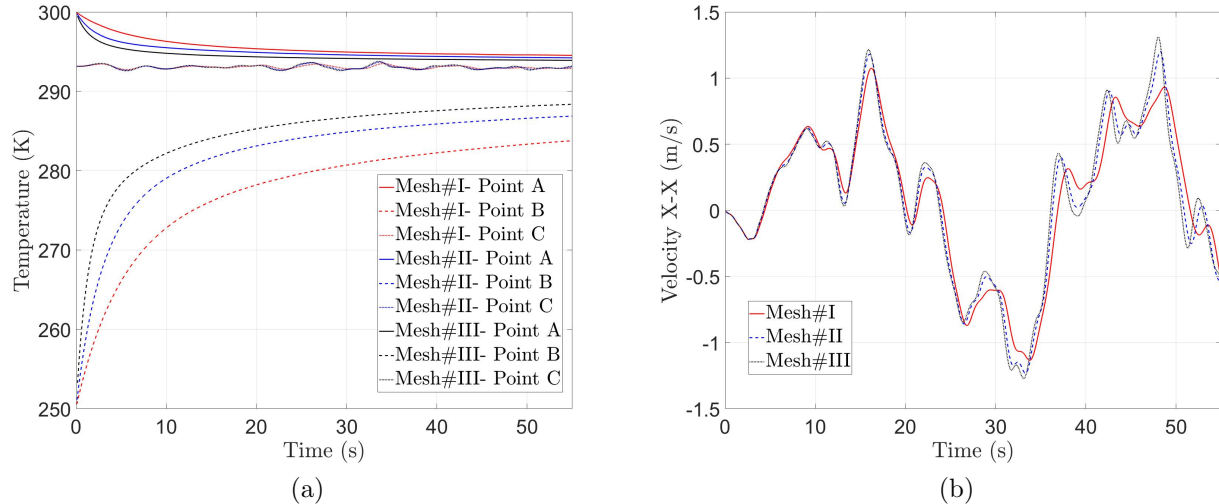


Figure 5: L-shaped block: time evolution of (a) temperature at three different points $\{A, B, C\}$, and (b) velocity v_x at point A. Point A refers to position $[0, 10, 0]^T$, point B refers to position $[6, 0, 0]^T$ and point C refers to $[3, 3, 3]^T$. A polyconvex Mie-Grüneisen thermo-elastic constitutive model as described in (48) is used. Their corresponding material parameters are summarised in Table 5.

and is then left floating in space.

The initial temperature profile of the disk is homogeneously distributed and equal to the reference temperature, that is $\theta|_{t=0} = \theta_R$. To achieve heat build-up within the disk, a negative value of the boundary heat flux is prescribed on a quarter of its lateral boundary surface (see Figure 8) within a period of time $t \in [0, 4]$ s. This is described as

$$Q_B(t) = -1591.5 f(t) (\text{W/m}^2) \quad \text{where} \quad f(t) = \begin{cases} \sin\left(\frac{\pi t}{4}\right) & t \leq 4s \\ 0 & t > 4s. \end{cases} \quad (125)$$

The remaining boundary surfaces are assumed to be thermally insulated. A polyconvex Mie-Grüneisen model (48) is chosen and their material parameters are summarised in Table 6.

As illustrated in Figure 9a, the new PG-FEM is capable of preserving the global angular momentum within the underlying thermo-mechanical system. When time $t \leq 4$ s, the total energy of the system is expected to increase due to the prescribed heat flux described in (125), that is heat flows into the system. When time $t > 4$ s, that is after the removal of heat flux, the system is considered as closed. This implies that the total energy should either stay constant or possibly decrease as the result of numerical dissipation. This is shown in Figure 9b, where the total energy decreases slightly over time. Perhaps more importantly, the amount of numerical dissipation decreases with the reduction in mesh size (see Figure 9c). No numerical instability is observed.

In order to ensure the algorithm correctly reproduces the second law of thermodynamics, the global entropy is monitored (see Figure 9d). As expected, the global entropy of the system increases during the period $t \in [0, 4]$ s. As the system is closed (after $t > 4$ s), the global entropy of the system is a non-decreasing function over time, whereby the irreversibility is caused by heat conduction.

For visualisation purposes, a sequence of deformation pattern of the disk is displayed in

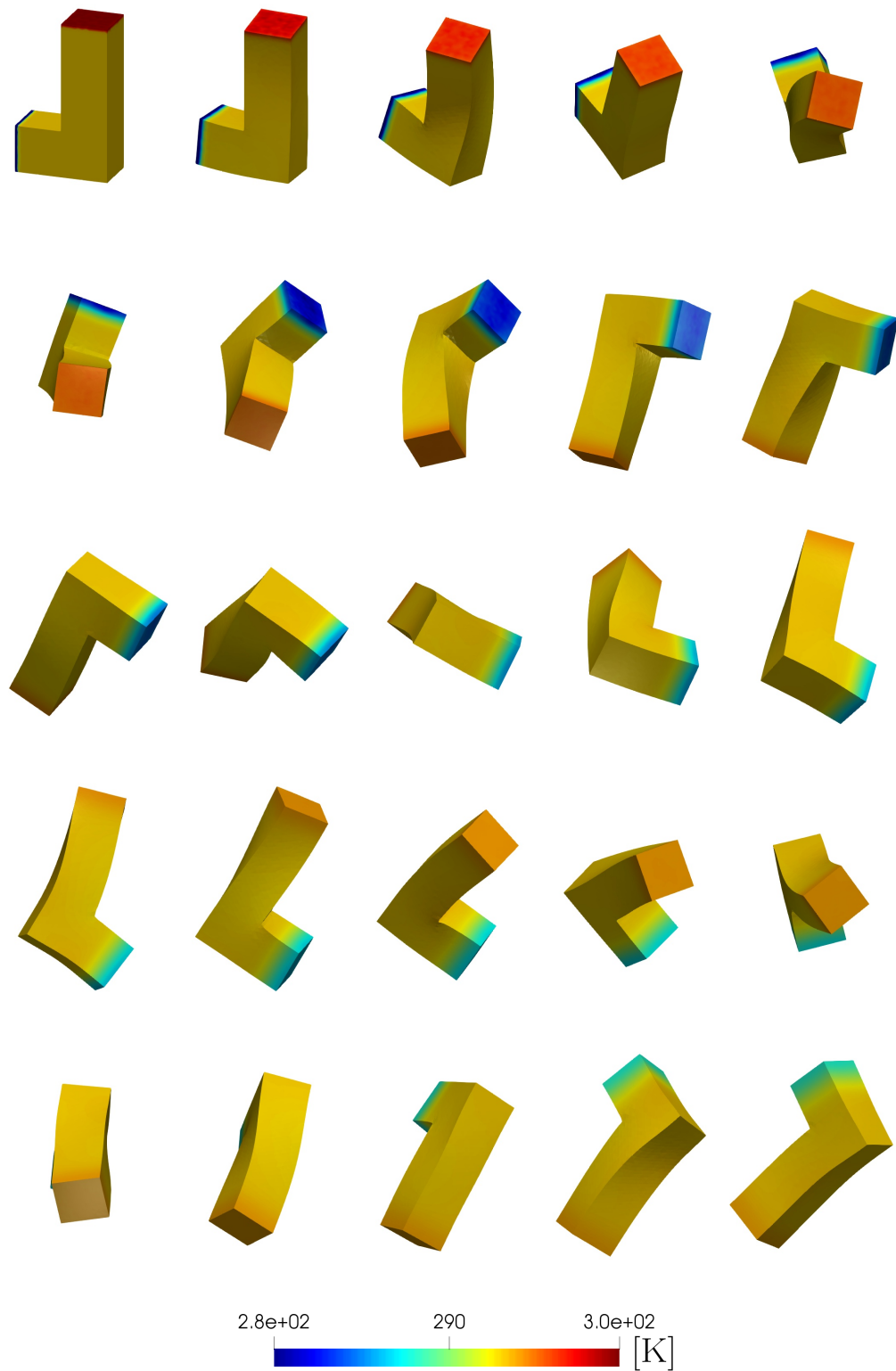


Figure 6: L-shaped block: a sequence of deformed structures with temperature distribution at times $t = \{0, 1, 2, 3, \dots, 48\}$ s (left to right and top to bottom), respectively. Results obtained using a polyconvex Mie-Grüneisen equation of state as described in (48). Their corresponding material parameters are summarised in Table 5.

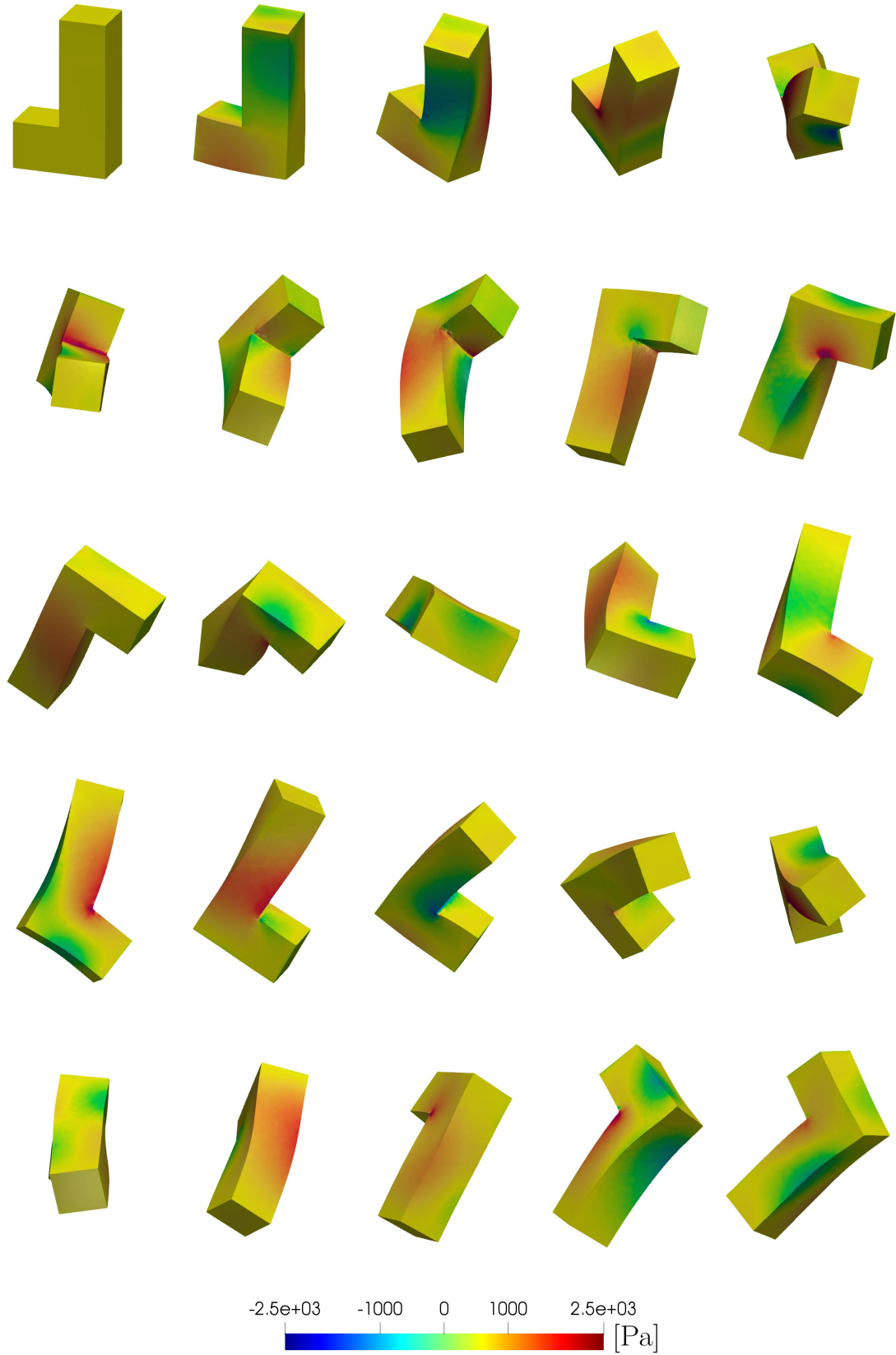


Figure 7: L-shaped block: a sequence of deformed structures with pressure distribution at times $t = \{0, 1, 2, 3, \dots, 48\}$ s (left to right and top to bottom), respectively. Results obtained using a polyconvex Mie-Grüneisen equation of state as described in (48). Their corresponding material parameters are summarised in Table 5.

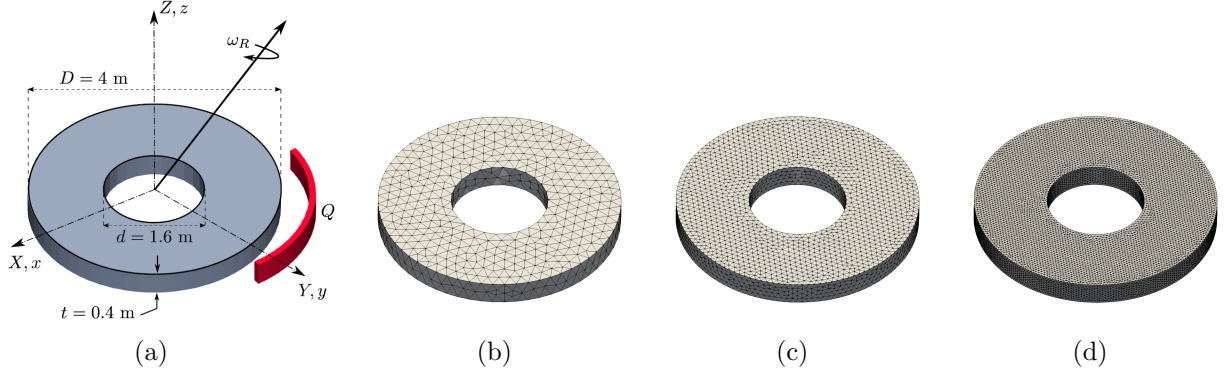


Figure 8: Rotating disk: (a) geometry and its finite element discretisation, namely (b) **Mesh#I** (3,328 linear tetrahedra), (c) **Mesh#II** (21,520 linear tetrahedra) and (d) **Mesh#III** (159,596 linear tetrahedra).

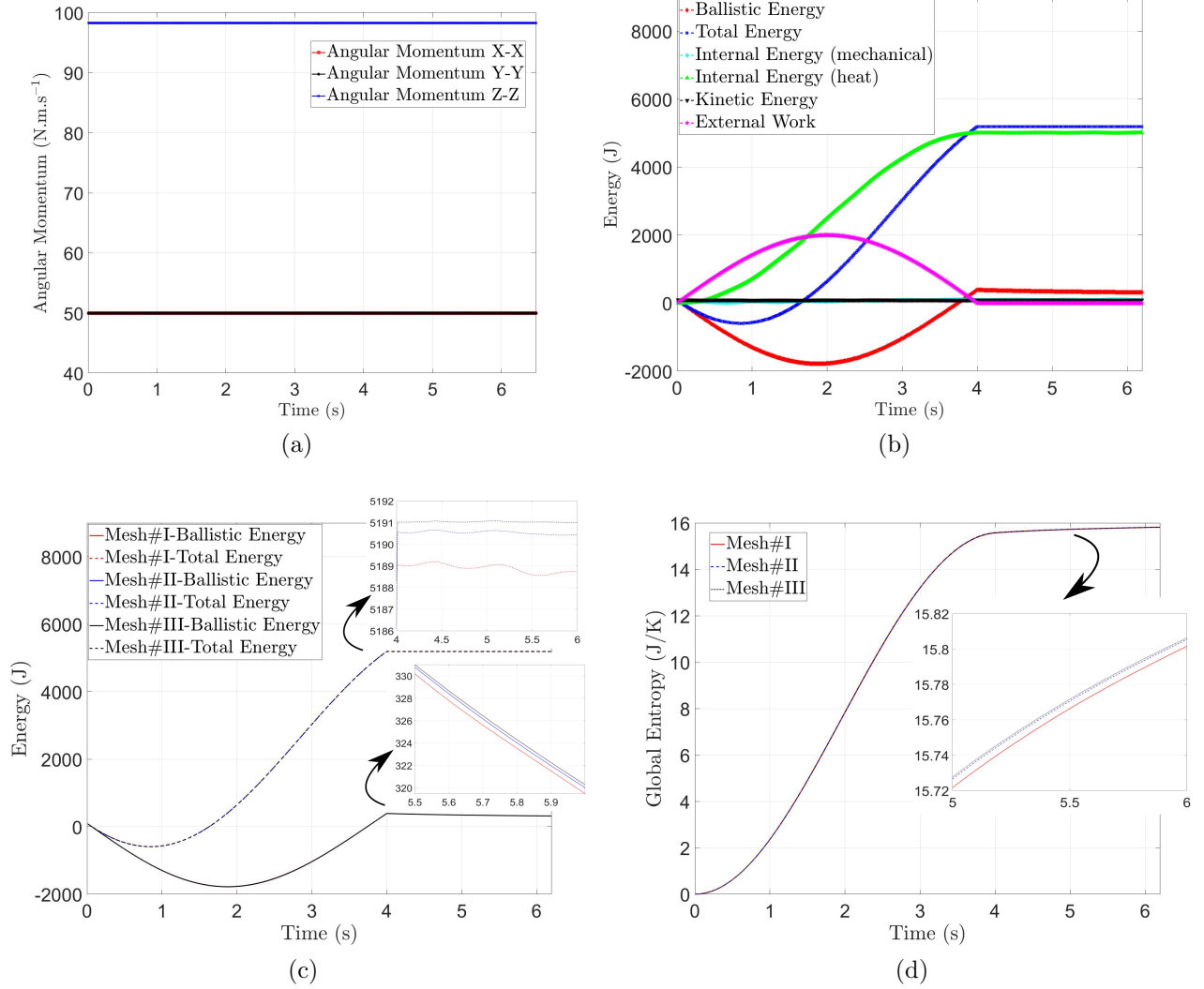


Figure 9: Rotating disk: time evolution of (a) global angular momentum, (b) various energy forms, (c) Ballistic and total energy with mesh refinement, and (d) global entropy with mesh refinement. A polyconvex Mie-Grüneisen thermo-elastic constitutive model as described in (48) is used. Their corresponding material parameters are summarised in Table 6.

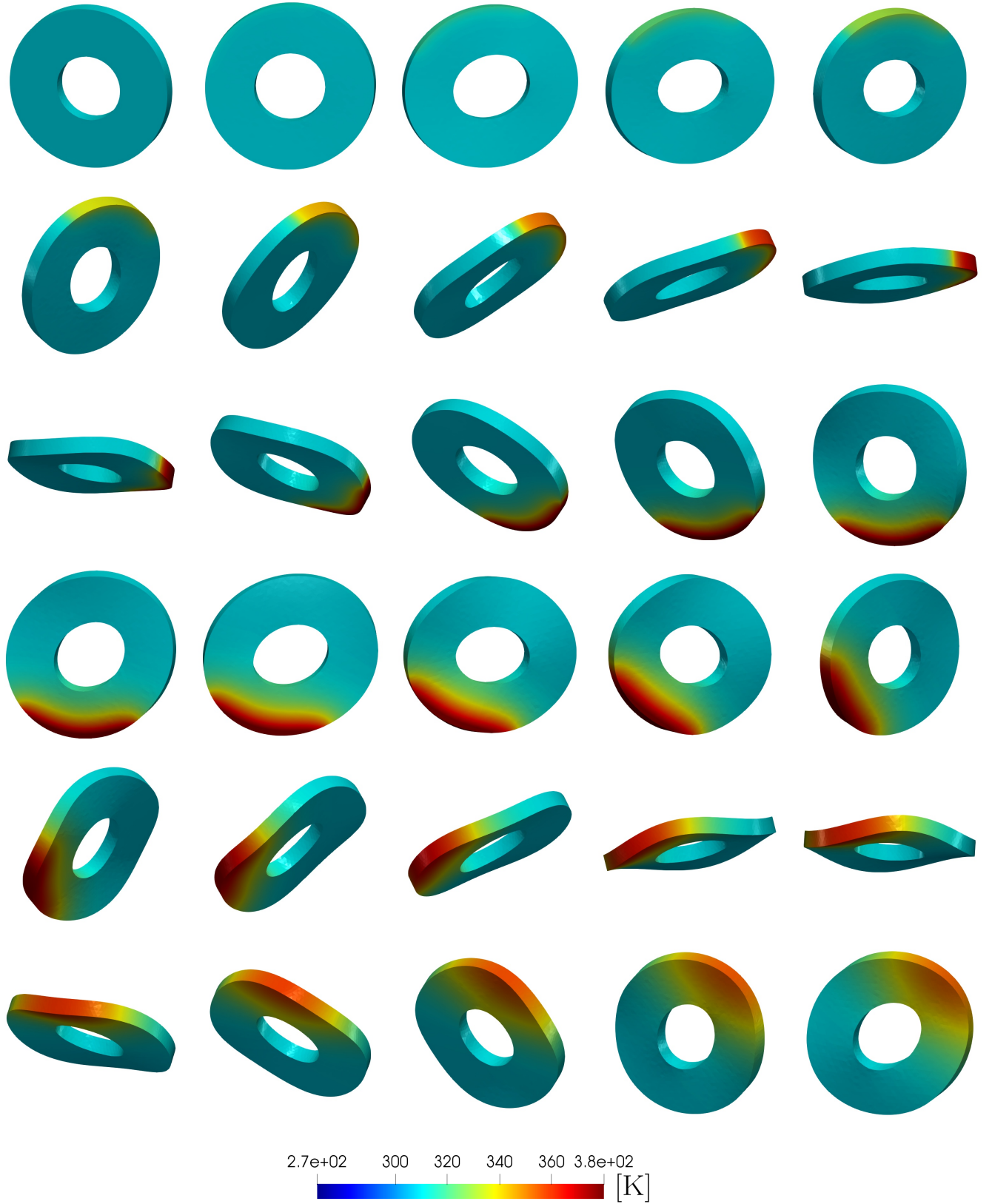


Figure 10: Rotating disk: a sequence of deformed structures with temperature distribution at times $t = \{0, 1, 2, 3, \dots, 58\}$ s (left to right and top to bottom). Results obtained using a polyconvex Mie-Grüneisen equation of state as described in (48). Their corresponding material parameters are summarised in Table 6.

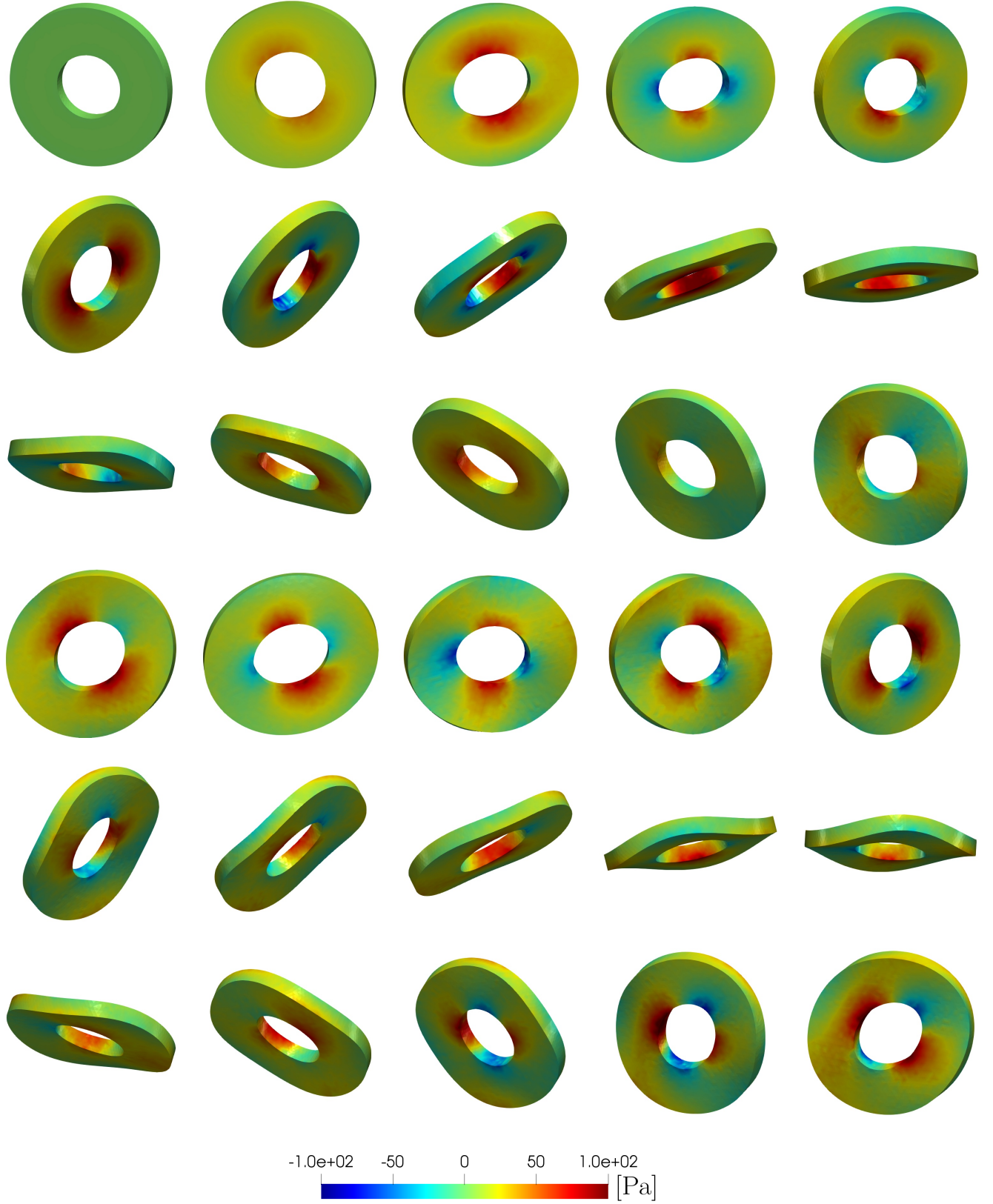


Figure 11: Rotating disk: a sequence of deformed structures with pressure distribution at times $t = \{0, 1, 2, 3, \dots, 58\}$ s (left to right and top to bottom). Results obtained using a polyconvex Mie-Grüneisen equation of state as described in (48). Their corresponding material parameters are summarised in Table 6.

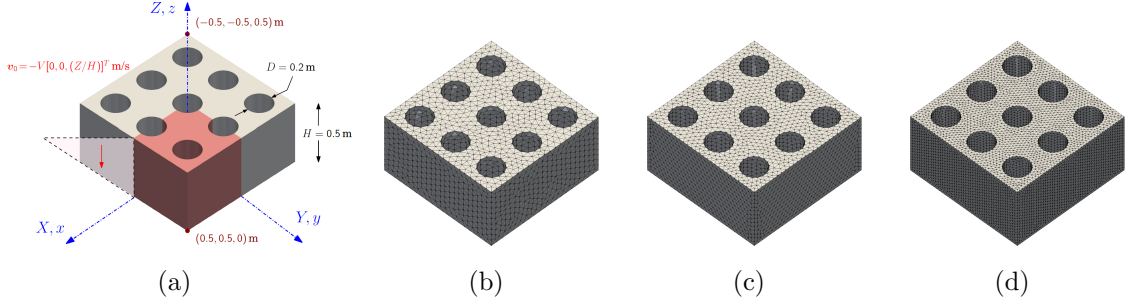


Figure 12: Punch block: (a) geometry and its finite element discretisation, namely (b) **Mesh#I** (15,931 linear tetrahedra), (c) **Mesh#II** (36,722 linear tetrahedra) and (d) **Mesh#III** (113,846 linear tetrahedra).

Table 7: Punch block: material parameters used in the simulation

Lamé parameters	μ	6.5385	MPa
	λ	9.8077	MPa
Specific heat capacity	C_v	1	$\text{JK}^{-1}\text{kg}^{-1}$
Reference temperature	θ_R	293.15	K
Thermal conductivity	h	10	$\text{WK}^{-1}\text{m}^{-1}$
Material density	ρ_R	1100	kgm^{-3}
Mie-Grüneisen coefficients	q	1	
	Γ_0	8.5889	

Figures 10 and 11 with snapshots at successive points in time. Both temperature and pressure distributions are shown.

8.3. Locking and pressure instability

8.3.1. Spurious modes of a constrained punch block

Previously explored in [60] for non-thermal elasticity, an extension of this example to include thermal effects is now carried out. We consider a block with 3×3 of vertical holes with a diameter of D . Dimensions of the block are shown in Figure 12. The block is left free on its top surface and is constrained with roller support (i.e. symmetric boundary conditions) on the rest of the surfaces. The deformation of the block is initiated with a compressive (punch) velocity profile in quarter of the domain ($X \geq 0$ and $Y \geq 0$), described as

$$\mathbf{v}|_{t=0} = -5 \begin{bmatrix} 0 \\ 0 \\ Z/H \end{bmatrix} \text{ (m/s)}. \quad (126)$$

For inclusion of thermal effects, we assume that the initial temperature profile across the structure is not homogeneous, given as

$$\theta|_{t=0} = \theta_R + 10 \frac{Z}{H} \text{ (K)}. \quad (127)$$

Moreover, a polyconvex Mie-Grüneisen model as presented in (48) is used, where the material parameters are summarised in Table 7.

In this example, three different meshes are explored, namely (**Mesh#I**) 15,931, (**Mesh#II**) 36,722, and (**Mesh#III**) 113,846 linear tetrahedral elements. It is interesting to notice, from

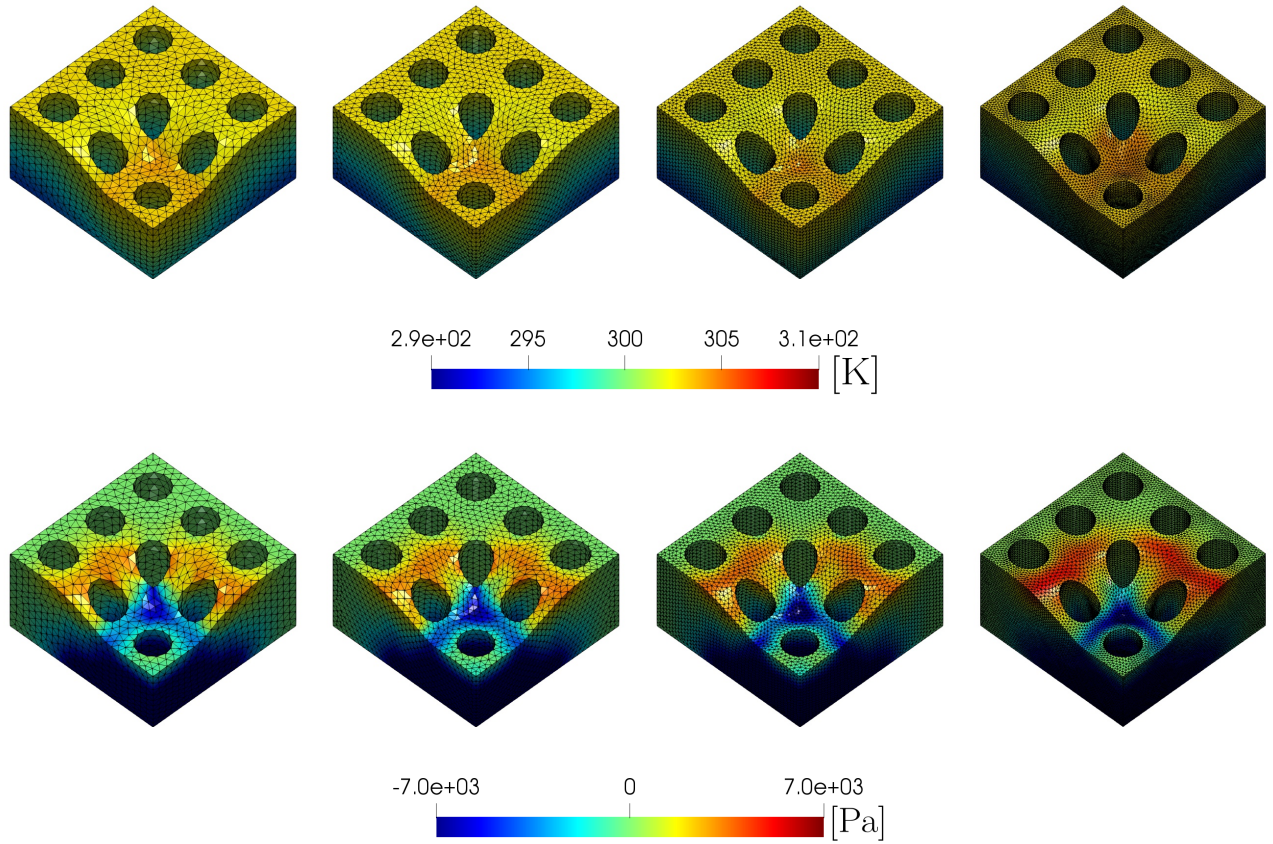


Figure 13: Punch block: comparison of deformed shapes at time $t = 0.05$ s. The first three columns ($\{\mathbf{Mesh\#I}, \mathbf{Mesh\#II}, \mathbf{Mesh\#III}\}$, from left to right) show the mesh refinement of a structure simulated using PG-FEM, whereas the last column shows a deformed structure via Upwind-VCFVM. The first row depicts the temperature contour and the second row illustrates pressure contour. A polyconvex Mie-Grüneisen thermo-elastic constitutive model described in (48) is used, with material parameters being summarised in Table 7.

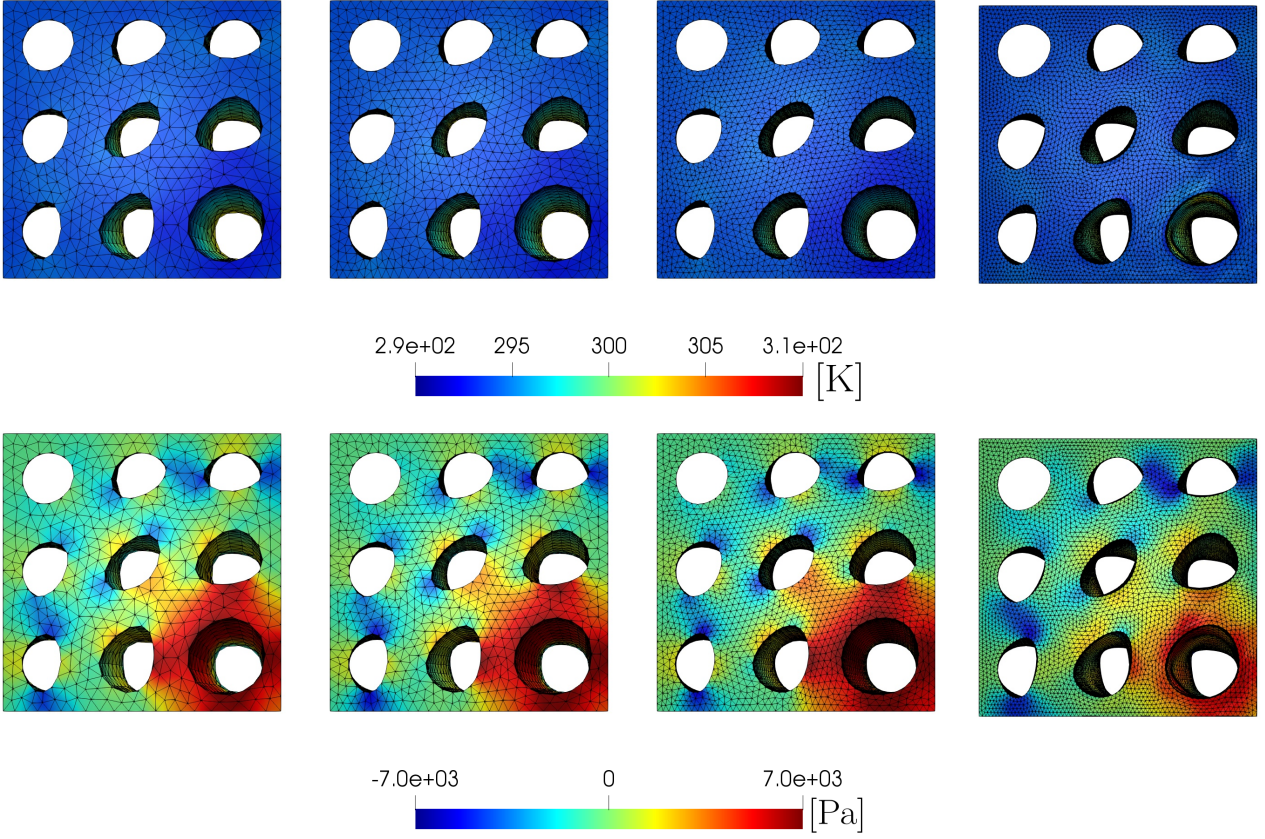


Figure 14: Punch block: comparison of deformed shapes at bottom view at time $t = 0.12$ s. The first three columns ($\{\text{Mesh\#I, Mesh\#II, Mesh\#III}\}$, from left to right) show the mesh refinement of a structure simulated using PG-FEM, whereas the last column shows a deformed structure via Upwind-VCFVM. The first row depicts the temperature contour and the second row illustrates pressure contour. A polyconvex Mie-Grüneisen thermo-elastic constitutive model as described in (48) is used, with material parameters being summarised in Table 7.

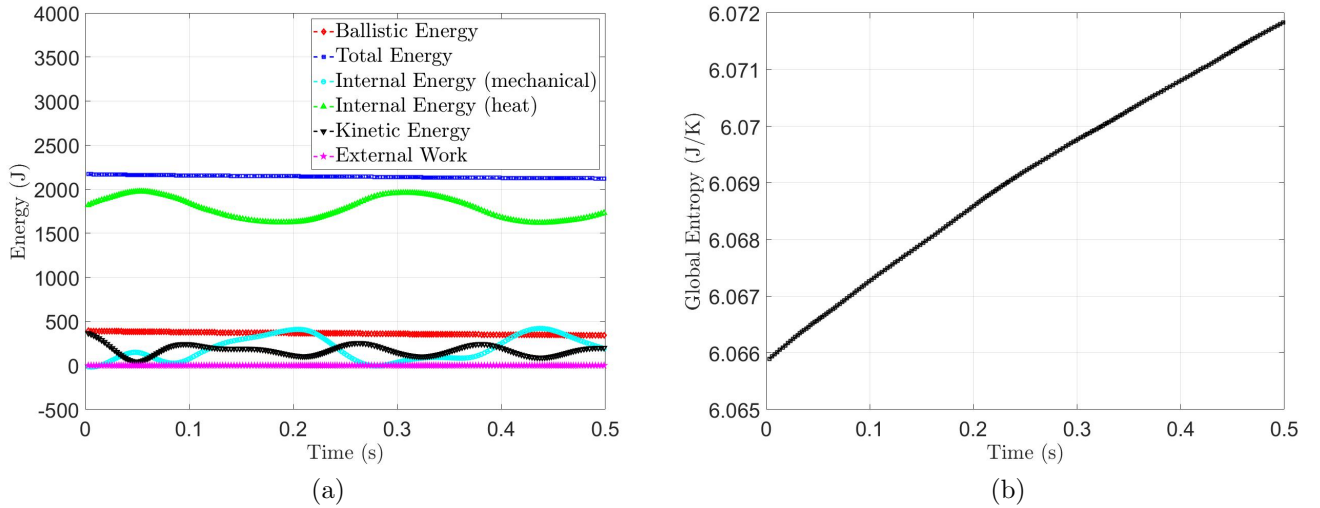


Figure 15: Punch block: time evolution of (a) various energy measures and (b) global entropy with mesh refinement. A polyconvex Mie-Grüneisen thermo-elastic constitutive model as described in (48) is used. Their corresponding material parameters are summarised in Table 7.

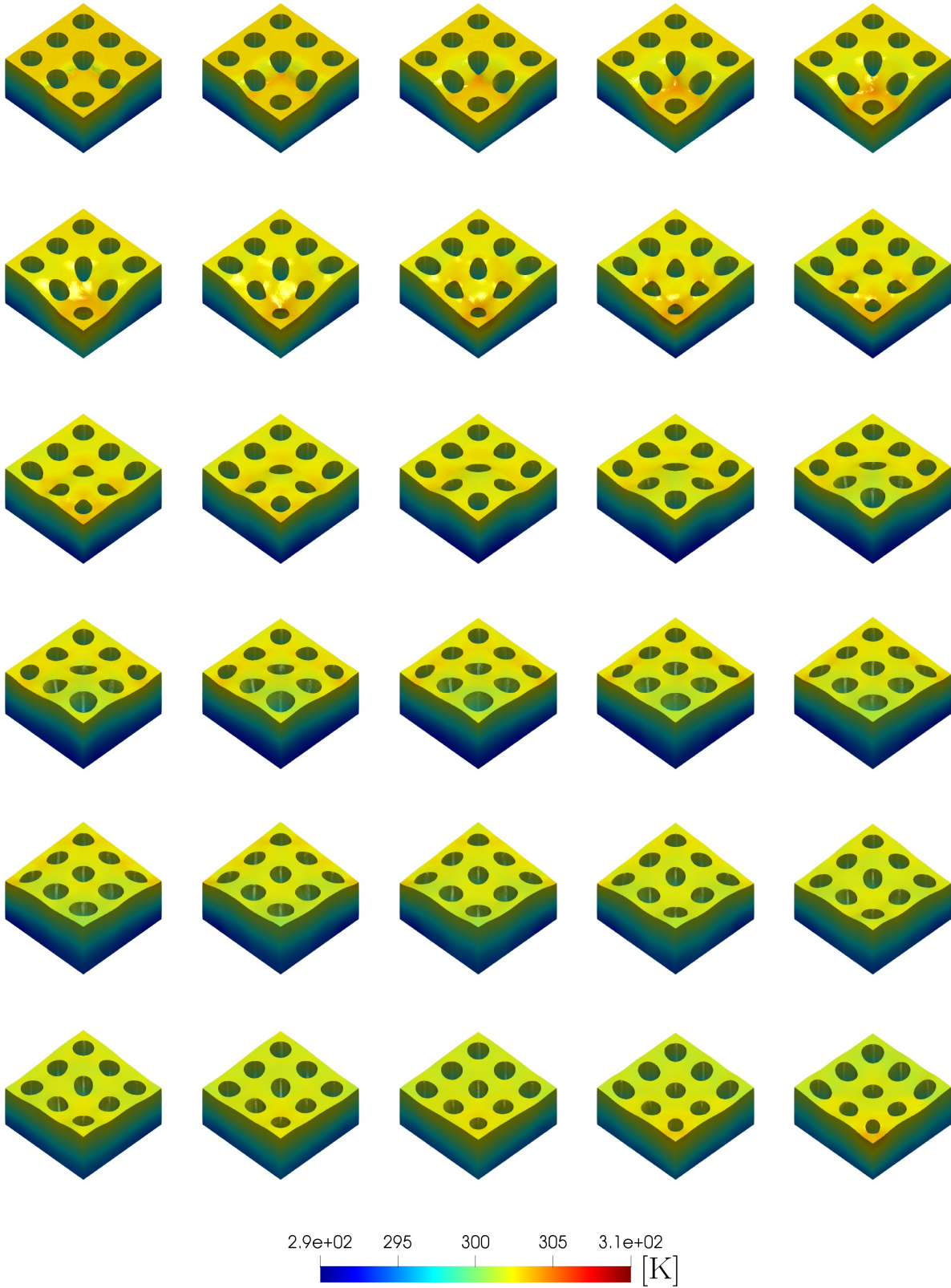


Figure 16: Punch block: a sequence of deformed structures with temperature distribution at times $t = \{10, 20, 30, \dots, 300\}$ ms (left to right and top to bottom). Results obtained using a polyconvex Mie-Grüneisen equation of state as described in (48). Their corresponding material parameters are summarised in Table 7.

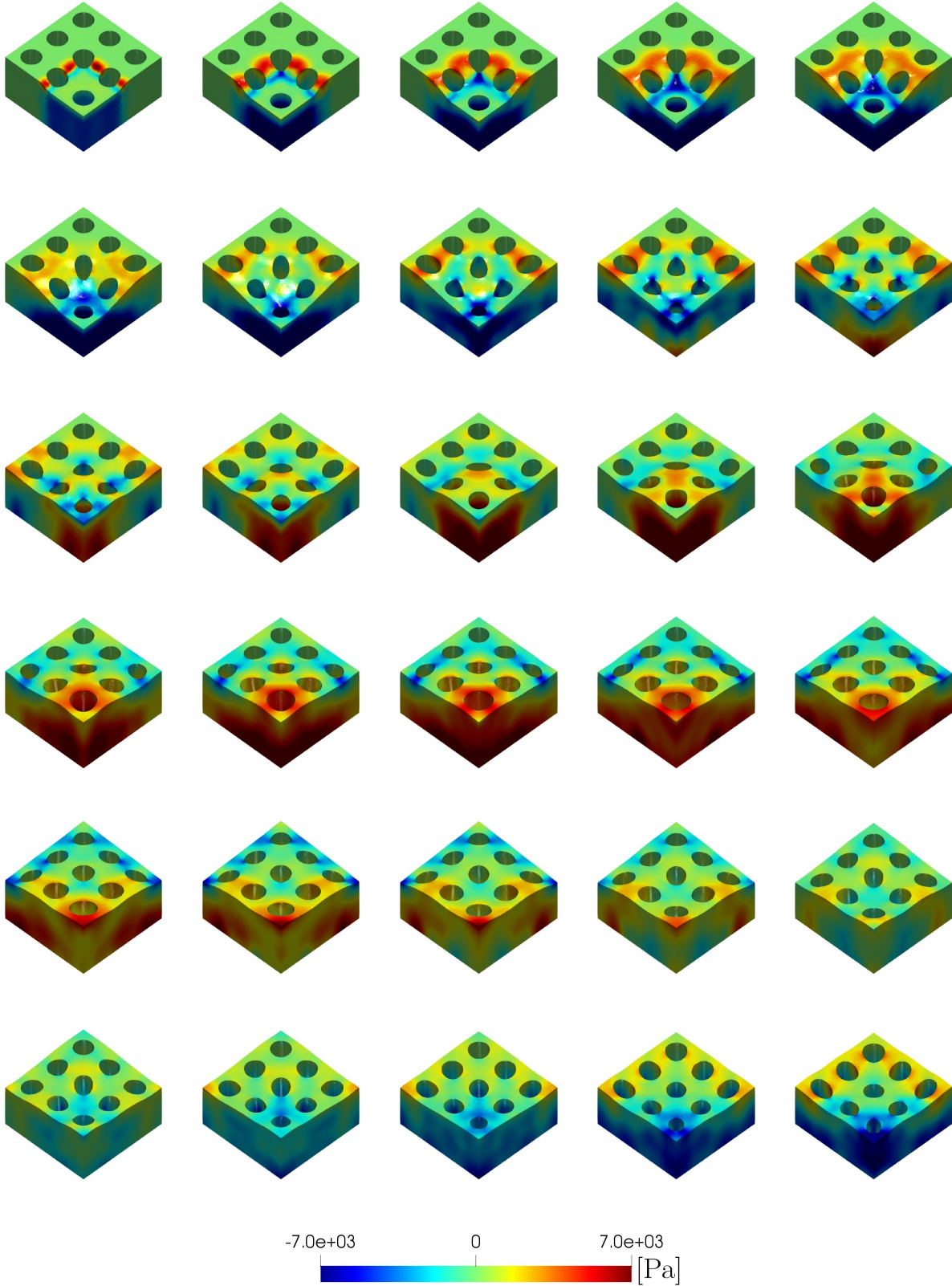


Figure 17: Punch block: a sequence of deformed structures with pressure distribution at times $t = \{10, 20, 30, \dots, 300\}$ ms (left to right and top to bottom). Results obtained using a polyconvex Mie-Grüneisen equation of state as described in (48). Their corresponding material parameters are summarised in Table 7.

Figures 13 and 14, that despite increasing the number of elements from 15,931 to 113,846, the deformation patterns predicted by the PG-FEM scheme are practically identical, but with improved resolution in pressure and temperature. The proposed PG-FEM scheme can clearly capture the extreme deformation of holes near the bottom plane, showing extremely good agreement with the results simulated using Upwind-VCFVM.

In Figure 15a, the evolution in time of the kinetic energy, internal energies (e.g. heat and mechanical contributions), total energy and ballistic energy are monitored. Notice that the difference between the total energy (blue discontinuous line) and the ballistic energy (red discontinuous line) is regarded as the global entropy associated with irreversible heat conduction, which is positive in this case. This is proven in Figure 15b as the value of global entropy is non-negative and increases over time. Figures 16 and 17 show a series of deformed states without experiencing any locking difficulties. No spurious pressure and/or temperature instabilities are observed despite simulating a rather complex geometry.

8.3.2. Bending of a thin plate

The bending behaviour of a thin structure is assessed [41] (see Figure 18a). The main aim of this example is to verify that PG-FEM circumvents the usual locking difficulties when simulating a thin structure. The thin plate is subjected to an initial velocity profile given by the following expression

$$\mathbf{v}|_{t=0} = \sqrt{\frac{2}{\pi}} \left[\exp\left(-\frac{(X-5)^2}{10}\right) + \exp\left(-\frac{(Y-5)^2}{10}\right) \right] \begin{bmatrix} 0 \\ 0 \\ 1 \end{bmatrix} \text{ (m/s)}. \quad (128)$$

For consideration of thermal effects, the plate is initially subjected to a uniform temperature distribution of $\theta|_{t=0} = \theta_R$, and a boundary (outflow) heat flux prescribed on the bottom surface of the plate defined as

$$Q_B(t) = \begin{cases} 10^3 \text{ (W/m}^2\text{)} & 0 \leq t \leq 2 \text{ s,} \\ 0 & t > 2 \text{ s.} \end{cases} \quad (129)$$

A polyconvex Mie-Grüneisen model (48) is chosen and a summary of the data simulation used is detailed in Table 8.

Aiming to show mesh convergence, three successively refined meshes are used. These include (**Mesh#I**) 39,366, (**Mesh#II**) 108,342 and (**Mesh#III**) 276,102 linear tetrahedral elements. Figure 19 compares the deformation process of the structure at time $t = \{1.5, 3, 4.5, 6\}$ s using those three meshes previously described. Similar results in terms of deformed shape and pressure field are observed. Figures 20a,b show the time history of the components of the global linear and angular momenta of the system. In particular, the global linear momentum is conserved under translation in space, whereas the angular momentum is perfectly conserved with the activation of angular momentum projection algorithm. In terms of energy plot, both the total energy and total entropy of the system first decrease as a result of heat loss induced by a positive value of external (heat) work, that is heat flows from inside to outside of the structure. After removal of the external heat flux at time $t = 2$ s, the total energy should stay constant in time. For satisfaction of the second law of thermodynamics, the total entropy of the underlying system should increase over time due to heat conduction. These are displayed in Figures 20c,d.

Finally, Figure 21 illustrates the time evolution of the deformation of a plate, displaying a smooth pressure. Top view and bottom view of the deformed structures are also displayed

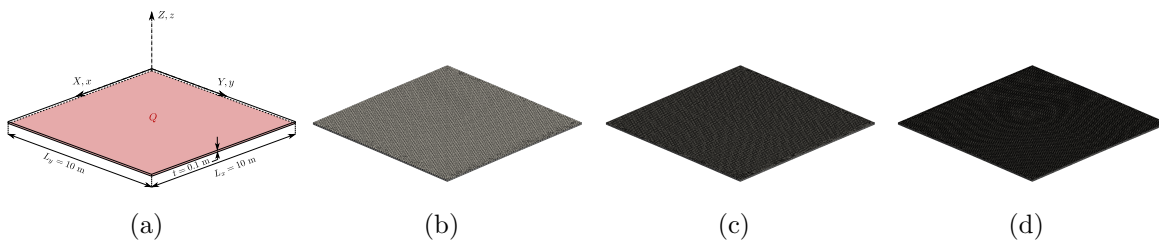


Figure 18: Thin plate: (a) geometry and its finite element discretisation, namely (b) **Mesh#I** (39,366 linear tetrahedra), (c) **Mesh#II** (108,340 linear tetrahedra) and (d) **Mesh#III** (276,192 linear tetrahedra).

Table 8: Thin plate: material parameters used in the simulation

Lamé parameters	μ	19.423	kPa
	λ	29.135	kPa
Specific heat capacity	C_v	1	$\text{JK}^{-1}\text{kg}^{-1}$
Reference temperature	θ_R	308.15	K
Thermal conductivity	h	10	$\text{WK}^{-1}\text{m}^{-1}$
Material density	ρ_R	1000	kgm^{-3}
Mie-Grüneisen coefficients	q	1	
	Γ_0	0.0281	

in Figure 22. It is remarkable seeing how the deformation behaviour of the structure can be captured.

8.4. Robustness

In order to assess the applicability and robustness of the proposed method, a challenging example is presented in this section. Specifically, implosion of a thin-walled bottle of thickness T is examined. Both the initial height H and outer diameter D_0 of the bottle, as well as the dimensions of its cross section, are shown in Figure 23. The bottle is subjected to (1) a constant internal pressure $p = -7.5$ (kPa) on the side walls thereby creating a suction effect, (2) an initial (uniform) temperature distribution of $\theta|_{t=0} = \theta_R$, and (3) a time-varying prescribed heat flux $Q_B(t)$ applied on the outer surface of the bottle, defined as

$$Q_B(t) = \begin{cases} -10^3 \sin\left(\frac{\pi t}{a}\right) \text{ (W/m}^2\text{)} & 0 \leq t \leq a, \\ 0 & t > a, \end{cases} \quad a = 5 \times 10^{-3} \text{ (s)}. \quad (130)$$

For computational efficiency, the problem is simplified by considering the existence of two symmetry planes and hence only a quarter of the domain is simulated. In this case, a polyconvex

Table 9: Bottle: material parameters used in the simulation

Lamé parameters	μ	6.5385	MPa
	λ	9.8077	MPa
Specific heat capacity	C_v	1	$\text{JK}^{-1}\text{kg}^{-1}$
Reference temperature	θ_R	293.15	K
Thermal conductivity	h	10	$\text{WK}^{-1}\text{m}^{-1}$
Material density	ρ_R	1100	kgm^{-3}
Mie-Grüneisen coefficients	q	1	
	Γ_0	8.5889	

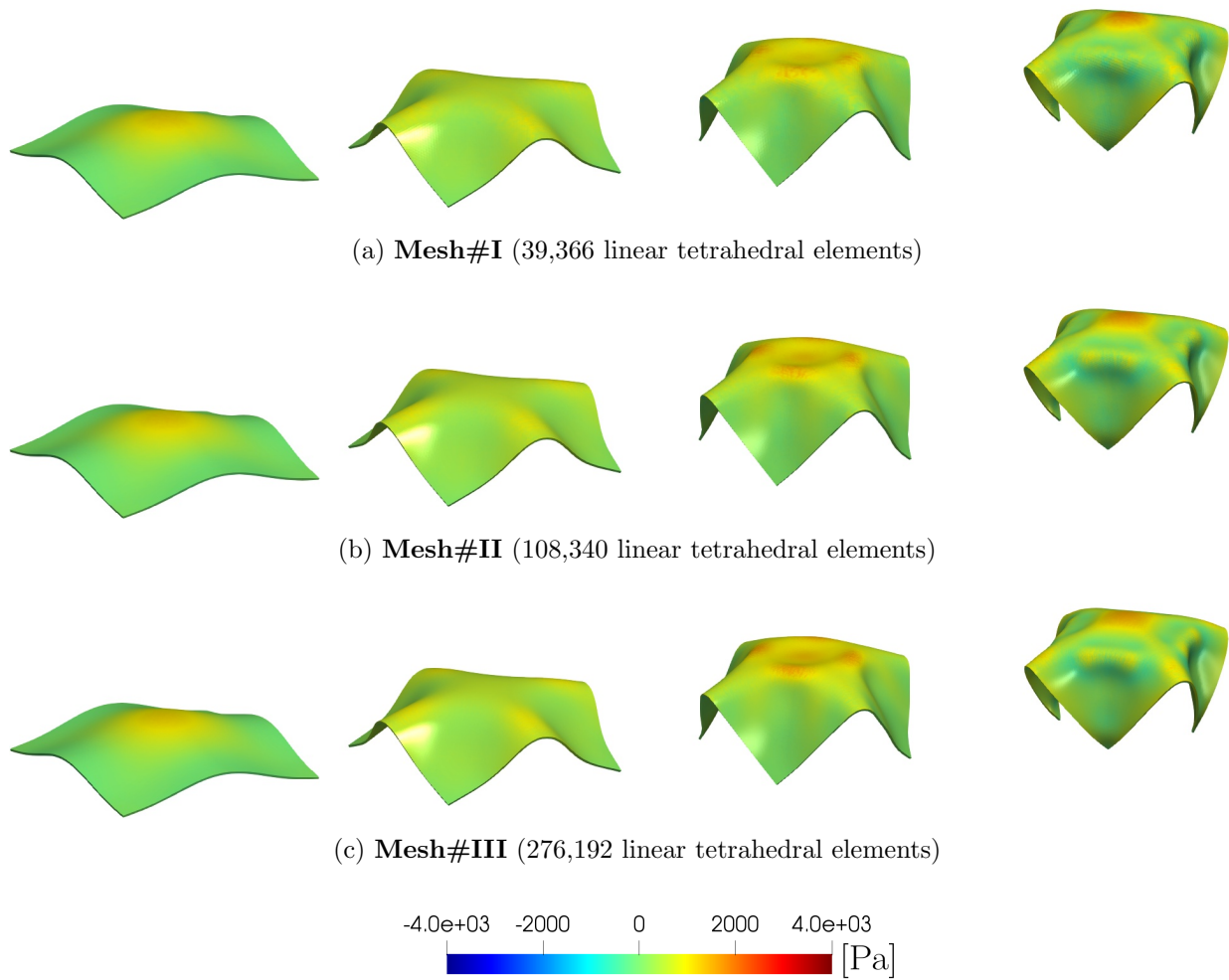
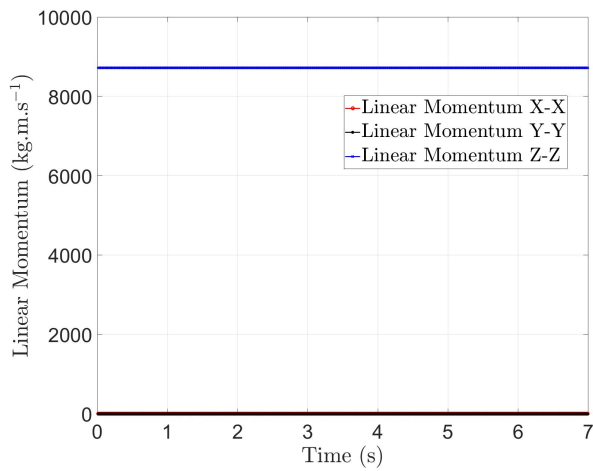
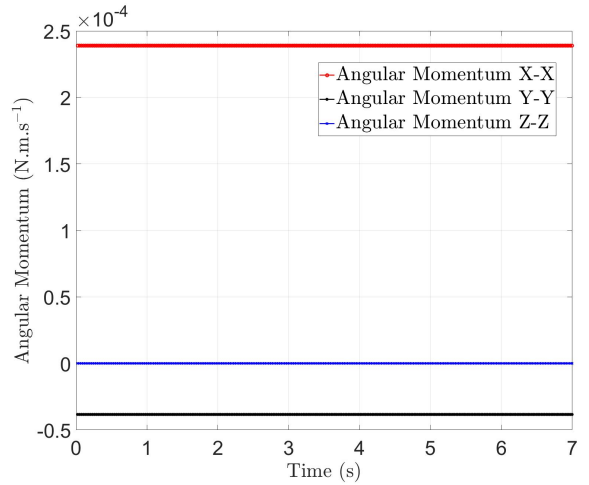


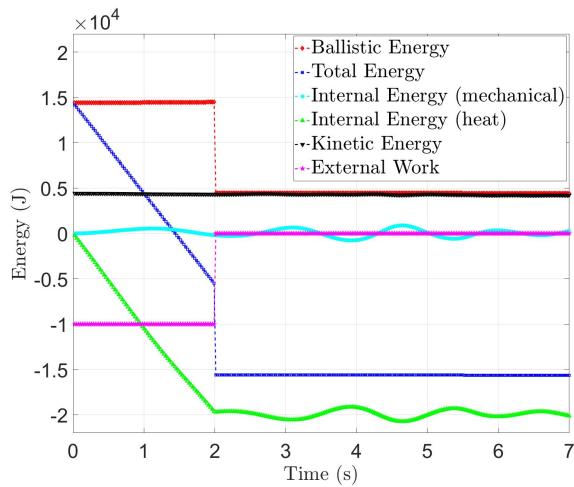
Figure 19: Thin plate: comparison of deformed shapes at time $t = \{1.5, 3, 4.5, 6\}$ s using three different meshes, where the colour contour plot indicates pressure field. A polyconvex Mie-Grüneisen thermo-elastic constitutive model as described in (48) is used, with material parameters being summarised in Table 8.



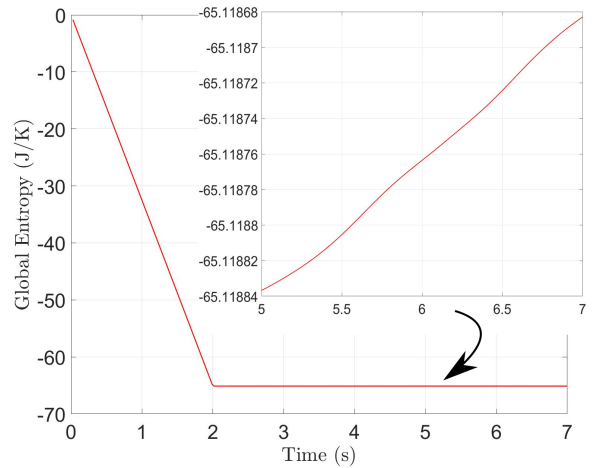
(a)



(b)



(c)



(d)

Figure 20: Thin plate: time evolution of (a) global linear momentum, (b) global angular momentum, (c) various energy measures, and (d) global entropy. A polyconvex Mie-Grüneisen thermo-elastic constitutive model as described in (48) is used. Their corresponding material parameters are summarised in Table 8.

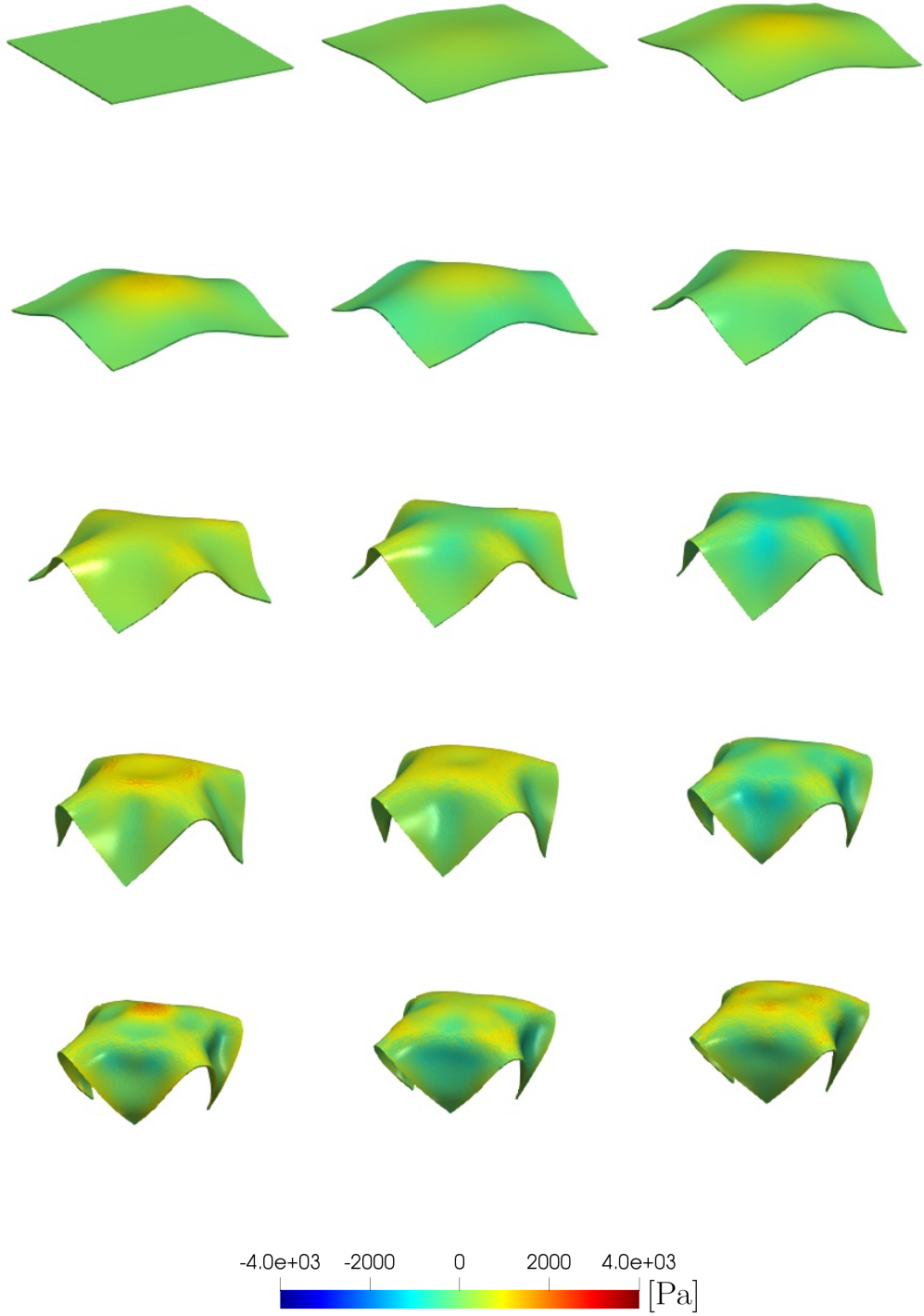
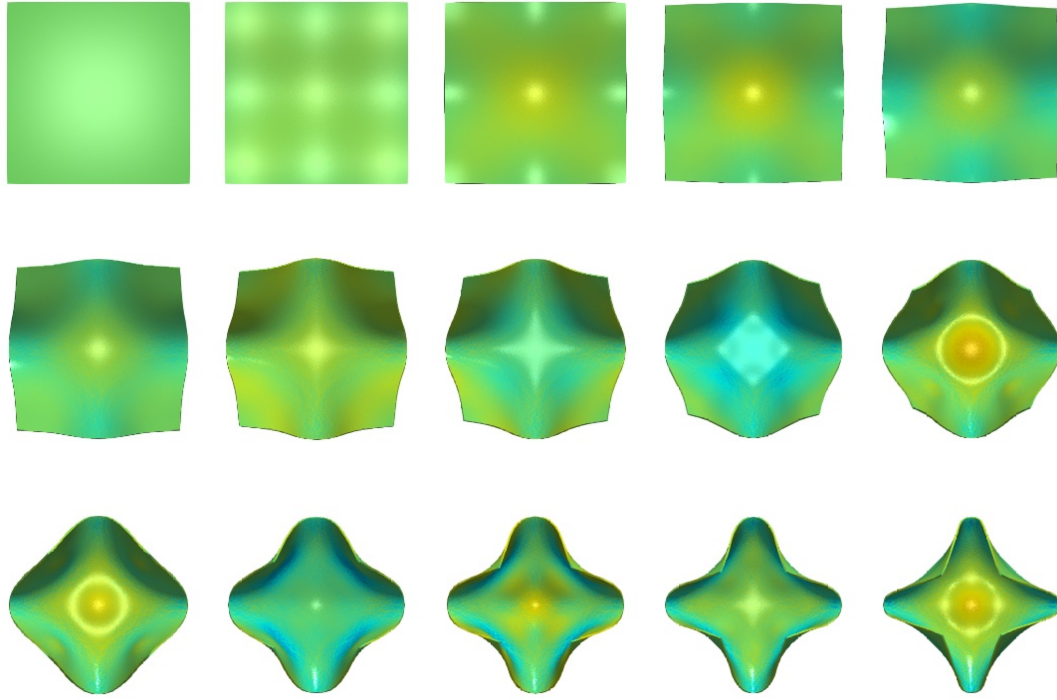
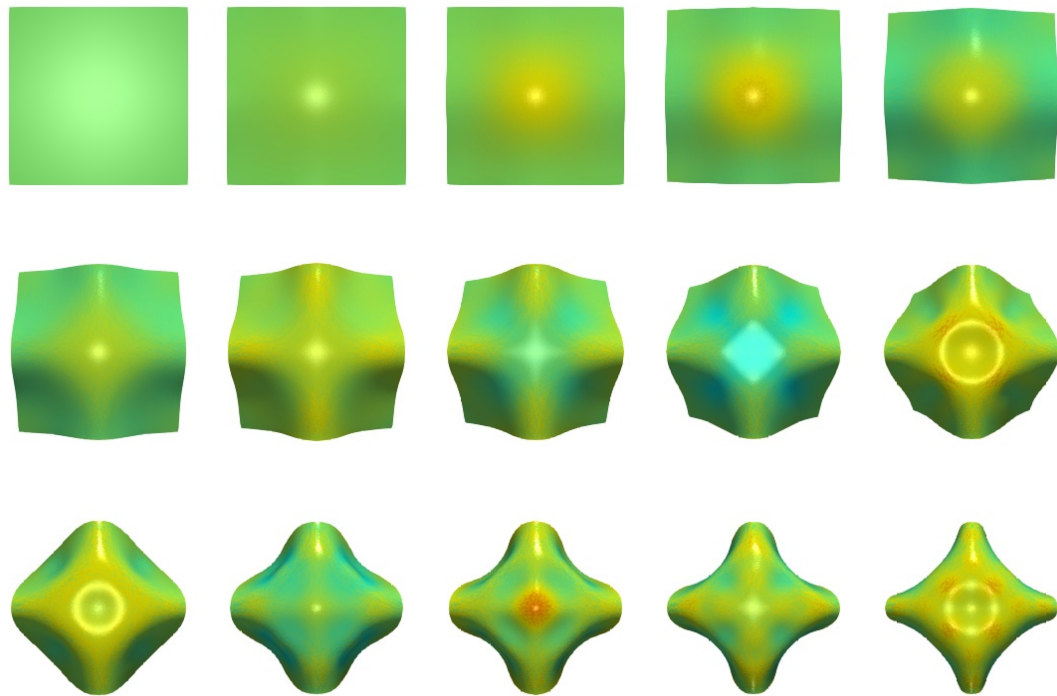


Figure 21: Thin plate: a sequence of deformed structures with pressure distribution at times $t = \{0, 0.5, 1, 1.5, 2, \dots, 7\}$ s (left to right and top to bottom). Results obtained using a polyconvex Mie-Grüneisen equation of state as described in (48). Their corresponding material parameters are summarised in Table 8.



(a) Bottom view



(b) Top view

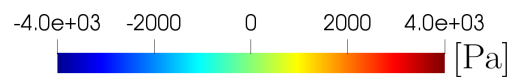


Figure 22: Thin plate: a sequence of deformed structures with pressure distribution at times $t = \{0, 0.5, 1, 1.5, 2, \dots, 7\}$ s (left to right and top to bottom): (a) bottom view and (b) top view. Results obtained using a polyconvex Mie-Grüneisen equation of state as described in (48). Their corresponding material parameters are summarised in Table 8.

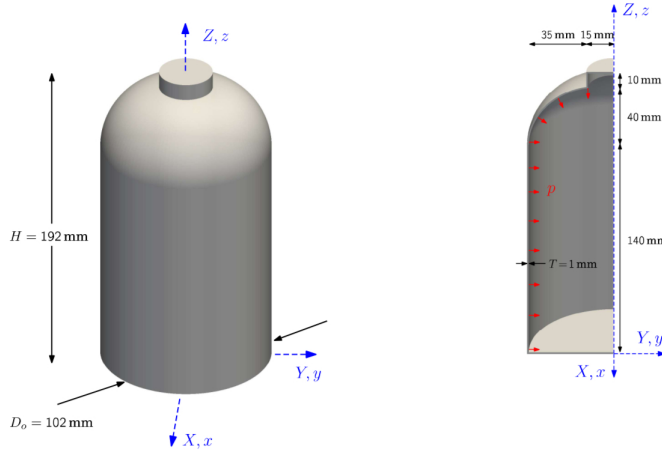


Figure 23: Implosive bottle: geometry of a bottle and its cross section

Mie-Grüneisen model is utilised. Both the geometry and material properties are presented in Table 9.

Aiming to show mesh independent convergence for this problem, successive refinement of meshes are explored and compared. For a quarter of the domain, we generate three dimensional linear tetrahedral mesh of (**Mesh#I**) 14,046, (**Mesh#II**) 30,022, (**Mesh#III**) 46,837 and (**Mesh#IV**) 53,535 number of elements. As shown in Figure 24, the pressure contour is smooth without showing any zero-energy modes. Convergence for both deformed shape and pressure profile can be observed when increasing the mesh density. It is worth pointing out that a noticeable change in the deformation pattern is observed as the mesh density is increased from **Mesh#I** to **Mesh#III**. Further mesh refinement (**Mesh#IV**) ensures that its deformation behaviour remains practically identical, thus guaranteeing mesh independence. For visualisation purposes, time evolution of the complex implosive process is shown in Figure 25. Complex deformation modes comprising wrinkled patterns are observed.

9. Conclusions

In this paper, a new computational framework has been introduced for the analysis of thermo-elasticity in the context of fast transient solid dynamics. In addition to conservation laws for the linear momentum \mathbf{p} , the deformation gradient tensor \mathbf{F} , its co-factor \mathbf{H} and its Jacobian J , formerly exploited in this series [1, 2] in the context of isothermal elasticity, a further conservation law, representing the first law of thermodynamics in terms of the entropy η (or total energy E), is incorporated to extend the range of applications into thermally coupled smooth (non-smooth) hyperelasticity.

From the continuum standpoint, the methodology is built upon the careful definition of polyconvex internal energy density functionals with respect to the extended set $\{\mathbf{F}, \mathbf{H}, J, \eta\}$ [47] by establishing sufficient conditions on the internal energy density and the entropy, when both are measured at a reference temperature. It is then shown how the ballistic energy [53] corresponds to a convex entropy function which, along with appropriate entropy fluxes, guarantees not only the hyperbolicity of the system but also the existence of a symmetrisation strategy when using appropriate entropy conjugate fields $\{\mathbf{v}, \Sigma_{\mathbf{F}}, \Sigma_{\mathbf{H}}, \Sigma_J, \vartheta\}$.

From the discretisation standpoint, and following previous work in the series, an explicit stabilised Petrov-Galerkin method is presented and implemented in the form of a Variational

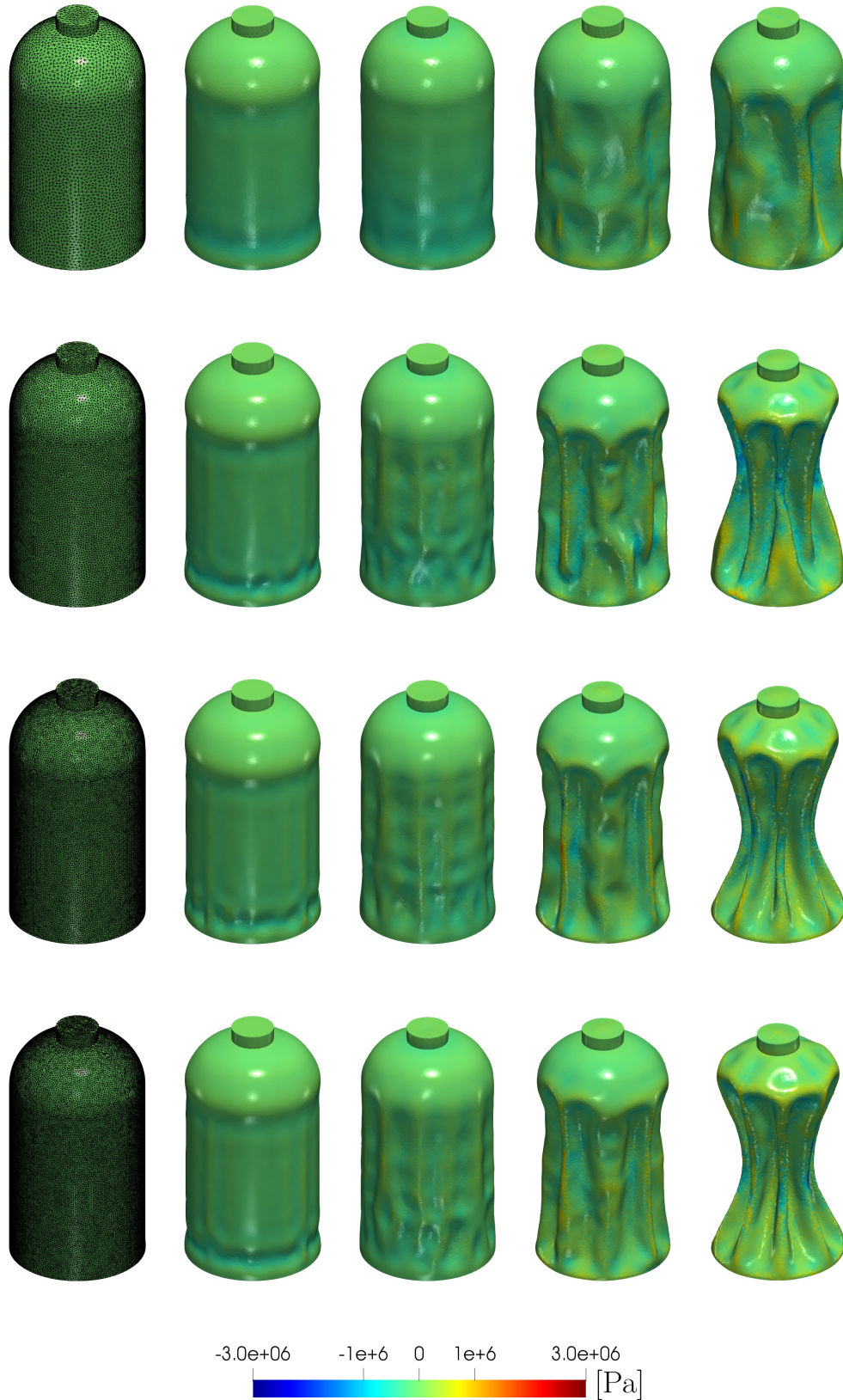


Figure 24: Imploding bottle: results obtained with meshes comprising of **Mesh#I** , **Mesh#II**, **Mesh#III** and **Mesh#IV** (top to bottom). First column shows four different mesh sizes, whereas the remaining columns show pressure contour plot at time $t = \{1.5, 3, 4.5, 6\}$ ms (from left to right). Both geometry and material properties used in the simulation are presented in Table 9.



Figure 25: Imploding bottle: results obtained with **Mesh#IV**. A sequence of deformation pattern at various time $t = \{0.3, 0.6, 0.9, \dots, 6\}$ ms (from left to right and top to bottom). Both geometry and material properties used in the simulation are presented in Table 9.

MultiScale method. This discretisation strategy is restricted to the case when the entropy η is used as unknown. Crucially, to ensure time stability of the explicit time integrator, the Courant-Friedrichs-Lewy number is computed based on an accurate estimation of the pressure and shear wave speeds, for which a detailed eigenvalue analysis is presented for two well-established thermo-elastic constitutive models, namely, the deviatoric-volumetric Mie-Grüneisen model and the modified entropic elasticity model.

An ample set of numerical examples is presented in order to assess the applicability and robustness of the proposed formulation. Both velocities, stresses (volumetric and deviatoric) and entropy display the same (second order) rate of convergence when using linear finite elements, in contrast to standard displacement based algorithms. The consideration of inelastic effects and the formulation of the problem in alternative descriptions, namely Eulerian and Arbitrary Lagrangian–Eulerian, constitute the next steps of our work.

Appendix A. Entropic elasticity

The simplest model that satisfies the sufficient conditions (i) to (iii) discussed in Section 3.4 is the case of modified entropic elasticity. In this model, the energy function $\tilde{\mathcal{E}}_R(\boldsymbol{\mathcal{X}})$ is postulated to be only a function of the volume ratio $\tilde{\mathcal{E}}_R(J)$, that is $\tilde{\mathcal{E}}_R(\boldsymbol{\mathcal{X}}) \approx \tilde{\mathcal{E}}_R(J)$. Following the work of [69, 89, 90], a simple linear energy potential for $\tilde{\mathcal{E}}_R(J)$ is adopted as

$$\tilde{\mathcal{E}}_R(J) = c_v \theta_R \Gamma_0 (J - 1). \quad (\text{A.1})$$

In order to obtain the coupling term $\tilde{\eta}_R(\boldsymbol{\mathcal{X}})$, recall first that the Helmholtz free energy at reference temperature ψ_R is

$$\psi_R(\boldsymbol{\mathcal{X}}) = \tilde{\mathcal{E}}_R(J) - \theta_R \tilde{\eta}_R(\boldsymbol{\mathcal{X}}), \quad (\text{A.2})$$

which, after rearranging, enables the entropy to be expressed as

$$-\tilde{\eta}_R(\boldsymbol{\mathcal{X}}) = \frac{1}{\theta_R} \left(\psi_R(\boldsymbol{\mathcal{X}}) - \tilde{\mathcal{E}}_R(J) \right). \quad (\text{A.3})$$

Since the function $\tilde{\mathcal{E}}_R(J)$ (A.1) is linear in J (and hence, $\frac{d^2 \tilde{\mathcal{E}}_R(J)}{dJ^2} = 0$), it is easy to show that $-\tilde{\eta}_R(\boldsymbol{\mathcal{X}})$ (A.3) is polyconvex in $\boldsymbol{\mathcal{X}}$ provided that $\psi_R(\boldsymbol{\mathcal{X}})$ is polyconvex in $\boldsymbol{\mathcal{X}}$. For instance, consider the possible polyconvex Helmholtz energy function proposed in Part I [1] as

$$\psi_R(\boldsymbol{\mathcal{X}}) = \alpha_R (II_{\mathbf{F}} - 3) + \beta_R (II_{\mathbf{H}} + 1) - 4\beta_R J - 2\alpha_R \ln J + \frac{\lambda_R}{2} (J - 1)^2, \quad (\text{A.4})$$

thus, a universally polyconvex internal energy density for modified entropic elasticity is

$$\mathcal{E}(\boldsymbol{\mathcal{X}}_\eta) = \tilde{\mathcal{E}}_R(J) + c_v \theta_R \left(e^{\eta/c_v} e^{(\psi_R(\boldsymbol{\mathcal{X}}) - \tilde{\mathcal{E}}_R(J))/c_v \theta_R} - 1 \right). \quad (\text{A.5})$$

With this, the conjugate stresses (10) become

$$\boldsymbol{\Sigma}_{\mathbf{F}}(\boldsymbol{\mathcal{X}}_\eta) = \frac{\Theta(\boldsymbol{\mathcal{X}}_\eta)}{\theta_R} \frac{\partial \psi_R}{\partial \mathbf{F}} = \frac{\Theta(\boldsymbol{\mathcal{X}}_\eta)}{\theta_R} (2\alpha_R \mathbf{F}); \quad \boldsymbol{\Sigma}_{\mathbf{H}}(\boldsymbol{\mathcal{X}}_\eta) = \frac{\Theta(\boldsymbol{\mathcal{X}}_\eta)}{\theta_R} \frac{\partial \psi_R}{\partial \mathbf{H}} = \frac{\Theta(\boldsymbol{\mathcal{X}}_\eta)}{\theta_R} (2\beta_R \mathbf{H}), \quad (\text{A.6})$$

and

$$\Sigma_J(\boldsymbol{\mathcal{X}}_\eta) = \frac{\Theta(\boldsymbol{\mathcal{X}}_\eta)}{\theta_R} \frac{\partial \psi_R}{\partial J} - \tilde{\vartheta}_{c_v} \Gamma_0 = \frac{\Theta(\boldsymbol{\mathcal{X}}_\eta)}{\theta_R} \left(-4\beta_R - \frac{2\alpha_R}{J} + \lambda_R (J - 1) \right) - \tilde{\vartheta}_{c_v} \Gamma_0. \quad (\text{A.7})$$

Here, $\tilde{\vartheta} = \tilde{\vartheta}(\boldsymbol{\mathcal{X}}_\eta) = \Theta(\boldsymbol{\mathcal{X}}_\eta) - \theta_R$ represents the temperature increment with $\Theta(\boldsymbol{\mathcal{X}}_\eta)$ being defined in (25). The Hessian operator $[\mathbb{H}_\mathcal{E}]$ adopts the following simple expression as

$$[\mathbb{H}_\mathcal{E}] = \begin{bmatrix} \mathcal{E}_{\mathbf{F}\mathbf{F}} & \mathcal{E}_{\mathbf{F}\mathbf{H}} & \mathcal{E}_{\mathbf{F}J} & \mathcal{E}_{\mathbf{F}\eta} \\ \mathcal{E}_{\mathbf{H}\mathbf{F}} & \mathcal{E}_{\mathbf{H}\mathbf{H}} & \mathcal{E}_{\mathbf{H}J} & \mathcal{E}_{\mathbf{H}\eta} \\ \mathcal{E}_{J\mathbf{F}} & \mathcal{E}_{J\mathbf{H}} & \mathcal{E}_{JJ} & \mathcal{E}_{J\eta} \\ \mathcal{E}_{\eta\mathbf{F}} & \mathcal{E}_{\eta\mathbf{H}} & \mathcal{E}_{\eta J} & \mathcal{E}_{\eta\eta} \end{bmatrix}, \quad (\text{A.8})$$

where Hessian components are

$$\begin{aligned} \mathcal{E}_{\mathbf{F}\mathbf{F}} &= \frac{\Theta}{\theta_R} \left[2\alpha_R \mathbf{I} + \frac{4\alpha_R^2}{c_v \theta_R} \mathbf{F} \otimes \mathbf{F} \right]; & \mathcal{E}_{\mathbf{H}\mathbf{H}} &= \frac{\Theta}{\theta_R} \left[2\beta_R \mathbf{I} + \frac{4\beta_R^2}{c_v \theta_R} \mathbf{H} \otimes \mathbf{H} \right]; \\ \mathcal{E}_{JJ} &= \frac{\Theta}{\theta_R} \left[f'' + \frac{1}{c_v \theta_R} (f' - c_v \theta_R \Gamma_0)^2 \right]; & \mathcal{E}_{\mathbf{F}\mathbf{H}} &= \frac{\Theta}{\theta_R} \frac{4\alpha_R \beta_R}{c_v \theta_R} \mathbf{F} \otimes \mathbf{H}; & \mathcal{E}_{\mathbf{H}\mathbf{F}} &= \frac{\Theta}{\theta_R} \frac{4\alpha_R \beta_R}{c_v \theta_R} \mathbf{H} \otimes \mathbf{F}; \\ \mathcal{E}_{\mathbf{F}J} &= \mathcal{E}_{J\mathbf{F}} = \frac{\Theta}{\theta_R} \frac{2\alpha_R}{c_v \theta_R} (f' - c_v \theta_R \Gamma_0) \mathbf{F}; & \mathcal{E}_{\mathbf{H}J} &= \mathcal{E}_{J\mathbf{H}} = \frac{\Theta}{\theta_R} \frac{2\beta_R}{c_v \theta_R} (f' - c_v \theta_R \Gamma_0) \mathbf{H}; \\ \mathcal{E}_{\mathbf{F}\eta} &= \mathcal{E}_{\eta\mathbf{F}} = \frac{\Theta}{c_v \theta_R} 2\alpha_R \mathbf{F}; & \mathcal{E}_{\mathbf{H}\eta} &= \mathcal{E}_{\eta\mathbf{H}} = \frac{\Theta}{c_v \theta_R} 2\beta_R \mathbf{H}; & \mathcal{E}_{J\eta} &= \mathcal{E}_{\eta J} = \frac{\Theta}{c_v \theta_R} (f' - c_v \theta_R \Gamma_0); \\ \mathcal{E}_{\eta\eta} &= \frac{\Theta}{c_v}, \end{aligned} \quad (\text{A.9})$$

with $f' = -4\beta_R - \frac{2\alpha_R}{J} + \lambda_R(J-1)$ and $f'' = \lambda_R + \frac{2\alpha_R}{J^2}$.

Using the Hessian components (A.8) described above, and repeating the exact same procedure carried out in Section 4, the thermo-mechanical acoustic tensor for this particular model (A.5) yields

$$\mathbf{C}_{NN} = \frac{\Theta}{\theta_R} \mathbf{C}_{NN}^\chi + \frac{\Theta}{\theta_R} \frac{1}{c_v \theta_R} [2(\alpha_R \Lambda_F + \beta_R \Lambda_M) + \Lambda_H (f' - c_v \theta_R \Gamma_0)]^2 \mathbf{n} \otimes \mathbf{n}, \quad (\text{A.10})$$

where \mathbf{C}_{NN}^χ represents the acoustic tensor associated with the polyconvex (isothermal) model described in (A.4). This term is already presented in Part I [1] and is repeated here for convenience (refer to equation (75) in [1])

$$\mathbf{C}_{NN}^\chi = 2\alpha_R \mathbf{I} + f'' \Lambda_H^2 \mathbf{n} \otimes \mathbf{n} + 2\beta_R (\Lambda_T^2 \mathbf{I} - \Lambda_T). \quad (\text{A.11})$$

As shown in Section 4, we can now obtain bounds of the wave speeds by assuming \mathbf{N} is a principal direction. This is achieved by substituting equation (A.10) into (77) and taking $\delta \mathbf{v} = \mathbf{v}_\alpha = \mathbf{n}$ to give

$$\rho_R c_p^2 = \frac{\Theta}{\theta_R} (2\alpha_R + \Lambda_H^2 f'' + 2\beta_R \Lambda_T^2) + \frac{\Theta}{\theta_R} \frac{1}{c_v \theta_R} [2(\alpha_R \Lambda_F + \beta_R \Lambda_M) + \Lambda_H (f' - c_v \theta_R \Gamma_0)]^2, \quad (\text{A.12})$$

from which the first set of eigenvalues corresponding to pressure wave c_p is

$$c_{1,2} = \pm c_p; \quad c_p = \sqrt{\frac{\Theta}{\theta_R} \left[\frac{2\alpha_R + \Lambda_H^2 f'' + 2\beta_R \Lambda_T^2}{\rho_R} + \frac{[2(\alpha_R \Lambda_F + \beta_R \Lambda_M) + \Lambda_H (f' - c_v \theta_R \Gamma_0)]^2}{c_v \theta_R \rho_R} \right]}. \quad (\text{A.13})$$

The remaining four eigenvalues correspond to shear waves where the vibration takes place on the propagation plane. The corresponding velocity vectors are orthogonal to \mathbf{n} and in the

directions of the unit eigenvectors $\{\mathbf{t}_1, \mathbf{t}_2\}$ of the rank two tensor $\mathbf{\Lambda}_T$. The wave speeds are given by $c_{3,4} = \pm c_{s_1}$ and $c_{5,6} = \pm c_{s_2}$ where

$$c_{s_1} = \sqrt{\frac{\Theta}{\theta_R} \left[\frac{2\alpha_R + 2\beta_R(\Lambda_T^2 - \lambda_1^2)}{\rho_R} \right]}; \quad c_{s_2} = \sqrt{\frac{\Theta}{\theta_R} \left[\frac{2\alpha_R + 2\beta_R(\Lambda_T^2 - \lambda_2^2)}{\rho_R} \right]}. \quad (\text{A.14})$$

Appendix B. Alternative conservation formulation for thermo-elasticity

In order to derive a suitable generalised entropy function for the alternative set of conservation variables $\hat{\mathbf{U}} = [\mathbf{p}, \mathbf{F}, \mathbf{H}, J, E]^T$, the convex entropy function as presented in (87) must now be re-written in terms of linear momentum \mathbf{p} , the triplet of deformation measures $\mathcal{X} = \{\mathbf{F}, \mathbf{H}, J\}$ and total energy E as

$$\hat{S}(\mathbf{p}, \mathcal{X}_E) = \hat{B}(\mathbf{p}, \mathcal{X}_E) = E - \theta_R \hat{\eta}(\mathbf{p}, \mathcal{X}_E); \quad \mathcal{X}_E = \{\mathcal{X}, E\} = \{\mathbf{F}, \mathbf{H}, J, E\}. \quad (\text{B.1})$$

As shown by Wagner in [74], the function $-\hat{\eta}(\mathbf{p}, \mathcal{X}_E)$ is convex in \mathbf{p} and \mathcal{X}_E . In this representation, and noticing that $\hat{\mathcal{E}}(\mathcal{X}, \hat{\eta}(\mathbf{p}, \mathcal{X}_E)) = E - \frac{1}{2\rho_R} \mathbf{p} \cdot \mathbf{p}$, the entropy $\hat{\eta}(\mathbf{p}, \mathcal{X}_E)$ is obtained implicitly via the following expression $\varphi(\mathbf{p}, \mathcal{X}_E, \hat{\eta})$ defined as [74]

$$0 = \varphi(\mathbf{p}, \mathcal{X}_E, \hat{\eta}) = \hat{\mathcal{E}}(\mathcal{X}, \hat{\eta}) - \left(E - \frac{1}{2\rho_R} \mathbf{p} \cdot \mathbf{p} \right). \quad (\text{B.2})$$

Differentiating $\hat{S}(\mathbf{p}, \mathcal{X}_E)$ (B.1) gives the conjugate entropy variables $\hat{\mathbf{V}}$ as

$$\hat{\mathbf{V}} = \frac{\partial \hat{S}(\mathbf{p}, \mathcal{X}_E)}{\partial \hat{\mathbf{U}}} = \begin{bmatrix} \frac{\partial \hat{S}}{\partial \mathbf{p}} \\ \frac{\partial \hat{S}}{\partial \mathbf{F}} \\ \frac{\partial \hat{S}}{\partial \mathbf{H}} \\ \frac{\partial \hat{S}}{\partial J} \\ \frac{\partial \hat{S}}{\partial E} \end{bmatrix} = \begin{bmatrix} \Gamma_{\mathbf{p}} \\ \Gamma_{\mathbf{F}} \\ \Gamma_{\mathbf{H}} \\ \Gamma_J \\ \Gamma_E \end{bmatrix} = \begin{bmatrix} -\theta_R \frac{\partial \hat{\eta}(\mathbf{p}, \mathcal{X}_E)}{\partial \mathbf{p}} \\ -\theta_R \frac{\partial \hat{\eta}(\mathbf{p}, \mathcal{X}_E)}{\partial \mathbf{F}} \\ -\theta_R \frac{\partial \hat{\eta}(\mathbf{p}, \mathcal{X}_E)}{\partial \mathbf{H}} \\ -\theta_R \frac{\partial \hat{\eta}(\mathbf{p}, \mathcal{X}_E)}{\partial J} \\ 1 - \theta_R \frac{\partial \hat{\eta}(\mathbf{p}, \mathcal{X}_E)}{\partial E} \end{bmatrix}. \quad (\text{B.3})$$

To complete the above equation, it is now necessary to compute the derivatives of $\hat{\eta}(\mathbf{p}, \mathcal{X}_E)$ by differentiation of φ (B.2) with respect to each component of $\hat{\mathbf{U}}$. By using the chain rule, the derivative of $\hat{\eta}(\mathbf{p}, \mathcal{X}_E)$ with respect to \mathbf{p} can first be achieved as

$$\mathbf{0} = \frac{\partial \varphi(\mathbf{p}, \mathcal{X}_E, \hat{\eta}(\mathbf{p}, \mathcal{X}_E))}{\partial \mathbf{p}} + \frac{\partial \varphi(\mathbf{p}, \mathcal{X}_E, \hat{\eta})}{\partial \hat{\eta}} \frac{\partial \hat{\eta}(\mathbf{p}, \mathcal{X}_E)}{\partial \mathbf{p}}. \quad (\text{B.4a})$$

Since $\frac{\partial \varphi(\mathbf{p}, \mathcal{X}_E, \hat{\eta})}{\partial \hat{\eta}} = \frac{\partial \hat{\mathcal{E}}(\mathcal{X}, \hat{\eta})}{\partial \hat{\eta}} = \theta$, equation above after rearranging becomes

$$-\frac{\partial \hat{\eta}(\mathbf{p}, \mathcal{X}_E)}{\partial \mathbf{p}} = \left(\frac{\partial \varphi}{\partial \hat{\eta}} \right)^{-1} \frac{\partial \varphi}{\partial \mathbf{p}} = \frac{\mathbf{v}}{\theta}. \quad (\text{B.5})$$

Repeating the same procedure on the derivatives of $\hat{\eta}$ with respect to \mathbf{F} , \mathbf{H} , J and E ,

results in

$$-\frac{\partial \hat{\eta}(\mathbf{p}, \boldsymbol{\chi}_E)}{\partial \mathbf{F}} = \left(\frac{\partial \varphi}{\partial \hat{\eta}} \right)^{-1} \frac{\partial \varphi}{\partial \mathbf{F}} = \frac{1}{\theta} \boldsymbol{\Sigma}_{\mathbf{F}}; \quad (\text{B.6a})$$

$$-\frac{\partial \hat{\eta}(\mathbf{p}, \boldsymbol{\chi}_E)}{\partial \mathbf{H}} = \left(\frac{\partial \varphi}{\partial \hat{\eta}} \right)^{-1} \frac{\partial \varphi}{\partial \mathbf{H}} = \frac{1}{\theta} \boldsymbol{\Sigma}_{\mathbf{H}}; \quad (\text{B.6b})$$

$$-\frac{\partial \hat{\eta}(\mathbf{p}, \boldsymbol{\chi}_E)}{\partial J} = \left(\frac{\partial \varphi}{\partial \hat{\eta}} \right)^{-1} \frac{\partial \varphi}{\partial J} = \frac{1}{\theta} \boldsymbol{\Sigma}_J; \quad (\text{B.6c})$$

$$-\frac{\partial \hat{\eta}(\mathbf{p}, \boldsymbol{\chi}_E)}{\partial E} = \left(\frac{\partial \varphi}{\partial \hat{\eta}} \right)^{-1} \frac{\partial \varphi}{\partial E} = \frac{1}{\theta}. \quad (\text{B.6d})$$

Finally, by combining equations (B.6) and (B.1), components of the conjugate entropy variables (B.3) are

$$\Gamma_{\mathbf{p}} = \frac{\theta_R}{\theta} \mathbf{v}; \quad \Gamma_{\mathbf{F}} = \frac{\theta_R}{\theta} \boldsymbol{\Sigma}_{\mathbf{F}}; \quad \Gamma_{\mathbf{H}} = \frac{\theta_R}{\theta} \boldsymbol{\Sigma}_{\mathbf{H}}; \quad \Gamma_J = \frac{\theta_R}{\theta} \boldsymbol{\Sigma}_J; \quad \Gamma_E = \frac{\vartheta}{\theta}, \quad (\text{B.7})$$

respectively.

Appendix C. Linearisation of thermo-elasticity equations

This Appendix is included to derive a linearised version of internal strain energy \mathcal{E}^{Lin} followed by the computation of the first Piola Kirchoff stress tensor. To derive this, we use the concept of directional derivative [71] by linearising an internal energy $\mathcal{E}(\boldsymbol{\chi}_\eta)$ with respect to a reference configuration $\{\boldsymbol{\chi}_I, \eta = 0\}$ demonstrated as below

$$\begin{aligned} \mathcal{E}^{\text{Lin}}(\delta \boldsymbol{\chi}, \delta \eta) &\approx \underbrace{\mathcal{E}(\boldsymbol{\chi}_I, \eta = 0)}_0 + D\mathcal{E}|_{\boldsymbol{\chi}_{I,0}}[\delta \boldsymbol{\chi}, \delta \eta] + \frac{1}{2}D(D\mathcal{E}[\delta \boldsymbol{\chi}, \delta \eta])|_{\boldsymbol{\chi}_{I,0}}[\delta \boldsymbol{\chi}, \delta \eta] \\ &\approx D\mathcal{E}|_{\boldsymbol{\chi}_{I,0}}[\delta \boldsymbol{\chi}, \delta \eta] + \frac{1}{2}D(D\mathcal{E}[\delta \boldsymbol{\chi}, \delta \eta])|_{\boldsymbol{\chi}_{I,0}}[\delta \boldsymbol{\chi}, \delta \eta]. \end{aligned} \quad (\text{C.1})$$

To achieve this, recall first that the general internal strain energy function (48) is

$$\mathcal{E}(\boldsymbol{\chi}_\eta) = \tilde{\mathcal{E}}_R(\boldsymbol{\chi}) + c_v (\Theta_0(J) e^{\eta/c_v} - 1); \quad \Theta_0(J) = \theta_R e^{-\tilde{\eta}_R(J)/c_v}, \quad (\text{C.2})$$

and also notice that $\frac{d\Theta_0(J)}{dJ} = -\frac{\Theta_0}{c_v} \frac{d\tilde{\eta}_R(J)}{dJ}$, the directional derivative of the energy above becomes

$$\begin{aligned} D\mathcal{E}(\boldsymbol{\chi}_\eta)[\delta \boldsymbol{\chi}, \delta \eta] &= D\tilde{\mathcal{E}}_R(\boldsymbol{\chi})[\delta \boldsymbol{\chi}] + c_v D(\Theta_0(J) e^{\eta/c_v})[\delta J, \delta \eta] \\ &= \left(\frac{\partial \tilde{\mathcal{E}}_R}{\partial \mathbf{F}} + \frac{\partial \tilde{\mathcal{E}}_R}{\partial \mathbf{H}} \boldsymbol{\times} \mathbf{F} + \frac{\partial \tilde{\mathcal{E}}_R}{\partial J} \mathbf{H} \right) : \delta \mathbf{F} + c_v e^{\eta/c_v} \left[\left(\frac{d\Theta_0}{dJ} \delta J \right) + \left(\frac{\Theta_0(J)}{c_v} \delta \eta \right) \right] \\ &= \left(\frac{\partial \tilde{\mathcal{E}}_R}{\partial \mathbf{F}} + \frac{\partial \tilde{\mathcal{E}}_R}{\partial \mathbf{H}} \boldsymbol{\times} \mathbf{F} + \frac{\partial \tilde{\mathcal{E}}_R}{\partial J} \mathbf{H} \right) : \delta \mathbf{F} + \Theta_0(J) e^{\eta/c_v} \left(\delta \eta - \frac{d\tilde{\eta}_R(J)}{dJ} \delta J \right) \\ &= \left(\frac{\partial \tilde{\mathcal{E}}_R}{\partial \mathbf{F}} + \frac{\partial \tilde{\mathcal{E}}_R}{\partial \mathbf{H}} \boldsymbol{\times} \mathbf{F} + \left(\frac{\partial \tilde{\mathcal{E}}_R}{\partial J} - \Theta \frac{d\tilde{\eta}_R(J)}{dJ} \right) \mathbf{H} \right) : \delta \mathbf{F} + \Theta \delta \eta \\ &= \mathbf{P} : \delta \mathbf{F} + \Theta \delta \eta, \end{aligned} \quad (\text{C.3})$$

with $\Theta(J, \eta) = \Theta_0(J)e^{\eta/c_v}$. Consequently, further application of directional derivative on the above expression gives

$$\begin{aligned}
D(D\mathcal{E}[\delta\boldsymbol{\mathcal{X}}, \delta\eta])[\delta\boldsymbol{\mathcal{X}}, \delta\eta] &= D\mathbf{P}[\delta\boldsymbol{\mathcal{X}}, \delta\eta] : \delta\mathbf{F} + D\Theta[\delta J, \delta\eta]\delta\eta \\
&= \begin{bmatrix} \delta\mathbf{F} \\ \mathbf{F} \times \delta\mathbf{F} \\ \mathbf{H} : \delta\mathbf{F} \\ \delta\eta \end{bmatrix}^T \underset{[\mathbb{H}\mathcal{E}]}{\begin{bmatrix} \delta\mathbf{F} \\ \mathbf{F} \times \delta\mathbf{F} \\ \mathbf{H} : \delta\mathbf{F} \\ \delta\eta \end{bmatrix}} + e^{\eta/c_v} \frac{d\Theta_0(J)}{dJ} \delta\eta \delta J + \frac{\Theta_0(J)}{c_v} e^{\eta/c_v} (\delta\eta)^2 \\
&= \begin{bmatrix} \delta\mathbf{F} \\ \mathbf{F} \times \delta\mathbf{F} \\ \mathbf{H} : \delta\mathbf{F} \\ \delta\eta \end{bmatrix}^T \underset{[\mathbb{H}\mathcal{E}]}{\begin{bmatrix} \delta\mathbf{F} \\ \mathbf{F} \times \delta\mathbf{F} \\ \mathbf{H} : \delta\mathbf{F} \\ \delta\eta \end{bmatrix}} + \frac{\Theta}{c_v} \left((\delta\eta)^2 - \frac{d\tilde{\eta}_R}{dJ} \delta J \delta\eta \right).
\end{aligned} \tag{C.4}$$

With these at hand, we are now in a position to derive the linearised internal energy $\mathcal{E}^{\text{Lin}}(\mathbf{F}, \eta)$ as described in (C.1). This indeed can be achieved by first noticing that both derivatives (C.3) and (C.4) defined at reference state $\{\boldsymbol{\mathcal{X}}_I, \eta = 0\}$ become

$$D\mathcal{E}|_{\boldsymbol{\mathcal{X}}_I, 0}[\delta\boldsymbol{\mathcal{X}}, \delta\eta] = \theta_R \delta\eta \tag{C.5}$$

and

$$D(D\mathcal{E}[\delta\boldsymbol{\mathcal{X}}, \delta\eta])|_{\boldsymbol{\mathcal{X}}_I, 0}[\delta\boldsymbol{\mathcal{X}}, \delta\eta] = \delta\mathbf{F} : \mathbf{C}^{\text{Lin}} : \delta\mathbf{F} + \frac{\theta_R}{c_v} (\delta\eta - c_v \Gamma_0 \text{tr} \delta\mathbf{F})^2 + (1-q) \theta_R c_v \Gamma_0 (\text{tr} \delta\mathbf{F})^2, \tag{C.6}$$

where the fourth order linear elasticity tensor is defined as

$$\mathbf{C}^{\text{Lin}} = \lambda \mathbf{I} \otimes \mathbf{I} + \mu (\boldsymbol{\mathcal{I}} + \tilde{\boldsymbol{\mathcal{I}}}), \tag{C.7}$$

with $[\mathbf{I} \otimes \mathbf{I}]_{iIjJ} = \delta_{iI} \delta_{jJ}$, $[\boldsymbol{\mathcal{I}}]_{iIjJ} = \delta_{ij} \delta_{IJ}$ and $[\tilde{\boldsymbol{\mathcal{I}}}]_{iIjJ} = \delta_{iJ} \delta_{Ij}$. Using these expressions, and replacing $\delta\mathbf{F}$ with \mathbf{F} and $\delta\eta$ with η , the linearised internal energy (C.1) becomes

$$\mathcal{E}^{\text{Lin}}(\mathbf{F}, \eta) = \tilde{\mathcal{E}}_R^{\text{Lin}}(\mathbf{F}) + \theta_R \eta + \frac{\theta_R}{2c_v} (\eta - c_v \Gamma_0 (\text{tr} \mathbf{F} - 3))^2 + \frac{1}{2} (1-q) \theta_R c_v \Gamma_0 (\text{tr} \mathbf{F} - 3)^2, \tag{C.8}$$

with the classical linear elastic model [71] being defined as

$$\tilde{\mathcal{E}}_R^{\text{Lin}}(\mathbf{F}) = \frac{\mu_R}{4} [(\mathbf{F} + \mathbf{F}^T - 2\mathbf{I}) : (\mathbf{F} + \mathbf{F}^T - 2\mathbf{I})] + \frac{\lambda_R}{2} (\text{tr} \mathbf{F} - 3)^2. \tag{C.9}$$

The first Piola-Kirchhoff stress now follows

$$\mathbf{P}(\mathbf{F}, \eta) = \mu_R (\mathbf{F} + \mathbf{F}^T - 2\mathbf{I}) + \hat{\lambda}_R (\text{tr} \mathbf{F} - 3) \mathbf{I} - \theta_R \Gamma_0 (\eta - c_v \Gamma_0 (\text{tr} \mathbf{F} - 3)) \mathbf{I}; \quad \hat{\lambda}_R = \lambda_R + (1-q) \theta_R c_v \Gamma_0. \tag{C.10}$$

Alternatively, and noting that the linearised entropy function is in the form of [62]

$$\tilde{\eta}(\mathbf{F}, \theta) = c_v \Gamma_0 (\text{tr} \mathbf{F} - 3) + c_v \left(\frac{\theta}{\theta_R} - 1 \right), \tag{C.11}$$

the first Piola-Kirchhoff stress (C.10) can now be written in terms of $\{\mathbf{F}, \theta\}$ as

$$\tilde{\mathbf{P}}(\mathbf{F}, \theta) = \mu_R (\mathbf{F} + \mathbf{F}^T - 2\mathbf{I}) + \hat{\lambda}_R (\text{tr} \mathbf{F} - 3) \mathbf{I} - c_v \Gamma_0 \theta_R \left(\frac{\theta}{\theta_R} - 1 \right) \mathbf{I}. \tag{C.12}$$

Acknowledgements

The second author gratefully acknowledges the support provided by the EPSRC Strategic Support Package: Engineering of Active Materials by Multiscale/Multiphysics Computational Mechanics - EP/R008531/1. The third author acknowledges the financial support received through the European Training Network Protection (Project ID: 764636). The third and fourth authors would also like to acknowledge the financial support received through the European Commission EACEA Agency, Framework Partnership Agreement 2013-0043 Erasmus Mundus Action 1b, as a part of the EM Joint Doctorate “Simulation in Engineering and Entrepreneurship Development (SEED)”.

References

- [1] J. Bonet, A. J. Gil, C. H. Lee, M. Aguirre, R. Ortigosa, A first order hyperbolic framework for large strain computational solid dynamics. Part I: Total Lagrangian isothermal elasticity, *Computer Methods in Applied Mechanics and Engineering* 283 (2015) 689–732.
- [2] A. J. Gil, C. H. Lee, J. Bonet, R. Ortigosa, A first order hyperbolic framework for large strain computational solid dynamics. Part II: Total Lagrangian compressible, nearly incompressible and truly incompressible elasticity, *Computer Methods in Applied Mechanics and Engineering* 300 (2016) 146–181.
- [3] C. H. Lee, A. J. Gil, J. Bonet, Development of a cell centred upwind finite volume algorithm for a new conservation law formulation in structural dynamics, *Computers and Structures* 118 (2013) 13–38.
- [4] J. Bonet, A. J. Burton, A simple average nodal pressure tetrahedral element for incompressible and nearly incompressible dynamic explicit applications, *Communications in Numerical Methods in Engineering* 14 (1998) 437–449.
- [5] C. R. Dohrmann, M. W. Heinstein, J. Jung, S. W. Key, W. R. Witkowski, Node-based uniform strain elements for three-node triangular and four-node tetrahedral meshes, *International Journal for Numerical Methods in Engineering* 47 (2000) 1549–1568.
- [6] J. Bonet, H. Marriott, O. Hassan, An averaged nodal deformation gradient linear tetrahedral element for large strain explicit dynamic applications, *Communications in Numerical Methods in Engineering* 17 (2001) 551–561.
- [7] J. Bonet, H. Marriott, O. Hassan, Stability and comparison of different linear tetrahedral formulations for nearly incompressible explicit dynamic applications, *International Journal for Numerical Methods in Engineering* 50 (2001) 119–133.
- [8] M. W. Gee, C. R. Dohrmann, S. W. Key, W. A. Wall, A uniform nodal strain tetrahedron with isochoric stabilization, *International Journal for Numerical Methods in Engineering* 78 (2009) 429–443.
- [9] T. J. R. Hughes, Generalization of selective integration procedures to anisotropic and nonlinear media, *International Journal for Numerical Methods in Engineering* 15 (1980) 1413–1418.
- [10] E. A. de Souza Neto, D. Peric, M. Dutko, D. R. J. Owen, Design of simple low order finite elements for large strain analysis of nearly incompressible solids, *International Journal of Solids and Structures* 33 (1996) 3277–3296.
- [11] Y. Onishi, K. Amaya, A locking-free selective smoothed finite element method using tetrahedral and triangular elements with adaptive mesh rezoning for large deformation problems, *International Journal for Numerical Methods in Engineering* 99 (2014) 354–371.
- [12] S. K. Lahiri, J. Bonet, J. Peraire, A variationally consistent mesh adaptation method for triangular elements in explicit Lagrangian dynamics, *International Journal for Numerical Methods in Engineering* 82 (2010) 1073–1113.

- [13] J. Chung, G. M. Hulbert, A time integration algorithm for structural dynamics with improved numerical dissipation: The generalized α method, *Journal of Applied Mechanics* 60 (1993) 371–375.
- [14] S. K. Lahiri, J. Bonet, J. Peraire, L. Casals, A variationally consistent fractional time-step integration method for incompressible and nearly incompressible Lagrangian dynamics, *International Journal for Numerical Methods in Engineering* 63 (2005) 1371–1395.
- [15] A. J. Gil, P. D. Ledger, A coupled *hp*-finite element scheme for the solution of two-dimensional electrostrictive materials, *International Journal for Numerical Methods in Engineering* 91 (2012) 1158–1183.
- [16] J. A. Trangenstein, A second-order Godunov algorithm for two-dimensional solid mechanics, *Computational Mechanics* 13 (1994) 343–359.
- [17] J. A. Trangenstein, P. Colella, A higher-order Godunov method for modelling finite deformation in elastic-plastic solids, *Communications on Pure and Applied Mathematics* 44 (1991) 41–100.
- [18] B. Després, C. Mazeran, Lagrangian gas dynamics in two dimensions and Lagrangian systems, *Archive for Rational Mechanics and Analysis* 178 (2005) 327–372.
- [19] G. Kluth, B. Després, Discretization of hyperelasticity on unstructured mesh with a cell-centered Lagrangian scheme, *Journal of Computational Physics* 229 (2010) 9092–9118.
- [20] G. Georges, J. Breil, P. H. Maire, A 3D finite volume scheme for solving the updated Lagrangian form of hyperelasticity, *International Journal for Numerical Methods in Fluids* 84 (2017) 41–54.
- [21] G. Scovazzi, B. Carnes, X. Zeng, S. Rossi, A simple, stable, and accurate linear tetrahedral finite element for transient, nearly and fully incompressible solid dynamics: A dynamic variational multiscale approach, *International Journal for Numerical Methods in Engineering* 106 (2016) 799–839.
- [22] S. Rossi, N. Abboud, G. Scovazzi, Implicit finite incompressible elastodynamics with linear finite elements: A stabilized method in rate form, *Computer Methods in Applied Mechanics and Engineering* 311 (2016) 208–249.
- [23] N. Abboud, G. Scovazzi, Elastoplasticity with linear tetrahedral elements: A variational multiscale method, *International Journal for Numerical Methods in Engineering* 115 (2018).
- [24] X.Zeng, G. Scovazzi, N. Abboud, O. Colomes, S. Rossi, A dynamic variational multiscale method for viscoelasticity using linear tetrahedral elements, *International Journal for Numerical Methods in Engineering* 112 (2018).
- [25] G. Scovazzi, T. Song, X. Zeng, A velocity/stress mixed stabilized nodal finite element for elastodynamics: Analysis and computations with strongly and weakly enforced boundary conditions, *Computer Methods in Applied Mechanics and Engineering* 325 (2017) 532 – 576.

- [26] M. Cervera, M. Chiumenti, R. Codina, Mixed stabilized finite element methods in nonlinear solid mechanics: Part I: Formulation, *Computer Methods in Applied Mechanics and Engineering* 199 (2010) 2559–2570.
- [27] M. Cervera, M. Chiumenti, R. Codina, Mixed stabilized finite element methods in nonlinear solid mechanics. Part II: Strain localization, *Computer Methods in Applied Mechanics and Engineering* 199 (2010) 2571 – 2589.
- [28] M. Cervera, M. Chiumenti, L. Benedetti, R. Codina, Mixed stabilized finite element methods in nonlinear solid mechanics. Part III: Compressible and incompressible plasticity, *Computer Methods in Applied Mechanics and Engineering* 285 (2015) 752 – 775.
- [29] M. Chiumenti, M. Cervera, R. Codina, A mixed three-field finite element formulation for stress accurate analysis including the incompressible limit, *Computer Methods in Applied Mechanics and Engineering* 283 (2015) 1095 – 1116.
- [30] I. Castanar, J. Baiges, R. Codina, A stabilized mixed finite element approximation for incompressible finite strain solid dynamics using a Total Lagrangian formulation, *Computer Methods in Applied Mechanics and Engineering* 368 (2020) 113164.
- [31] C. H. Lee, A. J. Gil, J. Bonet, Development of a stabilised Petrov-Galerkin formulation for conservation laws in Lagrangian fast solid dynamics, *Computer Methods in Applied Mechanics and Engineering* 268 (2014) 40–64.
- [32] C. H. Lee, A. J. Gil, G. Greto, S. Kulasegaram, J. Bonet, A new Jameson-Schmidt-Turkel Smooth Particle Hydrodynamics algorithm for large strain explicit fast dynamics, *Computer Methods in Applied Mechanics and Engineering* 311 (2016) 71–111.
- [33] M. Aguirre, A. J. Gil, J. Bonet, C. H. Lee, An upwind vertex centred finite volume solver for Lagrangian solid dynamics, *Journal of Computational Physics* 300 (2015) 387–422.
- [34] J. Haider, C. H. Lee, A. J. Gil, J. Bonet, A first order hyperbolic framework for large strain computational solid dynamics: An upwind cell centred Total Lagrangian scheme, *International Journal for Numerical Methods in Engineering* 109 (2017) 407–456.
- [35] A. J. Gil, C. H. Lee, J. Bonet, M. Aguirre, A stabilised Petrov-Galerkin formulation for linear tetrahedral elements in compressible, nearly incompressible and truly incompressible fast dynamics, *Computer Methods in Applied Mechanics and Engineering* 276 (2014) 659–690.
- [36] F. Armero, J. C. Simo, A new unconditionally stable fractional step method for nonlinear coupled thermomechanical problems, *International Journal for Numerical Methods in Engineering* 35 (1992) 737–766.
- [37] P. Betsch, M. Schiebl, Energy-momentum-entropy consistent numerical methods for large-strain thermoelasticity relying on the GENERIC formalism, *International Journal for Numerical Methods in Engineering* 119 (2019) 1216–1244.
- [38] C. Miehe, Entropic thermoelasticity at finite strains. aspects of the formulation and numerical implementation, *Computer Methods in Applied Mechanics and Engineering* 120 (1995) 243 – 269.

- [39] M. Franke, A. Janz, M. Schiebl, P. Betsch, An energy momentum consistent integration scheme using a polyconvexity-based framework for nonlinear thermo-elastodynamics, *International Journal for Numerical Methods in Engineering* 115 (2018) 549–577.
- [40] J. Simo, C. Miehe, Associative coupled thermoplasticity at finite strains: Formulation, numerical analysis and implementation, *Computer Methods in Applied Mechanics and Engineering* 98 (1992) 41 – 104.
- [41] R. Ortigosa, A. J. Gil, J. Martinez-Frutos, M. Franke, J. Bonet, A new energy-momentum time integration scheme for non-linear thermo-mechanics, *Computer Methods in Applied Mechanics and Engineering* (2020). Acceptedss.
- [42] J. M. Ball, Convexity conditions and existence theorems in nonlinear elasticity, *Archive for Rational Mechanics and Analysis* 63 (1976) 337–403.
- [43] J. M. Ball, Energy-minimising configurations in nonlinear elasticity, *Archive for Rational Mechanics and Analysis* 63 (1976) 337–403.
- [44] J. Schröder, P. Neff, Invariant formulation of hyperelastic transverse isotropy based on polyconvex free energy functions, *International Journal of Solids and Structures* 40 (2003) 401–445.
- [45] J. Schröder, P. Neff, D. Balzani, A variational approach for materially stable anisotropic hyperelasticity, *International Journal of Solids and Structures* 42 (2005) 4352–4371.
- [46] J. Schröder, P. Wriggers, D. Balzani, A new mixed finite element based on different approximations of the minors of deformation tensors, *Computer Methods in Applied Mechanics and Engineering* 200 (2011) 3583–3600.
- [47] M. Šilhavý, *The Mechanics and Thermodynamics of Continuous Media*, Springer Berlin Heidelberg, 1997.
- [48] M. Gurtin, E. Fried, L. Anand, *The Mechanics and Thermodynamics of Continua*, Cambridge University Press, 2010.
- [49] J. W. Gibbs, E. B. Wilson, *Vector analysis*, Yale University Press, ninth edition, 1947.
- [50] R. de Boer, *Vektor- und Tensorrechnung für Ingenieure*, Springer-Verlag, 1982.
- [51] J. Bonet, A. J. Gil, R. Ortigosa, A computational framework for polyconvex large strain elasticity, *Computer Methods in Applied Mechanics and Engineering* 283 (2015) 1061–1094.
- [52] J. Bonet, A. J. Gil, R. Ortigosa, On a tensor cross product based formulation of large strain solid mechanics, *International Journal of Solids and Structures* 84 (2016) 49–63.
- [53] J. L. Ericksen, *Introduction to the thermodynamics of solids*, pub-SV, New York, revised edition, 1998.
- [54] M. Kruger, M. GroB, P. Betsch, An energy-entropy-consistent time stepping scheme for nonlinear thermo-viscoelastic continua, *ZAMM - Journal of Applied Mathematics and Mechanics* 96 (2016) 141–178.

- [55] M. E. Gurtin, Thermodynamics and stability, *Archive for Rational Mechanics and Analysis* 59 (1975) 63–96.
- [56] C. M. Dafermos, Quasilinear hyperbolic systems with involutions, *Archive for Rational Mechanics and Analysis* 94 (1986) 373–389.
- [57] C. H. Lee, A. J. Gil, O. I. Hassan, J. Bonet, S. Kulasegaram, A variationally consistent Streamline Upwind Petrov Galerkin Smooth Particle Hydrodynamics algorithm for large strain solid dynamics, *Computer Methods in Applied Mechanics and Engineering* 318 (2017) 514–536.
- [58] O. I. Hassan, A. Ghavamian, C. H. Lee, A. J. Gil, J. Bonet, F. Auricchio, An upwind vertex centred finite volume algorithm for nearly and truly incompressible explicit fast solid dynamic applications: Total and updated lagrangian formulations, *Journal of Computational Physics: X* 3 (2019) 100025.
- [59] C. H. Lee, A. J. Gil, A. Ghavamian, J. Bonet, A total lagrangian upwind smooth particle hydrodynamics algorithm for large strain explicit solid dynamics, *Computer Methods in Applied Mechanics and Engineering* 344 (2019) 209 – 250.
- [60] J. Haider, C. H. Lee, A. J. Gil, A. Huerta, J. Bonet, An upwind cell centred total lagrangian finite volume algorithm for nearly incompressible explicit fast solid dynamic applications, *Computer Methods in Applied Mechanics and Engineering* 340 (2018) 684 – 727.
- [61] M. Aguirre, A. J. Gil, J. Bonet, A. A. Carreño, A vertex centred finite volume Jameson-Schmidt-Turkel (JST) algorithm for a mixed conservation formulation in solid dynamics, *Journal of Computational Physics* 259 (2014) 672–699.
- [62] O. Gonzalez, A. M. Stuart, *A first course in continuum mechanics*, Cambridge University Press, 2008.
- [63] J. M. Ball, *Geometry, Mechanics and Dynamics*, Springer, pp. 3–59.
- [64] J. M. Ball, F. Murat, Quasiconvexity and variational problems for multiple integrals, *Archive for Rational Mechanics and Analysis* 63 (1976) 337–403.
- [65] K. Zhang, A construction of quasiconvex functions with linear growth at infinity, *Annali della Scuola Normale Superiore di Pisa, Classe di Scienze* 97 (1992) 313–326.
- [66] B. Dacorogna, *Direct Methods in the Calculus of Variations*, Springer, 2008.
- [67] P. Ciarlet, Existence theorems in intrinsic nonlinear elasticity, *Journal des mathématiques pures et appliquées* 94 (2010) 229–243.
- [68] J. Bonet, A. J. Gil, R. D. Wood, *Nonlinear Solid Mechanics for Finite Element Analysis: Dynamics*, Cambridge University Press, 2020. Under review.
- [69] G. A. Holzapfel, *Nonlinear solid mechanics: A continuum approach for engineering*, Wiley and Sons, 2000.
- [70] G. Holzapfel, J. Simo, Entropy elasticity of isotropic rubber-like solids at finite strains, *Computer Methods in Applied Mechanics and Engineering* 132 (1996) 17 – 44.

- [71] J. Bonet, A. J. Gil, R. D. Wood, *Nonlinear Solid Mechanics for Finite Element Analysis: Statics*, Cambridge University Press, 2016.
- [72] E. Garcia-Blanco, R. Ortigosa, A. J. Gil, C. H. Lee, J. Bonet, A new computational framework for electro-activation in cardiac mechanics, *Computer Methods in Applied Mechanics and Engineering* 348 (2019) 796–845.
- [73] E. Garcia-Blanco, R. Ortigosa, A. J. Gil, J. Bonet, Towards an efficient computational strategy for electro-activation in cardiac mechanics, *Computer Methods in Applied Mechanics and Engineering* 356 (2019) 220–260.
- [74] D. H. Wagner, Symmetric-hyperbolic equations of motion for a hyperelastic material, *Journal of Hyperbolic Differential Equations* 06 (2009) 615–630.
- [75] Q. Tiehu, Symmetrizing nonlinear elastodynamic system, *Journal of Elasticity* 50 (1998) 245–252.
- [76] T. J. R. Hughes, L. P. Franca, M. Mallet, A new finite element formulation for computational fluid dynamics: I. Symmetric forms of the compressible Euler and Navier-Stokes equations and the second law of thermodynamics, *Computer Methods in Applied Mechanics and Engineering* 54 (1986) 223–234.
- [77] A. N. Brooks, T. J. R. Hughes, Streamline upwind/Petrov-Galerkin formulations for convection dominated flows with particular emphasis on the incompressible Navier-Stokes equations, *Computer Methods in Applied Mechanics and Engineering* 32 (1982) 199–259.
- [78] T. J. R. Hughes, L. P. Franca, M. Balestra, A new finite element formulation for computational fluid dynamics: V. Circumventing the Babuška-Brezzi condition: a stable Petrov-Galerkin formulation of the Stokes problem accommodating equal-order interpolations, *Computer Methods in Applied Mechanics and Engineering* 59 (1986) 85–99.
- [79] T. J. R. Hughes, L. P. Franca, M. Mallet, A new finite element formulation for computational fluid dynamics: Vi. Convergence analysis of the generalized SUPG formulation for linear time-dependent multidimensional advective-diffusive systems, *Computer Methods in Applied Mechanics and Engineering* 63 (1987) 97–112.
- [80] T. J. R. Hughes, M. Mallet, A new finite element formulation for computational fluid dynamics: III. The generalized streamline operator for multidimensional advective-diffusive systems, *Computer Methods in Applied Mechanics and Engineering* 58 (1986) 305–328.
- [81] T. J. R. Hughes, G. Scovazzi, T. E. Tezduyar, Stabilized methods for compressible flows, *Journal of Scientific Computing* 43 (2010) 343–368.
- [82] T. J. R. Hughes, T. E. Tezduyar, Finite element methods for first-order hyperbolic systems with particular emphasis on the compressible Euler equations, *Computer Methods in Applied Mechanics and Engineering* 45 (1984) 217–284.
- [83] T. E. Tezduyar, M. Senga, Stabilization and shock-capturing parameters in SUPG formulation of compressible flows, *Computer Methods in Applied Mechanics and Engineering* 195 (2006) 1621–1632.

- [84] I. A. Karim, C. H. Lee, A. J. Gil, J. Bonet, A two-step Taylor Galerkin formulation for fast dynamics, *Engineering Computations* 31 (2014) 366–387.
- [85] T. J. R. Hughes, Multiscale phenomena: Green’s functions, the Dirichlet-to-Neumann formulation, subgrid scale models, bubbles and the origins of stabilized methods, *Computer Methods in Applied Mechanics and Engineering* 127 (1995) 387–401.
- [86] T. J. R. Hughes, G. Scovazzi, L. P. Franca, in: E. Stein, R. de Borst, T. J. R. Hughes (Eds.), *Encyclopedia of Computational Mechanics*, John Wiley and Sons, 2004.
- [87] A. Ghavamian, A. J. Gil, C. H. Lee, J. Bonet, An entropy stable smooth particle hydrodynamics algorithm for large strain thermo-elasticity, *Computer Methods in Applied Mechanics and Engineering* (2020). Under review.
- [88] P. Betsch, A. Janz, C. Hesch, A mixed variational framework for the design of energy-momentum schemes inspired by the structure of polyconvex stored energy functions, *Computer Methods in Applied Mechanics and Engineering* 335 (2018) 660 – 696.
- [89] P. Chadwick, C. F. M. Creasy, Modified entropic elasticity of rubberlike materials, *Journal of the Mechanics and Physics of Solids* 32 (1984) 337–357.
- [90] R. W. Ogden, Aspects of the phenomenological theory of rubber thermoelasticity, *Polymer* 28 (1987) 379–385.